Biofuel Research Journal 46 (2025) 2432-2450

Biofuel Research Journal

Journal homepage: www.biofueljournal.com

Original Research Paper

Promoting methanogenesis and stability in anaerobic digestion with nano magnetite under VFA-induced stress

Xiaowen Zhu[1,*], Edgar Blanco[2], Manni Bhatti[1], Aiduan Borrion[1]

[1] *Department of Civil, Environmental and Geomatic Engineering, University College London, UK.*

[2] *Anaero Technology Limited, Cowley Road, Cambridge, UK.*

HIGHLIGHTS

- Nano magnetite increased methane yield by up to 8.7% under fatty acid stress.
- Direct interspecies electron transfer improved enzymatic and microbial resilience.
- Pretreatment with nano magnetite stabilised microbial diversity and methanogens.
- Economic analysis showed 8.8–12.8% more revenue and reduced carbon emissions in response to nano magnetite addition.
- Nano magnetite improved solid reduction and reduced disposal costs.

GRAPHICAL ABSTRACT

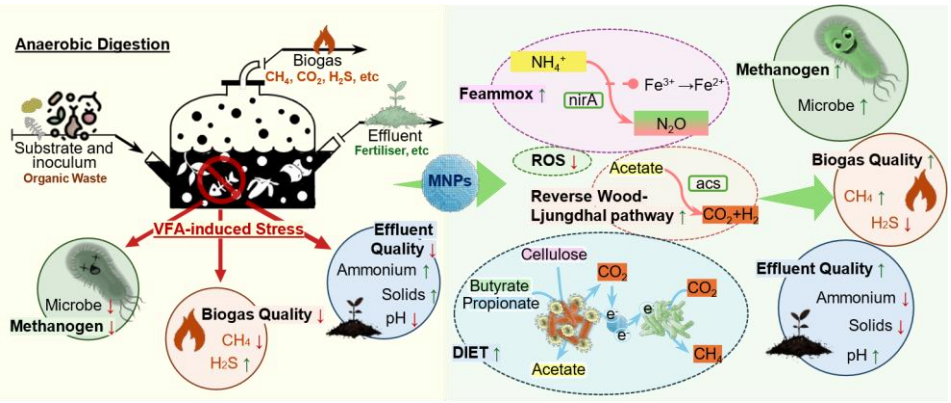

ARTICLE INFO

Article history:
Received 28 January 2025
Received in revised form 17 April 2025
Accepted 22 April 2025
Published 1 June 2025

Keywords:
Volatile fatty acid accumulation
Energy recovery
Nano magnetite
Anaerobic digestion
Metabolism
Waste-to-energy

ABSTRACT

Anaerobic digestion (AD) is a key waste-to-energy technology that transforms organic waste into biogas, contributing to renewable energy generation and environmental protection. However, AD systems are vulnerable to the accumulation of volatile fatty acids (VFAs), which disrupt methanogenesis and reduce system stability. Using batch tests to determine methanation kinetics, followed by long-term semi-continuous operations with stepwise butyrate and propionate additions, this study assessed both short- and long-term impacts of nano magnetite (magnetic nanoparticles, MNPs; specifically Fe_3O_4 nanoparticles) supplementation. Results demonstrated that MNPs facilitated VFA degradation within the VFA-stressed systems by promoting direct interspecies electron transfer (DIET), reducing oxidative stress, and enhancing enzymatic activity. The supplementation of MNPs improved methane production under VFA-induced stress, increasing yields by up to 7.9% and 8.7% in butyrate- and propionate-stressed systems, respectively. Moreover, MNP additions shortened the lag phases of butyrate and propionate methanation by over 24% while stabilised microbial viability above 85% compared to 70.7% in untreated systems during long-term operations. Smaller MNPs (20 nm) improved solid reduction rates by 4.01–6.82% within the stressed systems, reducing slurry disposal costs. Economic and environmental analysis demonstrated potential electricity revenue increases of 8.78–12.79%, while environmental assessments showed reduced carbon emissions. These findings suggest that MNPs provide a scalable and effective solution for industrial AD plants, particularly those treating cellulose-rich waste and substrates leading to rapid VFA production (e.g., food waste). Importantly, this study bridges lab-scale experimentation with practical applications, using batch-derived thresholds to inform semi-continuous operations. Future research should focus on long-term environmental impacts and MNP recovery strategies to ensure sustainable deployment.

* Corresponding author at:
E-mail address: zceszxi@ucl.ac.uk

Please cite this article as: Zhu X., Blanco E., Bhatti M., Borrion A. Promoting methanogenesis and stability in anaerobic digestion with nano magnetite under VFA-induced stress. Biofuel Research Journal 46 (2025) 2432-2450. DOI: 10.18331/BRJ2025.12.2.5.

Contents

Abbreviations

AD	Anaerobic digestion	SRB	Sulphate-reducing bacteria
ANOVA	One-way analysis of variance	TS	Total solid
BMP	Biochemical methane potential	VFA(s)	Volatile fatty acid(s)
DIET	Direct interspecies electron transfer	VS	Volatile solid
Feammox	Ammonium oxidation coupled with ferric iron reduction	VSS	Volatile suspended solids
HRT	Hydraulic retention time	λ	Duration of lag phase, h
IA:PA	Intermediate alkalinity to partial alkalinity	R_{max}	Maximum methanation rate, ml/h
KEGG	Kyoto Encyclopedia of Genes and Genomes	η	Substrate utilisation efficiency, %
MNP	Nano magnetite (magnetic nanoparticles)	$\mu_{max,\ ace}$	Maximum specific growth rate of acetogens, 1/d
NRB	Nitrate-reducing bacteria	$K_{S,\ ace}$	Maximum specific growth rate of methanogens, g/L
OLR	Organic loading rate	$\mu_{max,\ met}$	Acetogenic substrate half-saturation constant, 1/d
ORP	Oxidation-reduction potential	$K_{S,\ met}$	Methanogenic substrate half-saturation constant, g/L
PICTRSt2	Phylogenetic Investigation of Communities by Reconstruction of Unobserved States	Y	Overall synthesis yield, g cells/g substrate consumed
ROS	Reactive oxygen species	f_e	Electron flow for methanation
SMA	Specific methanogenic activity	f_s	Electron flow for microbial cell synthesis

1. Introduction

Anaerobic digestion (AD) is a well-established biochemical process that converts organic waste into biogas, primarily composed of methane and carbon dioxide. This renewable energy technology has gained attention for its potential to mitigate environmental pollution, reduce greenhouse gas emissions, and contribute to sustainable energy production (Subbarao et al., 2023). As global energy demand grows and the transition towards low-carbon energy systems accelerates, AD presents a scalable solution to generate clean energy from various waste streams. The methane-rich biogas produced by AD can be used directly as a fuel for electricity and heat generation (IEA, 2020). It can also be upgraded to biomethane for natural gas networks or as a renewable fuel for vehicles (IEA, 2020). Beyond energy production, AD contributes to the circular economy by reducing waste volumes, recovering nutrients, and mitigating carbon emissions associated with traditional waste disposal methods (Subbarao et al., 2023). However, the efficiency of AD systems is often hindered by process instabilities under stress conditions such as feedstock overload or high concentrations of volatile fatty acids (VFAs) (Barrena et al., 2023). Optimizing anaerobic digestion (AD) systems remains a critical priority, as underscored by previous studies, including Hansen et al. (2021).

Butyrate and propionate are intermediate VFAs formed during the fermentation stage of AD. They then break down into acetate, hydrogen, and formate, playing crucial roles in methanogenesis. Nevertheless, elevated concentrations of these VFAs often disrupt the microbial structures, causing pH reductions, inhibiting enzymatic activity, and

Please cite this article as: Zhu X., Blanco E., Bhatti M., Borrion A. Promoting methanogenesis and stability in anaerobic digestion with nano magnetite under VFA-induced stress. Biofuel Research Journal 46 (2025) 2432-2450. DOI: 10.18331/BRJ2025.12.2.5.

compromising methanogens` viability. Propionate degradation poses significant challenges due to its unfavourable thermodynamics and high toxicity to microbial communities (Li et al., 2020). Butyrate degradation, while thermodynamically favourable, can also induce metabolic bottlenecks under stress, resulting in delayed biogas production and system instability (Jin and Lu, 2023).

To address these challenges, direct interspecies electron transfer (DIET) has emerged as a promising pathway (Gahlot et al., 2020). DIET enhances syntrophic interactions between acetogens and methanogens by facilitating efficient electron flow, bypassing the need for hydrogen or formate as intermediates (Wu et al., 2022). The inclusion of conductive materials such as magnetite in AD systems has been shown to promote DIET, accelerating electron transfer and improving methanogenic activity under VFA-induced stress (Su et al., 2021). Acting as electron conduits, magnetite not only enhances DIET but also creates a more reductive environment conducive to methanogenesis (Giangeri et al., 2023).

Beyond their conductive properties, magnetite offers additional benefits to AD systems under stress. A critical challenge in AD is oxidative stress caused by reactive oxygen species (ROS), which disrupt enzymatic activity and damage microbial cells (Yan et al., 2023). Nano magnetite (magnetic nanoparticles, MNPs; specifically Fe_3O_4 nanoparticles) mitigate this by regulating ROS-associated enzymatic activities, which help neutralise oxidative damage and maintain redox balance (Kicheeva et al., 2023). This capacity to mitigate ROS toxicity creates a more favourable environment for methanogens, particularly under stress conditions (Yan et al., 2023).

In addition to addressing oxidative stress, magnetite actively participates in biochemical processes such as dissimilatory sulphate reduction and ammonium oxidation coupled with ferric iron reduction (Feammox) (Tan et al., 2022; Giangeri et al., 2023). By facilitating these pathways, magnetite reduces competition between sulphate-reducing bacteria (SRB), nitrate-reducing bacteria (NRB), and methanogens. This competitive inhibition is a major bottleneck in AD, and the enhanced sulphate degradation mediated by MNPs supports smoother methane production by mitigating sulphide-related toxicity and ammonia accumulation (Tan et al., 2022; Giangeri et al., 2023).

The small size and high surface area of MNPs enhance the colonisation of key microbial populations, creating microenvironments that support syntrophic interactions (Zhu et al., 2021; Jung et al., 2023). For example, MNPs can serve as bridges facilitating DIET by physically connecting acetogens and methanogens. This connectivity accelerates the electron flow during the degradation of VFAs, bypassing the need for hydrogen as an intermediate and improving the thermodynamics of methanogenic pathways (Jung et al., 2023). Additionally, the biofilm-forming properties of MNPs help protect microorganisms from environmental fluctuations and inhibitory substances, such as high VFA levels, ensuring stable microbial activity (Su et al., 2021). MNPs also influence the oxidation-reduction potential (ORP) within AD systems, shifting it to more reductive ranges conducive to methanogenesis. This reductive environment, combined with MNPs' ability to mitigate enzymatic inhibition, enhances methane production and stabilises the AD process during stress conditions (Su et al., 2021). It should be noted that the role of nanomaterials, including MNP, in enhancing electron transfer and system performance in bioenergy systems has been highlighted previously (Andrade et al., 2016; Mashkour et al., 2021).

As summarised in **Table 1**, several studies have shown that MNPs can enhance methane yields and support recovery in stressed AD. However, much of these works have been limited to batch-scale setups or lack mechanistic depth. The present study uniquely addresses both butyrate and propionate stress with different dosing strategies (pretreatment and post-treatment) while integrating kinetic, microbial, and metabolic evaluations in a long-term semi-continuous AD system, offering new mechanistic insights into MNP-mediated process stabilisation.

In light of the above, this study investigates the potential of MNPs as a novel strategy to mitigate VFA-induced stress in AD systems, with a focus on mitigating butyrate and propionate accumulation. This study hypothesises that these particles can facilitate the methanation of accumulated VFAs, stabilising AD performance under stress via enhanced

Table 1.
Summary of recent studies (2019–2025) about MNP to enhance the AD process under stress conditions.

MNP		Operation Condition					Main Features	Ref.
Concentration, mg/L	Size, nm	Feedstock	Inoculum	Temperature, °C	Type of Experiment	Induced Stress		
270[1]	6-13	Cellulose and glucose	Granular sludge or anaerobic flocculent sludge	37	Batch	Overloaded	• Focused on overload-induced VFA accumulation • Evaluated recovery via microbial shifts	Barrena et al. (2023)
200[1]	20	Synthetic wastewater with glucose	Anaerobic granular sludge	37±1	Batch	Salinity	• Tracked VFA profiles and methane yield • Explored high salinity-induced VFA accumulation	Guan et al. (2023)
4631[2]	50-100	Acetate anaerobic medium	Mesophilic anaerobic sludge	37	Batch and sequential batch	Acetate	• Quantified acetic acid degradation enhancement • Linked kinetics with MNP-mediated DIET	Kim et al. (2024)
100[1]	10-20	Acetic and propionic acids	Acclimated anaerobic granular sludge	35±2	Batch and sequential batch	Propionate	• Operated with acid-tolerant inoculum • Demonstrated lag-phase reduction with MNPs • Specific to syntrophic propionate oxidation	Li et al. (2021)
3200	50-100	Chicken manure	Anaerobic sludge for cattle manure	38	Batch	Ammonia	• Explored MNP-enhanced total ammonia nitrogen removal • Demonstrated DIET via enrichment of *Methanothrix* and *Syntrophomonas*	Ziganshina and Ziganshin (2023)
100	20 or 50	Cellulose-based synthetic feedstock	Mesophilic anaerobic sludge	38±1	Batch and Semi-continuous	Butyrate or propionate	• Dual boosting strategies (pretreatment and post-treatment) with long-term MNP exposure • Evaluated VFA thresholds and DIET mechanisms • Combined kinetic, microbial, and metabolic analysis	**Current Study**

[1]: Best performance.
[2]: Calculated based on the reported concentration of 20 mmol/L.

Please cite this article as: Zhu X., Blanco E., Bhatti M., Borrion A. Promoting methanogenesis and stability in anaerobic digestion with nano magnetite under VFA-induced stress. Biofuel Research Journal 46 (2025) 2432-2450. DOI: 10.18331/BRJ2025.12.2.5.

DIET, improved enzymatic activities, and regulated ROS. Moreover, considering their high surface area and small size, MNPs can promote the colonisation of syntrophic microbial populations, therefore enhancing AD system resilience for improved energy recovery. The hypothesis is tested through a combination of kinetic evaluations, microbial analyses, as well as performance assessments under controlled batch and long-term AD operations. By addressing these research questions, this study aims to provide a mechanistic understanding of MNP-enhanced AD processes and practical insights for improving waste-to-energy applications.

2. Materials and Methods

2.1. Experiment setup

Inoculum was collected from a biogas plant for food waste: Andigestion Ltd. (Holsworthy, UK), operating under a mesophilic condition with a hydraulic retention time (HRT) of 25 d and the organic loading rate (OLR) of 4.0 gVS/L/d. The inoculum was pretreated by sieving through a 2 mm mesh to remove large solid particles. Detailed characteristics of inoculum are provided in **Table S1**. The MNPs with a purity of 99% were obtained from Xiangtian Nano Material Company (Shanghai, China). This study examined the impact of MNP size on AD systems using MNPs with average diameters of 20 nm (specific surface area > 60 m²/g, bulk density 0.84 g/cm³) and 50 nm (specific surface area 50 m²/g, bulk density 0.67 g/cm³). Both particle sizes shared a density of 5.18 g/cm³. All experiments were conducted at a controlled temperature of 38±1°C and stirred at 40 rpm using the Nautilus system (Anaero Technology, UK, **Fig. 1**), including 15 one-litre reactors with a working volume of 750 mL each.

2.1.1. Batch experiment: methanogenesis of butyrate and propionate

The batch experiment assessed the degradation patterns of butyric acid and propionic acid over a three-day period, examining the effects with and without the addition of MNPs. These tests established the inhibition thresholds and served as the foundation for designing the subsequent long-term semi-continuous experiments. Six experimental groups were set up (**Fig. 1**), each featuring five dosage levels with elevated dosages of either butyric acid or propionic acid as the sole carbon source, together with 10 mL of mineral medium (**Table S2**). Additionally, a control group was established by operating the reactors without any substrate addition, serving as a baseline for comparison under the same operational conditions.

MNP treatment groups were amended with a constant concentration of 100 mg/L of magnetite (20 nm or 50 nm), a dosage selected based on previous studies reporting optimal AD performance while ensuring environmental safety (Zhu et al., 2021; Thu et al., 2023).

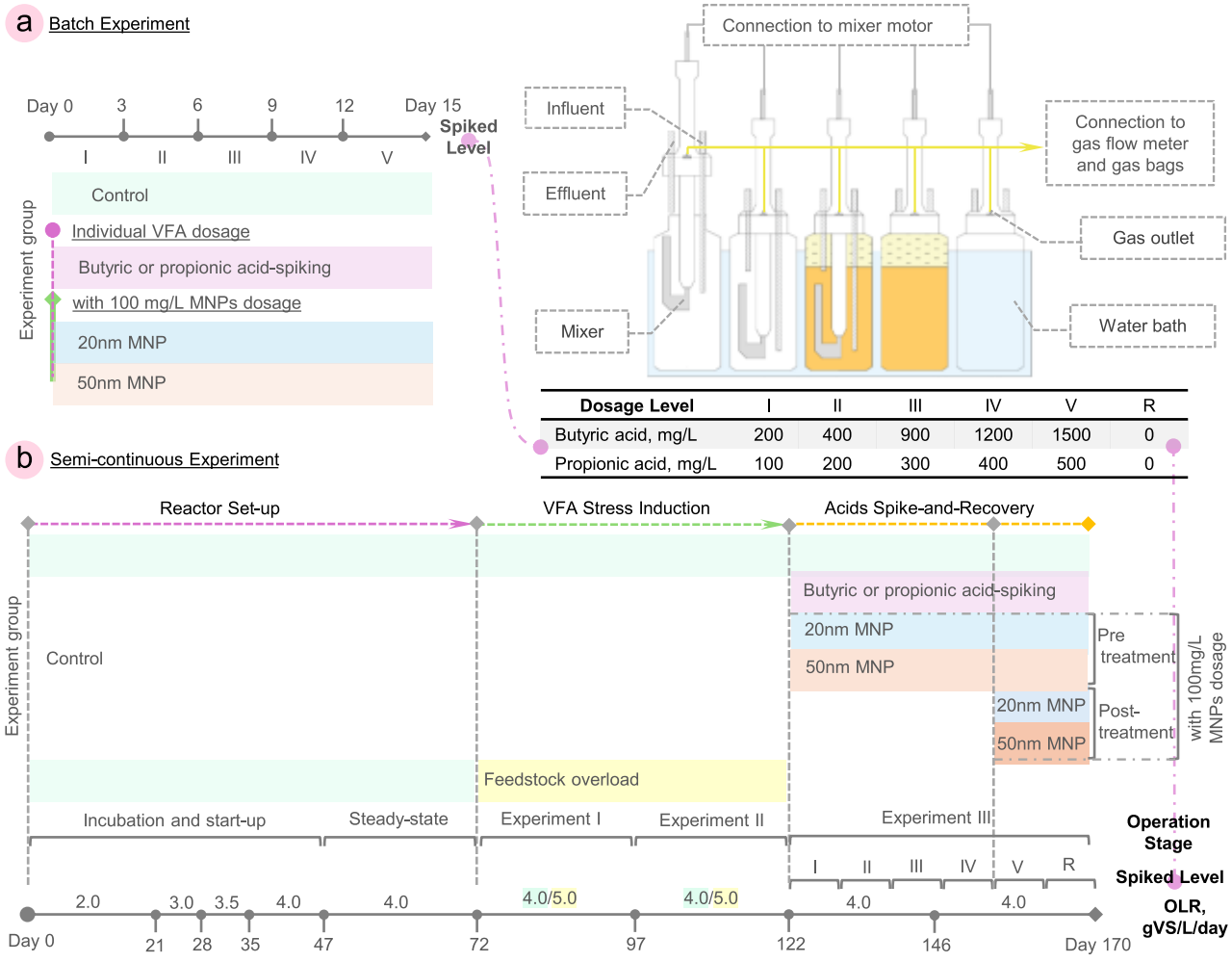

Fig. 1. Sectional view of Nautilus system and experimental design. (**a**) Batch experiment procedure; and (**b**) Semi-continuous experiment procedure.

Please cite this article as: Zhu X., Blanco E., Bhatti M., Borrion A. Promoting methanogenesis and stability in anaerobic digestion with nano magnetite under VFA-induced stress. Biofuel Research Journal 46 (2025) 2432-2450. DOI: 10.18331/BRJ2025.12.2.5.

VFA concentrations were selected based on reported inhibition thresholds for mesophilic systems (Wang et al., 2009). For butyrate, concentrations of 200, 400, 900, 1200, and 1500 mg/L were applied sequentially. Signs of inhibition were observed at 1200 mg/L, where the lag phase (λ) decreased by 74.3% and substrate utilisation efficiency (η) began to decline. To confirm the inhibitory trend, a final dose of 1500 mg/L was introduced before concluding the experiment. Detailed performance results are presented in *Section 3.1* and **Table S5**. A similar dosing strategy was employed for propionate.

A three-day dosing interval was adopted for each cycle, in line with previous reports indicating complete degradation of VFAs within 72 h under non-inhibitory mesophilic conditions (Dogan et al., 2005; Wang et al., 2009).

Each reactor was initially loaded with 750 mL of seed sludge and purged with nitrogen gas for 2 min to ensure anaerobic conditions. After a 24-h reactivation and degassing phase, configured doses of butyrate or propionate were introduced according to the levels specified in **Figure 1**. All experiments were conducted in triplicate to ensure data reliability.

2.1.2. Semi-continuous experiment: spike-and-recovery tests of butyrate and propionate

The semi-continuous AD operations used cellulose (Mereck, Germany) as the primary carbon source, while urea (≥99.5%, Sigma-Aldrich, UK) was added to maintain a carbon-to-nitrogen ratio of 21. To simulate the complexity and diversity of microbial communities similar to those in real-world feedstocks, these substrates were pre-mixed with a mineral medium (**Table S2**) before being introduced into the reactors (Isci and Demirer, 2007; Morita et al., 2011). The microbial community composition was assessed through sequencing and alpha diversity analyses, as described in *Section 2.4* and presented in **Figure S3**, enabling a comparison between the initial inoculum and samples collected after long-term reactor operation.

The operations followed a 24-h cycle of feeding, liquid sample collection, and waste removal, lasting 170 d and divided into three phases (**Fig. 1**): Phase 1 (Day 0-71), Phase 2 (Day 72-121), and Phase 3 (Day 122-170), each targeting specific operational goals. The semi-continuous experiments adopted the same MNP and VFA concentrations derived from batch tests to explore longer-term impacts and practical resilience.

During Phase 1, the seeded inoculum was reactivated by gradually increasing the OLR of each reactor from 2.0 to 4.0 gVS/L/d and maintained at 4.0 gVS/L/d for one HRT of 25 d. Phase 2 aimed to establish a stable operational baseline for Phase 3, with all eleven reactors operated at a constant OLR of 4.0 gVS/L/d for two HRTs.

Phase 3 explored the effect of MNPs on mitigating stress associated with varying dosages of butyric acid or propionic acid (**Fig. 1**). A control group was established without any additions of individual VFAs or MNPs. The VFA spike group consisted of two reactors, each subjected to increases in butyric acid or propionic acid according to the levels detailed in **Figure 1**. The MNP treatment groups received both individual VFA dosages and 100 mg/L MNPs, available in particle sizes of either 20 nm or 50 nm. In the pretreatment groups, MNPs were introduced together with the VFA spikes on the first day of Phase 3. The post-treatment groups were designed to simulate scenarios in which MNP treatments are added after the accumulation of target VFAs. To this end, MNPs were introduced on the first day of the last VFA dosage level (Day 157).

2.2. Analytical methods

Biogas volume was measured with a datalogger connected to the Nautilus model (**Fig. 1**). The methane and carbon dioxide concentrations were measured with a gas analyser (GasData GFM436, UK), together with the levels of hydrogen and hydrogen sulphide.

Analytical methods employed in this study were primarily based on the water and wastewater analysis methods outlined in the standard methods compiled by the American Public Health Association and the United States Environmental Protection Agency (USEPA, 1983; APHA, 2012). VFA concentrations and pH were measured 24 h and 72 h after each dosage, with the detailed methods provided in **Supplementary Material** (*Section S1*).

Sludge samples were collected to investigate the effects of different MNP dosing strategies under VFA accumulation on the microbial communities and metabolic functions within AD systems. Cell viability was measured using flow cytometry with the LIVE/DEAD BacLight Bacterial Viability Kit (Molecular Probes, Oregon, USA). The diversity of bacterial and archaeal communities of the semi-continuous spike-and-recovery experiment was analysed using 16S rRNA sequencing, with samples collected on the last day of VFA dosage level V and extracted with DNeasy Power Soil kit (QIAGEN, Germany) following the manufacturer's instructions. The purity and concentration of the extracted DNA were evaluated using a NanoDrop2000 micro-volume spectrophotometer (Thermo Fisher Scientific, USA). The V4 regions of the 16S rRNA were amplified with the universal primer set 515F/806R (Campanaro et al., 2018). Subsequent sequencing was performed on the Illumina NovaSeq PE250 platform by Novogene Co. Ltd. (Cambridge, UK). The details of the sequencing pipeline can be found in **Supplementary Material** (*Section S2*).

2.3. Kinetic evaluation

Kinetic parameters for methane production during batch spike-to-recovery tests were determined using the modified Gompertz equation. Specific methanogenic activity (SMA) and substrate utilisation efficiency (η) were calculated to evaluate methane production efficiency and substrate conversion rates (Boyle, 1977; Dogan et al., 2005). Microbial growth kinetics, including specific growth rate (μ) and synthesis yield (Y), were analysed using the Monod equation and stoichiometric modelling. The electron flow for methanation and microbial cell synthesis (fe and fs, respectively) was assessed using the stoichiometric oxidation-reduction reaction model, considering electron donor and acceptor contributions. Detailed equations and methodologies are provided in **Supplementary Material** (*Section S3*).

2.4. Statistical analysis

Statistical analyses were performed using R (v4.3.3). For batch operations, the mean was calculated at each spiked level, while both the mean and interquartile range were assessed for semi-continuous operations. Data from semi-continuous operations were analysed using one-way analysis of variance (ANOVA) and pairwise t-tests with Bonferroni correction to evaluate stability and performance differences at varying VFA concentrations and between treatment groups.

The metabolic capacities of microorganisms associated with each AD process were initially categorised using PICTRSt2 (Phylogenetic Investigation of Communities by Reconstruction of Unobserved States, version 2) results, which were informed by the KEGG (Kyoto Encyclopedia of Genes and Genomes) database and previous studies focused on the detailed reconstruction of microbial functions (Lv et al., 2020; You et al., 2023), nitrogen and sulphate cycling (Tan et al., 2022; Giangeri et al., 2023), DIET (You et al., 2023), as well as ROS in AD process (Yan et al., 2023). Further details are presented in **Supplementary Material** (*Section S2*), with gene expressions and enzyme activities summarised in **Tables S3** and **S4**. The Mantel test (Vegan package v2.6.4) was used to assess correlations between these microbial groups and AD performance indicators, with results evaluated using Mantel's p-value and Pearson's r. A significance level of $p < 0.05$ was applied to all tests.

3. Results and Discussion

This study systematically evaluated the methanation of butyrate and propionate, with and without MNP supplementation, to assess their impacts on AD performance. The section begins with kinetic assessments of butyrate and propionate degradation, establishing baseline system behaviour with a focus on methanogenesis, the most stress-sensitive AD phase (*Section 3.1*). This is followed by an analysis of semi-continuous reactor responses to increasing VFA dosages, both with and without MNP addition (*Sections 3.2* and *3.3*). *Section 3.4* explores long-term microbial community dynamics and metabolic pathway activities to mechanistically explain the observed performance trends, linking macro-scale outcomes to underlying biochemical processes. The broader implications of these findings are discussed in *Section 3.5*.

Please cite this article as: Zhu X., Blanco E., Bhatti M., Borrion A. Promoting methanogenesis and stability in anaerobic digestion with nano magnetite under VFA-induced stress. Biofuel Research Journal 46 (2025) 2432-2450. DOI: 10.18331/BRJ2025.12.2.5.

3.1. Methanation of butyrate and propionate

The typical methanogenic pathways for both butyrate and propionate involve cooperation between acetogens and methanogens, converting these acids into acetate and hydrogen, followed by methane production (Li et al., 2020). To assess the effects of MNPs on methanation kinetics, batch spike-to-recovery tests were conducted. These tests aimed to determine inhibition thresholds and assess the methanation kinetics of butyrate and propionate with and without MNP supplementation, as presented in **Table 2** and **Figure 2**. Kinetic parameters for each dosage level are summarised in **Table S5**. While direct microbial analysis was not performed for these batch assays, the results provided kinetic insights and served as a quantitative foundation for the subsequent long-term semi-continuous experiments (*Sections 3.2* and *3.3*), which adopted the same MNP and VFA concentrations to explore long-term AD performance under VFA-induced stress.

3.1.1. Methanogenesis response to evaluated butyrate and propionate concentrations

Overall methane production, SMA, and fermentation period duration increased with the increasing dosed substrate VFA concentrations (**Figs. 2a** and **2f**). Conversely, substrate utilisation efficiency (η) decreased with increasing substrate concentrations. For butyrate methanation, η values remained around 94.8±0.4% during the first three cycles but dropped to 90.1% in the last cycle. The maximum methanation rate (R_{max}, **Table S5**) of 13.8 mL/h in the fourth cycle shifted the maximum SMA from the first to the second day, with a 74.1% increase in the lag phase duration compared to the previous cycle. By the last cycle, the lag phase duration further increased to 20.8 h, and the maximum methanation rate decreased to 12.7 mL/h, indicating that a dosed concentration of 1500 mg/L hindered methanogenesis. Compared to fractions of electrons used for methanation (*fe*, **Table S5**), which decreased by 2.6% from the previous dosage level, this concentration exhibited greater impacts on substrate-to-cell synthesis (synthesis yield, Y and fractions of electrons for cell synthesis, *fs*, **Table S5**), which decreased by 6.5%.

Propionate degradation followed a similar pattern, with a maximum methanation rate of 3.2 mL/h at 300 mg/L and the longest lag phase of 16.1 h in the last cycle. The SMA for propionate was lower than for butyrate, with a 3.2-fold longer lag phase at 400 mg/L. The kinetic parameters (**Table 2**) showed that the specific growth rate of acetogens ($\mu_{max, met}$) for propionate was only half that for butyrate. Additionally, the acetogenic half-saturation constant ($K_{S, ace}$) was 2.5 times higher for propionate, suggesting that propionate is less readily degraded (Zhao et al., 2024). This is owing to the less favourable thermodynamics of propionate degradation and its higher toxicity to microorganisms compared to butyrate (Li et al., 2020), resulting in a notable drop in cell synthesis rate of 8.8% at the dosage concentration of 400 mg/L. Furthermore, a key player in butyrate degradation, such as *Syntrophomonas*, are generally more efficient and faster-growing than the syntrophic propionate-oxidising bacteria, including *Syntrophobacter* and *Pelotomaculum* (Westerholm et al., 2022; Jin and Lu, 2023), leading to higher overall cell synthesis yields

3.1.2. Effects of MNPs on butyrate and propionate methanation at lower dosages

During the first three cycles at lower dosages, MNPs increased three-day methane production from butyrate by an average of 3.8%, with η values improving from 94.8% to 98.4%. Similar patterns were observed for propionate methanation, with methane production increasing by 4.3% and η values averaging 98.2%. MNPs also reduced the lag phase for both substrates. For butyrate methanation, lag phase reductions averaged 24.1±2.2% for 20 nm MNPs and 24.0±0.1% for 50 nm MNPs during the first two dosage levels. In the second dosage level for propionate, both MNPs reduced the lag phase by 55.0%, indicating accelerated methanation similar to butyrate at the same concentration (dosage level I). These findings align with the patterns of SMAs. While the maximum SMA for the control group shifted from the first to the second day at the third dosage level of propionate-spiking, it remained on the first day in the MNP-treated groups.

Reductions in concentrations of acetic acid and substrate VFAs (**Figs. 2b** and **2g**) suggested that MNPs first accelerated VFA oxidation and then facilitated the conversion of intermediates (hydrogen, carbon dioxide, and acetate) to methane. These observations are consistent with the enhancements in acetogenesis and methanogenesis kinetic parameters (**Table 2**).

MNP additions increased the total fraction of electrons from the substrate (*fe+fs*) through improved syntrophic interactions between acetogens and methanogens (Fan et al., 2024), leading to more efficient oxidation and utilisation of substrate VFAs and resulting in more active microorganisms (**Figs. 2d** and **2i**). These findings were supported by previous studies that MNPs reduce energy loss and improve the thermodynamics of conversion processes by facilitating electron transfer, including DIET by acting as electron conductors during methanogenesis in AD systems (Gahlot et al., 2020; Wu et al., 2022).

3.1.3. Effects of MNPs on methanogenesis under VFA stress

The dosages of substrate VFAs hindered the methanogenesis process during the last two dosage levels in all experimental groups. At high VFA dosages, MNP-treated groups exhibited faster and more efficient substrate utilisation, resulting in enhanced and rapid degradation of VFAs, particularly noticeable in the final measurements of acetate and remaining substrate VFAs (**Figs. 2b** and **2g**). MNPs modified the redox potential (**Fig. S1**), creating favourable conditions for oxidising butyrate and propionate (Yang et al., 2019), thus enhancing methanogenesis.

When dosed with 1500 mg/L butyric acid, overall methane production improved by 7.2% and 6.6% for 20 nm and 50 nm MNPs, respectively, with

Table 2.
Average kinetic parameters of butyrate and propionate methanation.

Parameter		Butyrate			Propionate		
		Control	20 nm MNP	50 nm MNP	Control	20 nm MNP	50 nm MNP
Duration of lag phase (h)*	λ	20.817	12.518	12.651	16.054	12.637	12.842
Maximum methanation rate (ml/h) **	R_{max}	13.813	16.218	15.718	3.157	3.353	3.167
Substrate utilisation efficiency (%)	η	93.499	98.020	97.739	93.670	97.784	97.843
Maximum specific growth rate of acetogens (1/d)	$\mu_{max, ace}$	0.055	0.074	0.069	0.027	0.053	0.061
Maximum specific growth rate of methanogens (g/L)	$K_{S, ace}$	2.006	1.926	1.903	5.083	2.066	2.518
Acetogenic substrate half-saturation constant (1/d)	$\mu_{max, met}$	0.998	1.000	1.000	0.996	0.999	0.998
Methanogenic substrate half-saturation constant (g/L)	$K_{S, met}$	1.628	1.280	1.194	1.622	1.280	1.193
Overall synthesis yield (g cells/g substrate consumed)	Y	0.098	0.136	0.129	0.059	0.068	0.067
Total fraction of electrons from the donor	$f_e + f_s$	0.985	1.051	1.042	0.965	1.020	1.015

*: Maximum lag phase observed at the last dosage level.
**: Maximum methanation rate.

Please cite this article as: Zhu X., Blanco E., Bhatti M., Borrion A. Promoting methanogenesis and stability in anaerobic digestion with nano magnetite under VFA-induced stress. Biofuel Research Journal 46 (2025) 2432-2450. DOI: 10.18331/BRJ2025.12.2.5.

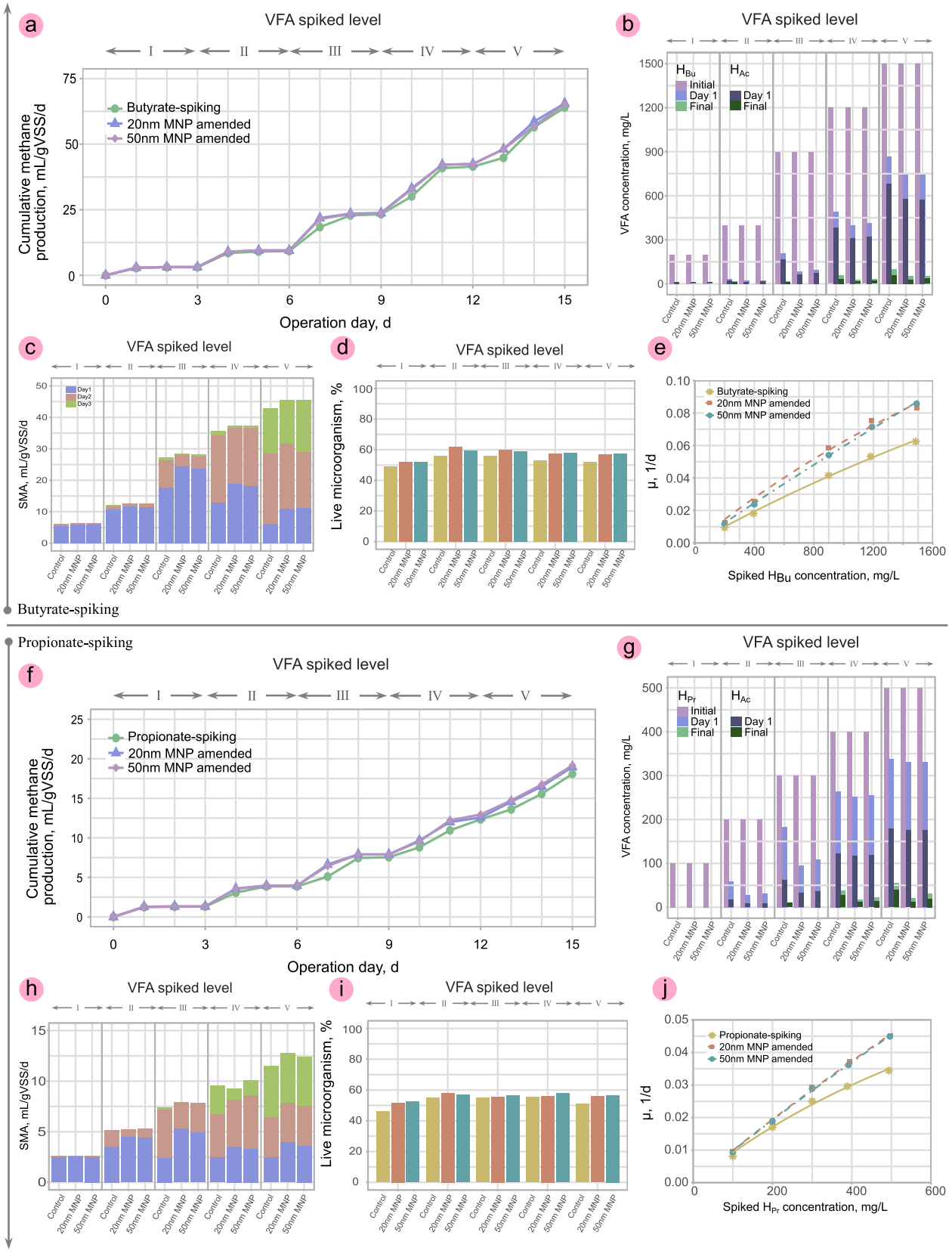

Fig. 2. Methanogenesis response to spiked butyric and propionic acids, with dosage concentrations of each spiked levels detailed in Figure 1. (**a,f**) Cumulative methane production; (**b,g**) Changes in VFA concentration at initial, Day 1, and the final day of each spiked level; (**c,h**) Specific methanogenic activity (SMA) over each spiked level; (**d,i**) Microbial viability at the end of each spiked level; and (**e,j**) The relationship between specific microbial growth rate and spiked VFA concentration.

Please cite this article as: Zhu X., Blanco E., Bhatti M., Borrion A. Promoting methanogenesis and stability in anaerobic digestion with nano magnetite under VFA-induced stress. Biofuel Research Journal 46 (2025) 2432-2450. DOI: 10.18331/BRJ2025.12.2.5.

similar η values of 96.3±0.3%, compared to 90.1% in the control. The pH of all experimental groups remained above 7.6, even with the highest dosages. Although the amount of dissolved iron cations from MNPs was negligible within this pH range, smaller MNPs tended to release more cations due to their larger surface-to-volume ratio (Ziganshina et al., 2021), promoting rapid electron transfer and enhancing microbial attachment (Fan et al., 2024), resulting in higher synthesis yields and microbial density compared to 50 nm MNPs. Moreover, 20 nm MNPs were more easily taken up by microorganisms *via* pinocytosis (Augustine et al., 2020), serving as nutrients and facilitating the butyrate oxidation process (Zhu et al., 2021; Guo et al., 2022).

During the last dosage level of propionate, overall methane production increased by 5.2% and 5.5% for 20 nm and 50 nm MNPs, respectively. The 50 nm MNPs achieved a higher η value of 97.2% with 500 mg/L propionic acid, compared to 96.7% with 20 nm MNPs and 92.1% in the control. While 20 nm MNPs enhanced electron transfer between microorganisms, leading to higher total fractions consumed for both cell synthesis and methane generation (*fe+fs*), 50 nm MNP-treated groups provided a more stable environment for microorganisms, with microbial viability averaged at 56.0±1.8%, compared to 55.5±2.7% for 20 nm MNPs. This suggested that 50 nm MNPs offered a more stable and efficient electron flow with an optimal balance between surface area and stability, facilitating a conducive environment for microbial richness and biofilm formation, thereby enhancing propionate utilisation efficiency. Moreover, larger-sized nanoparticles induce lower stress and toxicity to microorganisms, minimising inhibitory effects (Thu et al., 2023).

3.1.4. Effects of nano magnetite on microbial growth kinetics

The specific microbial growth rates (μ) for butyrate and propionate at various concentrations are shown in **Figures 2e** and **2j** for acid-spiking and MNP-treated groups. At the highest VFA dosages, these rates stabilised in control groups, aligning with decreased maximum methanation rates (R_{max}, **Table S3**). However, in the MNP-treated groups, no declines in μ or R_{max} were observed. Kinetic parameters for microbial growth during acetogenesis and methanogenesis were derived (**Table 2**) using the Monod equation (**Eq. S5**) and previous research on acetate kinetics (**Table S4**).

Fitting analysis demonstrated that MNPs increased $\mu_{max,ace}$ by over 90% for propionate oxidation to acetate and reduced the propionate $K_{S,ace}$ by over 50%. While $\mu_{max,ace}$ for butyrate improved by 34.5% and 25.5% for 20 nm and 50 nm MNPs, respectively, with a 4.6±0.6% reduction in butyrate $K_{S,ace}$. This difference is owing to the more complex propionate methanation process compared to butyrate (Jin and Lu, 2023). Additionally, both MNPs reduced the acetate $K_{S,met}$ by over 20% in both butyrate and propionate tests, highlighting MNPs' role in promoting microbial growth and metabolism during syntrophic methanation. These effects might lead to increased microbial density with effective biofilm formation, protecting bacteria from inhibitory factors and promoting efficient interspecies electron transfer (Chen et al., 2020).

Moreover, previous studies reported that MNPs improved the methanation of VFAs by stimulating enzymatic activities for converting intermediates, including hydrogen and acetate, into methane, as MNPs could act as nutrient suppliers for enzymes and coenzymes such as ferredoxin oxidoreductase and hydrogenases, thus enhancing electron transfer capabilities (Zhu et al., 2021; Jung et al., 2023).

3.2. System response to butyrate-spiking and different nano magnetite-boosting strategies

Based on the kinetic insights, *Sections 3.2* and *3.3* examine how the semi-continuous reactors responded to butyrate- and propionate-spiking, respectively. Before spiking with either butyrate or propionate, all the systems operated at an OLR of 4.0 gVS/L/d for three HRTs of 25 d to establish steady baselines (**Fig. S2**). The system's stability was assessed with pairwise t-tests on the selected indicators, and if no statistically significant differences ($p > 0.05$) were found between consecutive HRTs across all these indicators, the system was considered to have reached a steady state. Detailed measurements during these phases are provided in the supplementary material **Supplementary Material** (*Section S4* and **Figs. S2-S4**), showing stabilised methane yield, total VFA concentrations, and pH at 1395.2±145.0 mL/L/d, 822.13±323.5 mg/L, and 7.4±0.2, respectively. The intermediate alkalinity to partial alkalinity (IA:PA) ratio remained below 0.4, which was favourable for methanogens (Bai et al., 2025). This is in line with the microbial viability within the control group, which ranged between 91.7±4.0%.

3.2.1. System response to butyrate spiking

In the semi-continuous AD system with butyrate spiking, methane production (**Fig. 3a**) initially exhibited a modest improvement at lower spiked levels. At butyrate-spiking levels I (200 mg/L) and II (400 mg/L), methane production increased by 4.3% relative to the control, reaching an average of 1455.1±113.7 mL/L/d. During these stages, VFAs (**Figs. 3b** and **3c**) were rapidly consumed, indicating effective butyrate methanation, while no significant changes ($p > 0.05$) were observed across performance indicators, suggesting a steady-state operation.

At spiked level III (900 mg/L), the methane production remained stable, but hydrogen (**Fig. 3c**) and hydrogen sulphate (**Fig. 3d**) levels rose by 8.2±1.4% ($p < 0.05$) and 15.1±6.5% ($p < 0.001$), respectively. The IA:PA ratio (**Fig. 3f**) increased to 0.36±0.05, nearing the inhibition threshold of 0.4 (Bai et al., 2025), while microbial viability (**Fig. 3h**) dropped to 89.2±2.9% ($p < 0.001$). These shifts indicated emerging stress on the system, which became more pronounced at level IV (1200 mg/L), where methane production significantly declined by 10.5%, and VFA appeared to accumulate, with butyric acid reaching 127.9±22.1 mg/L. Notably, propionic acid concentrations (**Fig. 3c**) rose by 61.3% to 65.7±24.4 mg/L ($p<0.05$), signalling a shift towards a less energy-efficient propionate pathway (**Figs. 5d** and **S5**), while microbial viability further declined to 84.0±5.3%, suggesting a metabolic bottleneck within methanogenesis. Additionally, increased hydrogen sulphate and ammonium levels (**Fig. 3i**) (16.3% and 20.2% relative to the control, $p < 0.001$) suggested competitive activity from sulphate- and nitrogen-reducing bacteria (SRB and NRB), disrupting methanogenic efficiency (Giangeri et al., 2023).

At the final spiked level (1500 mg/L), methane production dropped further, with methane percentage decreasing from 48.1±2.3% (control) to 42.1±3.2%. The IA:PA ratio exceeded 0.4, pH fell below 7.0 (**Fig. 3g**), and microbial viability declined to 70.7%, marking conditions unfavourable for methanogens (Ali et al., 2019; Bai et al., 2025). VFA accumulation persisted, and hydrolysis was hindered, with total and volatile solids reaching 7.1% and 6.4%, respectively (compared to control levels of 4.5% and 3.2%).

During the recovery phase, the butyrate-spiked system began to alleviate the induced stress. Butyric acid levels declined while acetic acid increased, indicating a resumed acetogenesis. By the end of a four-day recovery, IA:PA returned to 0.34, pH rose to 7.19, and methane production increased from 987.3 to 1267.3 ml/L/d. Hydrogen levels stabilised at 112.8 ppm, indicating a recovery in methanogenic activity, particularly hydrogenotrophic methanogenesis, along with stabilised hydrolysis, as total and volatile solids settled at 5.5% and 5.1%, respectively.

3.2.2. Butyrate-spiking system response to nano magnetite pretreatment

In the semi-continuous AD system with MNP pretreatment, the response to butyrate spiking showed notable improvements over the butyrate-spiking system, particularly at lower spiked levels. At spiked levels I and II, both 20 nm and 50 nm MNPs enhanced butyrate methanation, increasing methane production (**Fig. 3a**) by 7.5% and 7.9%, respectively, compared to the butyrate-spiking system. The butyrate-spiking system presented a slight drop of 7.5% ($p < 0.05$) in hydrogen content at level II, while the MNP-amended system exhibited an increase in hydrogen levels (**Fig. 3d**), averaging 10.1% for the 50 nm MNP group and 18.7% for the 20 nm MNP group, indicating accelerated butyrate-to-acetate conversion and effective acetate methanation. VFA concentrations (**Figs. 3b** and **3c**) remained comparable to control, suggesting steady-state operation at these stages.

At spiked levels III and IV, methane production showed limited fluctuation, with hydrogen sulphide levels (**Fig. 3e**) being significantly lower than in the butyrate-spiking system, decreasing by 40.9% ($p < 0.001$) in the 50 nm MNP group and 46.3% ($p < 0.001$) in the 20 nm MNP group. Compared to the control, MNP-amended systems also maintained lower hydrogen sulphide concentrations by 33.8% ($p < 0.001$) and 39.6% ($p < 0.001$).

When dosed the butyric acid to the final concentration of 1500 mg/L, methane production decreased initially, reaching its lowest on the seventh

Please cite this article as: Zhu X., Blanco E., Bhatti M., Borrion A. Promoting methanogenesis and stability in anaerobic digestion with nano magnetite under VFA-induced stress. Biofuel Research Journal 46 (2025) 2432-2450. DOI: 10.18331/BRJ2025.12.2.5.

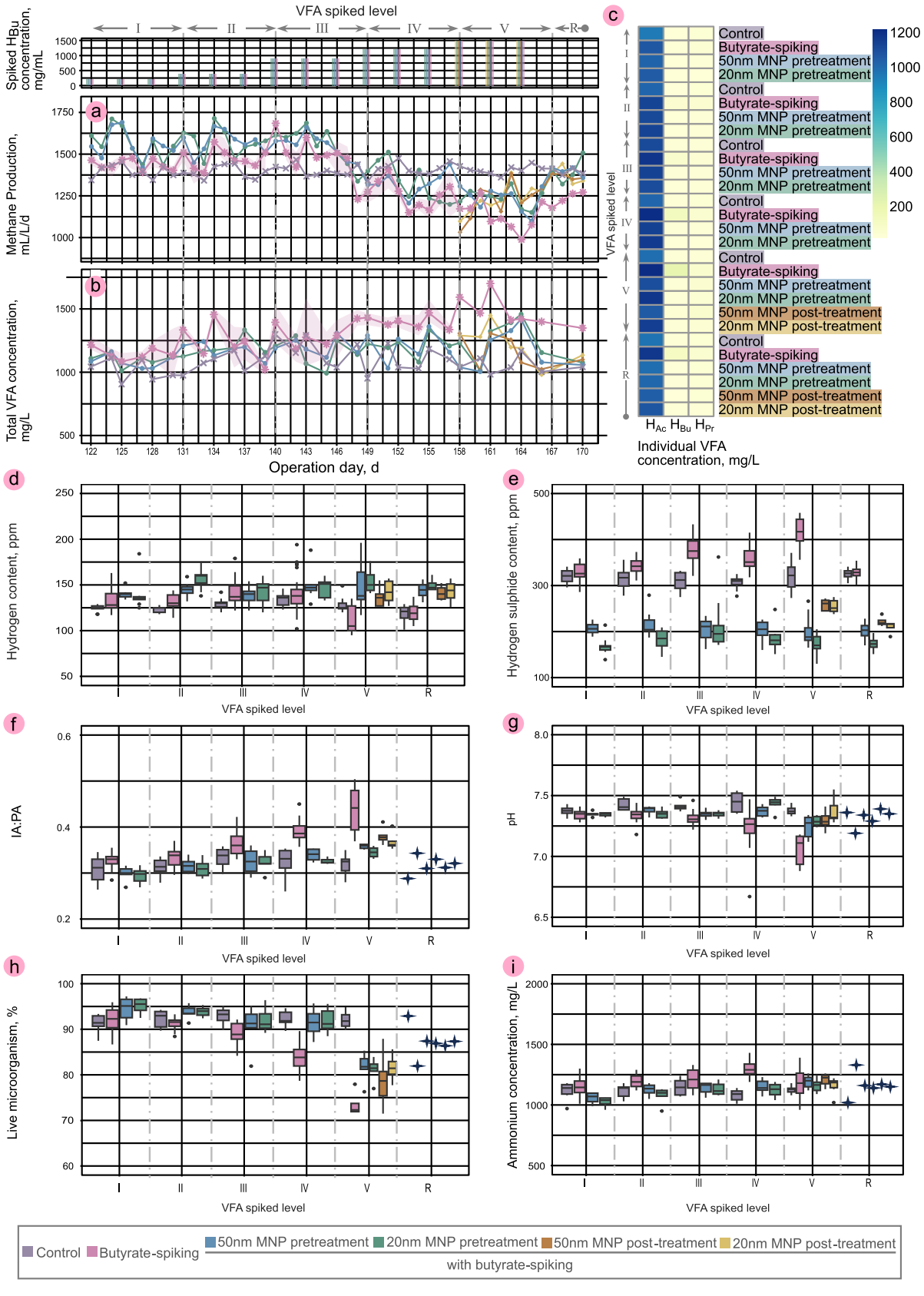

Fig. 3. System response to butyrate-induced stress with additions of MNPs, along with dosage concentrations of each spiked level. (**a**) Methane production; (**b**) Total VFA trends; (**c**) Heatmap represents the median concentration of each spiked level of three individual VFAs: H_{Ac} (acetate), H_{Bu} (butyrate); and H_{Pr} (propionate). Box plots summarise system performance during each spiked level (**d**) Hydrogen content; (**e**) Hydrogen sulphate concentrations; (**f**) IA:PA ratio; (**g**) pH; (**h**) Microbial viability; and (**i**) Ammonium concentration.

Please cite this article as: Zhu X., Blanco E., Bhatti M., Borrion A. Promoting methanogenesis and stability in anaerobic digestion with nano magnetite under VFA-induced stress. Biofuel Research Journal 46 (2025) 2432-2450. DOI: 10.18331/BRJ2025.12.2.5.

day (after the final dosing of this spiked level), but began to recover shortly after, along with a reduction in total VFA concentrations (**Fig. 3b**). No butyric acid accumulation was observed across the MNP-amended groups, suggesting effective acetogenesis and facilitated acetate conversion. Acetic acid concentrations remained low at 1077.3±263.7 mg/L, along with increased hydrogen production, possibly due to SRB activity using the reverse Wood-Ljungdahl pathway (see **Fig. 7**) that converts acetate into hydrogen and carbon (Ali et al., 2019; Bai et al., 2025).

Notably, throughout the spike-to-recovery test, hydrogen sulphate and ammonium levels (**Fig. 3i**) remained lower than in the butyrate-spiking system, suggesting that MNPs regulated the activities of both SRB and NRB, thus reducing competition with methanogens (Giangeri et al., 2023). Although the IA:PA ratio (**Fig. 3f**) and pH (**Fig. 3g**) remained within the optimal range for methanogens in the MNP-amended groups, methanogenesis was still limited by a capacity constraint. Additionally, the overall AD process, especially hydrolysis, slowed down under butyrate-induced stress, as indicated by the TS and VS contents in the MNP-amended groups, which were 40.0% and 65.6±6.2% higher than in control.

During the four-day recovery, methane production improved substantially in both MNP-amended groups, with the 20 nm group reaching 1507.7 mL/L/d and the 50 nm group reaching 1420.2 mL/L/d. Microbial viability increased to 86.9±0.6% in both groups, while acetic acid levels returned close to control. Moreover, hydrolysis recovered, with TS and VS contents averaging 5.3±0.2% and 4.4±0.1%, respectively, and the 20 nm MNP performed slightly better in stabilising these parameters.

3.2.3. Butyrate-spiking system response to nano magnetite post-treatment

In the MNP post-treatment groups, MNPs were introduced at the onset of spiked level V to simulate addition after butyrate-induced inhibition had been observed. Following MNP addition, methane production (**Fig. 3a**) rose from 1064.7±33.0 to 1386.1±6.7 mL/L/d, reaching 1412.6±29.9 mL/L/d by the end of the recovery phase. Total VFA concentrations (**Fig. 3b**) peaked after the second dose at spiked level V (1453.0±8.1 mg/L) but later declined to 997.1±16.9 mg/L, indicating improved methanogenesis. Compared to the butyrate-spiking system, hydrogen levels (**Fig. 3c**) in the MNP groups increased, with the 20 nm MNP group showing a 19.0% increase and the 50 nm group a 17.7% increase, suggesting enhanced hydrolysis. This was supported by lower TS and VS contents at the end of spiked level V, averaging 6.6±0.3% and 5.5±0.1%, respectively.

From spiked level V through recovery, butyric acid levels remained stable, while acetic acid concentrations fell by 7.0% and 11.6% in the 20 nm and 50 nm MNP groups, respectively (**Fig. 3c**). MNP addition also lowered the IA:PA ratio (**Fig. 3f**), hydrogen sulphide contents (**Fig. 3e**), and ammonium levels (**Fig. 3i**), creating a favourable environment for methanogens and reducing competition from SRB and NRB. Further reductions in TS and VS contents in recovery to 5.5±0.1% and 4.4%, respectively, indicate that MNP post-treatment effectively facilitated both methanogenesis and hydrolysis (**Figs. 7**, **S5**, and **S7a**), thus stabilising the AD system.

3.3. System response to propionate-spiking and different nano magnetite boosting strategies

Following the system's response to butyrate spiking, this section examines AD performance under stepwise propionate additions, which are typically more challenging to degrade within AD systems. The AD performance presented within this section, together with those in *Section 3.2*, provides critical context for the subsequent microbial and metabolic analyses. These results serve as a foundation for understanding how microbial function and gene activity contribute to system response and recovery under different VFA stresses and MNP supplementation conditions. To enhance reactor resilience under propionate stress, two MNP boosting strategies, using either 20 nm or 50 nm MNPs, were applied. These strategies mirrored those used in the butyrate-stressed systems. In the pretreatment groups, MNPs were added at the start of propionate spiking. In the post-treatment groups, MNPs were introduced during the initial three-day cycle at spiked level V after detecting propionic acid accumulation.

3.3.1. System response to propionate spiking

In the semi-continuous AD system response to propionate spiking, initial spiked levels I (100 mg/L) and II (200 mg/L) produced no significant fluctuations across all indicators (**Fig. 4**). At these lower concentrations, slight increases in acetic acid (8.0±0.3%, **Fig. 4c**) and hydrogen content (4.8±1.4%, $p < 0.05$, **Fig. 4d**) indicated effective propionate methanation, while hydrogen sulphide levels (**Fig. 4e**) showed modest increases relative to control values, 2.3% at the level I and 5.3% at the level II, suggesting limited competitive inhibition from SRBs.

At level III (300 mg/L), a 10.3% rise in hydrogen sulphide content was observed alongside a 3.8% increase in ammonium levels (**Fig. 4i**) relative to control. Methane production (**Fig. 4a**) began to decline after the second dosage of this level, although the system still supported propionate conversion to acetate, as indicated by slight increases in both hydrogen (6.6%) and acetic acid concentrations (7.9%). However, propionic acid (**Fig. 4c**) began accumulating within the system (4.8% increase from control), marking the start of metabolic stress.

With a further increase to level IV (400 mg/L), methanogenesis efficiency declined, especially after the final dosage at this concentration, as methane production dropped sharply and total VFA concentration (**Fig. 4b**) rose to 1616 mg/L. Hydrogen content stabilised, with no further increases from level III, while the IA:PA ratio surged to a range of 0.32 to 0.43, unfavourable for methanogenic activity. Microbial viability (**Fig. 4h**) correspondingly fell from 90.9±4.2% to 84.8±5.4% ($p < 0.001$). Compared to spiked level III, hydrogen sulphide and ammonium levels rose by 7.6% and 35.9% ($p < 0.001$), strengthening competition from SRB and NRB, resulting in a reduction of methane percentage from 48.1% to 39.5%.

At level V (500 mg/L), this trend continued, with methane production and microbial viability further declining as the total VFA concentration peaked at 1724 mg/L, reflecting severe stress within the system. The IA:PA ratio escalated to 0.44±0.06, while hydrogen content began to decrease, averaging 118.0 ppm. Although pH (**Fig. 4g**) remained above 7.0, maintaining an environment technically suitable for methanogenesis, hydrolysis was hindered, with TS and VS contents comparable to those observed in the butyrate-spiking system (7.0% and 6.4%, respectively).

During the recovery phase, in the absence of propionate spiking, the system gradually regained stability but at a slower pace compared to the butyrate-spiked system. This slower recovery was associated with a higher ORP of -268 mV in the propionate-stressed system by the end of the recovery phase, compared to -276 mV under butyrate-induced stress and -334 mV in the control. The increase in ORP suggested a potential metabolic shift within the propionate-stressed system toward the less energy-efficient propionate pathway, increasing energy demands and slowing the overall AD process (Sikora et al., 2019).

During the recovery phase, total VFA concentrations declined alongside propionate levels, IA:PA ratio decreased, along with rising acetic acid concentrations and increased hydrogen content, suggesting acetogenesis resumption. Methane concentration improved to 42.8%, though production remained within 1151.4 to 1084.7 mL/L/d. Although hydrogen sulphide (345.5±17.5 ppm) and ammonium (1350 mg/L) levels decreased, they remained unfavourable for methanogens (Sihlangu et al., 2024), indicating ongoing microbial competition.

3.3.2. Propionate-spiking system response to nano magnetite pretreatment

In the long-term propionate spike-to-recovery test, MNP pretreatment significantly improved system performance, along with limited fluctuations in pH and hydrogen sulphate observed within both MNP pretreatment systems. At levels I and II, both 20 nm and 50 nm MNPs enhanced propionate methanation, increasing methane production by 7.8% and 8.7% ($p < 0.001$, **Fig. 4a**), respectively, compared to the untreated propionate-spiking system. These improvements paralleled the enhancements observed in butyrate-spiking systems pretreated with MNPs, where MNPs facilitated butyrate-to-acetate conversion and effective methanogenesis. Similarly, slight increases in hydrogen content (averaged at 2.8±1.1%, **Fig. 4d**) further supported accelerated VFA conversion at lower spiked levels.

Methane production appeared to decline at spiked level III after the initial 300 mg/L dosage of propionic acid. However, the MNP-pretreated groups continued to surpass untreated systems, with methane production only 1.5%

Please cite this article as: Zhu X., Blanco E., Bhatti M., Borrion A. Promoting methanogenesis and stability in anaerobic digestion with nano magnetite under VFA-induced stress. Biofuel Research Journal 46 (2025) 2432-2450. DOI: 10.18331/BRJ2025.12.2.5.

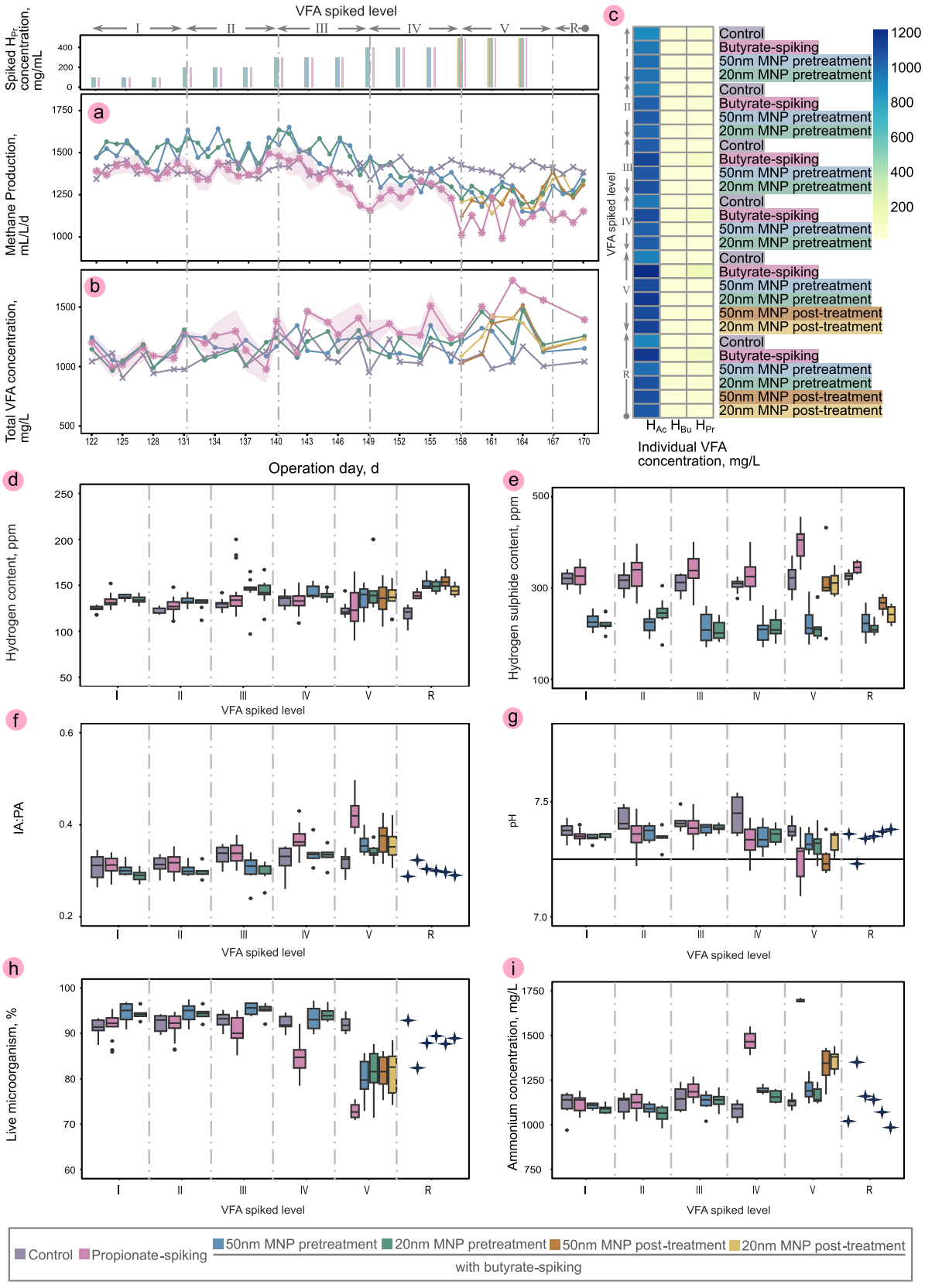

Fig. 4. System response to propionate-induced stress with additions of MNPs, along with dosage concentrations of each spiked level. (**a**) Methane production; (**b**) Total VFA trends; (**c**) Heatmap represents the median concentration of each spiked level of three individual VFAs: H_{Ac} (acetate), H_{Bu} (butyrate); and H_{Pr} (propionate). Box plots summarise system performance during each spiked level (**d**) Hydrogen content; (**e**) Hydrogen sulphate concentrations; (**f**) IA:PA ratio; (**g**) pH; (**h**) Microbial viability; and (**i**) Ammonium concentration.

Please cite this article as: Zhu X., Blanco E., Bhatti M., Borrion A. Promoting methanogenesis and stability in anaerobic digestion with nano magnetite under VFA-induced stress. Biofuel Research Journal 46 (2025) 2432-2450. DOI: 10.18331/BRJ2025.12.2.5.

below control levels but 11.1±0.8% higher than the propionate-spiking system without MNPs. IA:PA ratios (**Fig. 4f**) increased to 0.34 (20 nm MNP pretreatment group) and 0.32 (50 nm MNP pretreatment group), and ammonium concentrations (**Fig. 4i**) rose from 1090.0±45.5 mg/L to 1126.7±76.3 mg/L, suggesting a gradual increase in stress but sustained stability compared to untreated systems.

At level IV, methane production declined further but remained 8.1±0.4% higher than in untreated propionate-spiking groups. Total VFA accumulation (**Fig. 4b**) and limited fluctuations in hydrogen content indicated hindered methanogenesis, consistent with reduced microbial viability (<90%, **Fig. 4h**) and elevated ammonium concentrations (averaging 1176.7 mg/L). These patterns reflected the hindered pathway during VFA metabolism observed in both butyrate- and propionate-stressed systems, where MNPs mitigated but could not entirely overcome the inhibitory effects at higher stress levels.

By spiked level V, methane production dropped to 88.7±0.5% of control levels. While acetogenesis remained functional, as evidenced by low propionic acid and increasing acetic acid concentrations, methanogenesis was inhibited. The 20 nm MNP pretreatment group exhibited better performance, maintaining IA:PA ratios between 0.32–0.37 compared to 0.40 in the 50 nm MNP pretreatment group, which approached the inhibition threshold (Bai et al., 2025). Microbial viability followed a similar trend, averaging 81.3% for 20 nm MNPs and 80.1% for 50 nm MNPs.

During the recovery phase, methane production returned to control levels. Hydrogen content increased, IA:PA ratios dropped to 0.30, and hydrolysis resumed effectively, with TS and VS contents averaging 5.1% and 4.5%, respectively. These recovery trends were consistent with those observed in butyrate-spiking systems, demonstrating the ability of MNP pretreatment to stabilise AD processes under VFA-induced stress.

3.3.3. Propionate-spiking system response to nano magnetite post-treatment

The addition of MNPs significantly enhanced the recovery of AD systems under propionate stress. Methane production (**Fig. 4a**) increased from 1129.7±6.1 to 1307.1±1.3 mL/L/d within six days and further rose to 1374.55±8.0 mL/L/d by the end of the recovery phase. Total VFA concentrations (**Fig. 4b**) initially decreased following the final propionate dosage, reflecting effective VFA consumption before rising to 1230.5 mg/L, indicating efficient hydrolysis. Correspondingly, TS and VS contents decreased from 6.4±0.5% and 5.3±0.3% at spiked level V to 5.9±0.4% and 4.8±0.7%, respectively, during recovery, further confirming resumed hydrolytic activities (**Figs. 7** and **S7b**).

Hydrogen sulphide contents (**Fig. 4e**) and ammonium concentrations (**Fig. 4i**) were regulated to near-control levels after MNP addition, fostering a more optimal environment for methanogenesis and reducing competition from SRB and NRB. Notably, the 20 nm MNP group exhibited the lowest ammonium concentration of 985.6 mg/L by the recovery phase. Additionally, post-treatments with MNPs stabilised ORP at -311.0±2.6 mV by the end of the recovery phase, matching the MNP pretreatment system and contrasting with -264 mV in the untreated propionate-spiking system, suggesting a shift toward more energy-efficient acetate and butyrate metabolism pathways (**Figs. 7**, **S6** and **S7b**) (Sikora et al., 2019). These improvements were accompanied by increased hydrogen content (**Fig. 4c**), rising pH (**Fig. 4g**), and enhanced microbial viability (**Fig. 4h**), demonstrating that MNP post-treatment effectively supported methanogenesis, stabilised the AD system, and mitigated propionate-induced stress.

3.4. Microbial and metabolic responses to volatile fatty acid stress and mechanisms of nano magnetite mitigation

The AD process is governed by a complex network of microbial communities, each playing a vital role in system stability and performance. Earlier sections presented the methanogenic kinetics of butyrate and propionate degradation under different conditions (*Section 3.1*), followed by long-term system responses to stepwise VFA additions, with and without nano magnetite supplementation (*Sections 3.2* and *3.3*). To further understand these performance patterns, this section examines the microbial and metabolic mechanisms that support system recovery and resilience. *Section 3.4.1* compares microbial and functional responses across various stress scenarios, including feedstock overload and individual VFAs. Detailed performance data for overloaded and acetate-stressed systems with the same experimental setup were presented in a previous companion study (Zhu et al., 2025). *Section 3.4.2* assesses the impact of nano magnetite dosing strategies on microbial community structures, while *Section 3.4.3* explores how these changes influence key metabolic pathways.

3.4.1. Comparisons of microbial and metabolic responses across stress conditions

The microbial and metabolic responses to various stress conditions (feedstock overload, acetate, butyrate, and propionate) exhibited significant shifts in community structure and metabolic function (**Fig. 5**). Driven by hydrolytic bacteria such as *Treponema*, *Herbinix*, and *Ruminiclostridium* (**Fig. 5a**), feedstock overload enhanced microbial richness and diversity (**Fig. 5b**) (You et al., 2023). These bacteria are critical for carbohydrates, especially cellulose degradation, which supports efficient hydrolysis. Conversely, VFA stresses, particularly propionate, inhibited these bacteria, leading to reduced diversity and diminished hydrolytic activity, as confirmed by decreased cellulase activity. This limited hydrolysis under propionate stress resulted in incomplete cellulose breakdown, the primary carbon source in this study.

Acetogenic bacteria, such as *Syntrophomonadaceae* (butyrate-oxidising) and *Pelotomaculum* (propionate-oxidising), became more dominant in butyrate- and propionate-stressed systems, increasing from 1.2% to 3.8% and 0.5% to 3.3%, respectively (Liu and Lu, 2018). A similar enrichment was observed under feedstock overload, where these taxa reached 3.1%, suggesting a shift toward less energy-efficient VFA pathways under stress. Limited syntrophic acetate oxidation activity, particularly in propionate-stressed systems, further highlighted this shift.

Hydrogenotrophic methanogens, including *Methanoculleus* and *Methanosarcina*, predominated across all systems, highlighting their importance in maintaining methane production. Elevated OLR and VFA levels increased ROS-related gene expression (**Figs. 5c** and **S4c**), particularly *mdh*, associated with ROS generation and propionate metabolism (Lv et al., 2020; Yan et al., 2023). While PCA results could not directly confirm ROS toxicity, they highlighted metabolic responses to oxidative stress, with the highest ROS-related activity observed under feedstock overload, followed by propionate stress, then butyrate and acetate stress.

High VFA concentrations also correlated with elevated hydrogen sulphide and ammonium levels (**Figs. 5d** and **S4c**), suggesting potential competition between SRB and NRB with methanogens. This competition was further evidenced by the increased abundance of *Ruminiclostridium* across all stressed systems. Known for its role in cellulose fermentation, *Ruminiclostridium* produces lactate and succinate, which serve as substrates for SRB in a syntrophic relationship, where SRB consume lactate to generate hydrogen sulphide (Giangeri et al., 2023).

Additionally, propionate metabolism correlated strongly with residual solids (TS and VS), reflecting metabolic inefficiencies and the development of metabolic bottlenecks within the stressed systems. These inefficiencies were aggravated by elevated ORPs, which hindered AD processes by shifting the environment toward the less energy-efficient propionate metabolic pathway (Sikora et al., 2019). This interplay of microbial competition, substrate imbalance, and unfavourable environmental conditions highlights the challenges of maintaining methanogenesis efficiency under stress.

These findings align with the responses observed in butyrate- and propionate-stressed systems (*Subsections 3.2.1* and *3.2.2*), where VFA accumulation and microbial competition reduced methane yields and hydrolysis efficiency. Methanogens were particularly vulnerable to elevated hydrogen sulphide, ammonium, and VFAs, highlighting the critical need for intervention strategies to stabilise AD processes under VFA-induced stress.

3.4.2. Effects of nano magnetite-boosting strategies on butyrate- and propionate-stressed systems microbial community structures

The impacts of MNP treatments on microbial community structures varied over time and across stress conditions. Pretreatment groups consistently showed greater enhancements in microbial richness and diversity than post-treatment groups (**Figs. 6b** and **6f**). Community compositions in MNP-amended reactors shifted closer to those of the

Please cite this article as: Zhu X., Blanco E., Bhatti M., Borrion A. Promoting methanogenesis and stability in anaerobic digestion with nano magnetite under VFA-induced stress. Biofuel Research Journal 46 (2025) 2432-2450. DOI: 10.18331/BRJ2025.12.2.5.

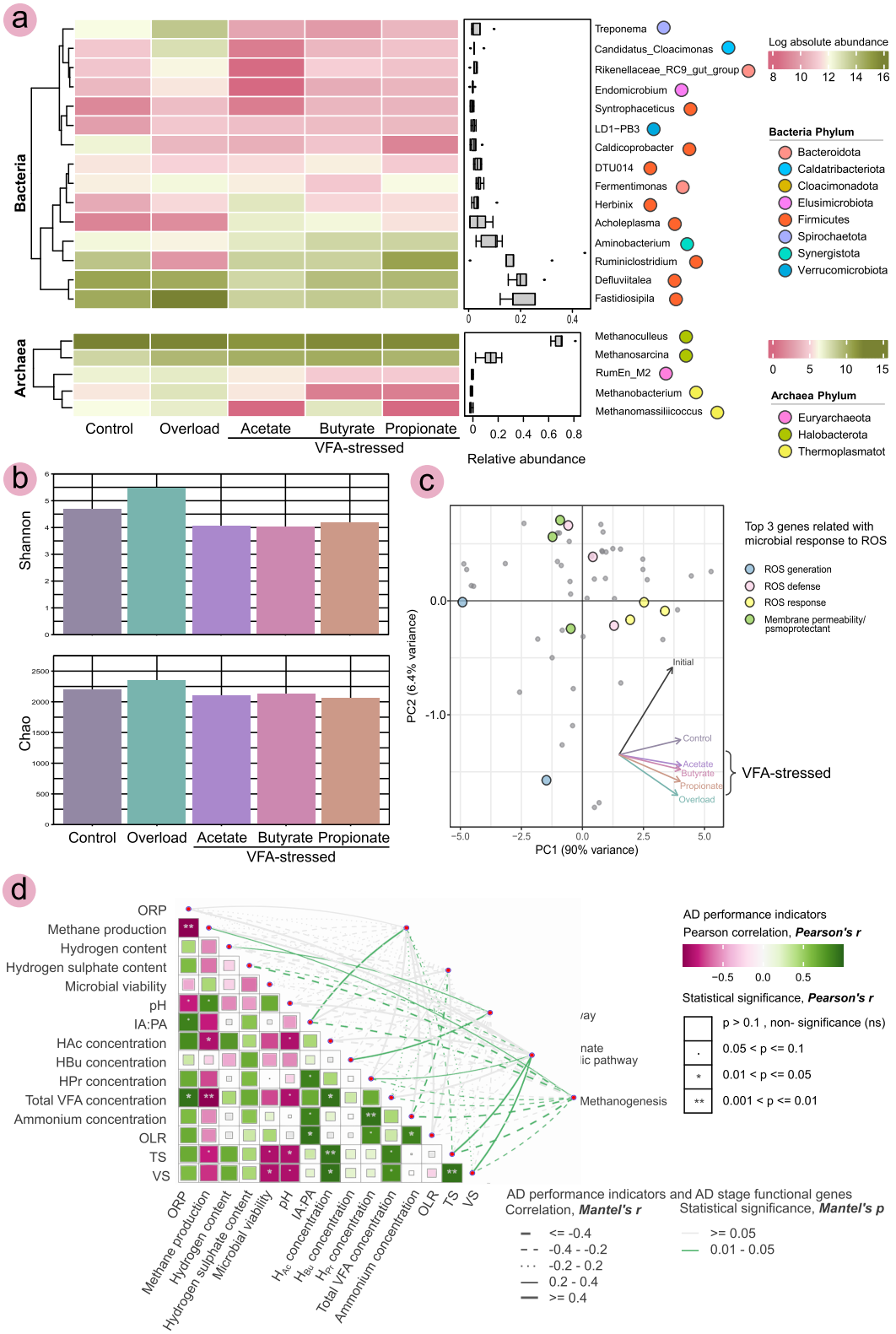

Fig. 5. Microbial and metabolic responses across various stress conditions. (**a**) Log-transformed absolute abundances of the dominant microbial genera, with bacterial relative abundance shown as a proportion of the total microbial community and archaeal relative abundance shown as a proportion of the archaeal community (box plots). (**b**) Alpha diversity metrics (Chao1 richness and Shannon diversity indices) across stress conditions, presenting microbial community diversity. (**c**) Principal component analysis (PCA) showing the first two principal components (96.4% cumulative variance) of the standardised matrix for microbial responses to ROS under different stress conditions, with sample "initial" collected at OLR of 3.5 g VS/L/d. Coloured circles highlight the top three genes linked to microbial ROS response. More details are presented in **Figure S8**. (**d**) Correlations between AD functional genes and key AD performance indicators across control and different stressed conditions. Pearson's correlations are shown with significance levels indicated, alongside Mantel's test results linking genes with AD stage functional processes. More details are presented in **Figures S5** and **S6**.

Please cite this article as: Zhu X., Blanco E., Bhatti M., Borrion A. Promoting methanogenesis and stability in anaerobic digestion with nano magnetite under VFA-induced stress. Biofuel Research Journal 46 (2025) 2432-2450. DOI: 10.18331/BRJ2025.12.2.5.

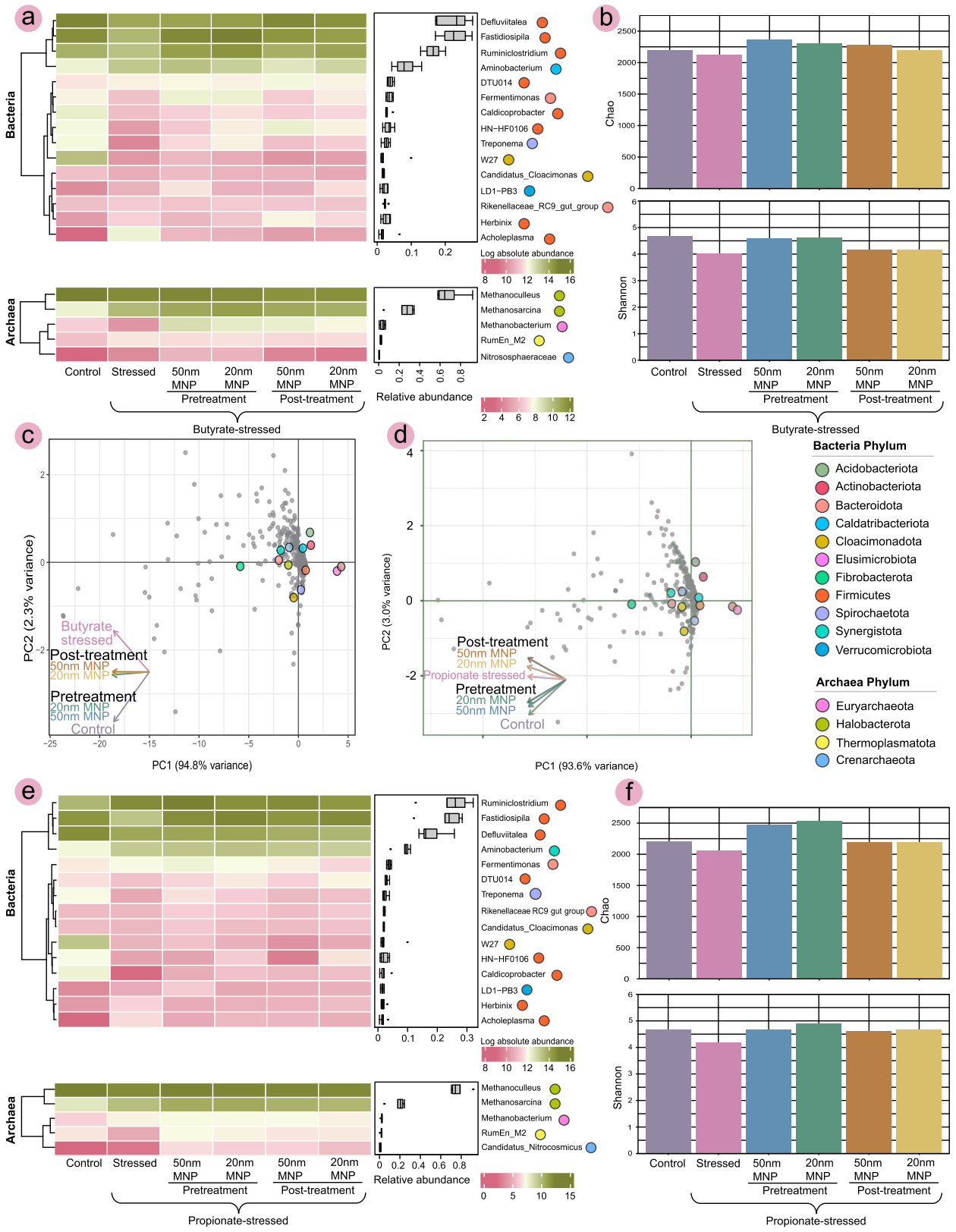

Fig. 6. Microbial responses across butyrate- (**a-c**) and propionate-stressed (**d-f**) conditions. (**a,e**) Log-transformed absolute abundances of the dominant microbial genera, with bacterial relative abundance shown as a proportion of the total microbial community and archaeal relative abundance shown as a proportion of the archaeal community (box plots). (**b,f**) Alpha diversity metrics (Chao1 richness and Shannon diversity indices) across stress conditions, presenting microbial community diversity. (**c,d**) PCA showing the first two principal components (97.1% and 96.6% cumulative variance, respectively for butyrate- and propionate-stressed systems) of the standardised matrix for microbial structures under different stress conditions. Coloured circles highlight the top ten bacterial phylum and top three archaea phylum.

Please cite this article as: Zhu X., Blanco E., Bhatti M., Borrion A. Promoting methanogenesis and stability in anaerobic digestion with nano magnetite under VFA-induced stress. Biofuel Research Journal 46 (2025) 2432-2450. DOI: 10.18331/BRJ2025.12.2.5.

control group, with the 20 nm pretreatment groups demonstrating the most similarity, followed by 50 nm pretreatment, 20 nm post-treatment, and 50 nm post-treatment groups (**Figs. 6c** and **6d**). This pattern was in line with long-term methane production results (*Section 3.2*), where the 20 nm MNP pretreatment group showed the highest improvements during dosage level V, increasing methane yields by 9.6% and 17.0% in butyrate- and propionate-stressed systems, respectively.

In butyrate-stressed systems, MNP pretreatment significantly enriched hydrolytic bacteria, including *Fastidiosipila*, *Ruminiclostridium*, and *Treponema* (**Fig. 6a**), which are involved in carbohydrate degradation (Bao et al., 2023; You et al., 2023). Similar trends were observed under propionate stress, though enhancements were less significant (**Fig. 6e**). Reductions in residual solids (TS and VS) across MNP-treated groups correlated with increased hydrolytic bacteria and iron-reducing bacteria, including *Ruminiclostridium*, which can degrade refractory organics while transferring extracellular electrons via type V pili to insoluble iron oxides (Peng et al., 2018; Zhang et al., 2019).

Two-step methanogenesis was required for both butyrate and propionate methanation. In butyrate-stressed systems, *Syntrophomonadaceae* increased from 1.2% to 3.4%, supporting butyrate methanation as evidenced by reduced butyric acid levels. Activated propionate metabolic pathways under butyrate stress led to increased *Pelotomaculum* (0.8% in MNP-treated systems compared to 2.2% in the untreated group). This indicates MNPs regulated propionate metabolism, reducing propionic acid levels in butyrate-stressed systems.

In propionate-stressed systems, *Pelotomaculum* remained at 0.5% in pretreatment groups but increased to 1.0% in post-treatment groups at the highest spiking level, suggesting enhanced propionate metabolism. However, higher remaining propionic acid levels in post-treatment groups indicated insufficient mitigation of propionate stress (**Figs. 6b** and **6c**). *Syntrophomonadaceae* increased to 2.7%, highlighting an enhanced butyrate metabolic pathway in MNP-treated propionate-stressed systems.

Methanogen populations, particularly hydrogenotrophic taxa including *Methanoculleus* and *Methanosarcina*, increased under MNP treatment. *Methanoculleus*, a DIET-associated methanogen, rose by 1.24–1.95 times, comprising 19.7–28.6% of the archaeal community (Holmes and Zhou, 2021). Other DIET-associated genera (*Geobacter*, *Pelotomaculum*, *Syntrophaceticus*) also increased by 10.3-92.5%, with the most significant enhancements in butyrate-stressed systems (Holmes and Zhou, 2021; Rotaru et al., 2022). These shifts aligned with improved methane production trends (*Sections 3.2* and *3.3*), supporting the hypothesis that MNPs enhanced syntrophic electron transfer.

MNPs act as electron conduits in AD systems by facilitating extracellular electron transfer between syntrophic bacteria and methanogens. This is achieved through the reversible cycling between Fe(II) and Fe(III) states within the magnetite structure, effectively serving as a redox-active bridge that enhances DIET (Wang et al., 2020). At the molecular level, this redox cycling supports microbial respiration by enabling continuous electron flow (Wang et al., 2020). The presence of conductive surfaces on magnetite has been shown to stimulate the expression of multiheme c-type cytochromes and type V pili, which are key components in microbial nanowire structures involved in DIET (Peng et al., 2018; Zhang et al., 2019). These conductive pathways bridge microbial partners, such as *Syntrophomonas* and *Methanothrix*, bypassing the need for interspecies hydrogen transfer and enhancing the thermodynamic favourability of syntrophic VFA degradation (Martins et al., 2019; Rotaru et al., 2022).

Moreover, the relative abundance of *Desulfovibrio*, a genus of SRB involved in hydrogen sulphide production during AD (Shu et al., 2025), decreased by an average of 42.9% in MNP-amended groups. This reduction aligned with observed decreases in hydrogen sulphide levels under both butyrate- and propionate-induced stress conditions. The most notable effect was observed in the 20 nm MNP pretreatment group under butyrate stress, where hydrogen sulphide concentrations dropped by 55.2% compared to the untreated butyrate-stressed system. These findings suggested that MNP treatments might induce a metabolic shift towards dissimilatory sulphate reduction pathways that are less competitive with methanogens (Giangeri et al., 2023), thereby enhancing methane production efficiency, with more details discussed in following *Section 3.4.3*.

3.4.3. Effects of nano magnetite-boosting strategies on butyrate- and propionate-stressed systems metabolic pathways

Evidence also supported that the addition of MNP enhanced the efficiency of metabolic pathways in AD systems under VFA-induced stress. Specifically, MNPs influenced methanogenesis at the biochemical level by modulating enzymatic activity and redox balance. Under stress conditions, the redox-buffering capacity of MNPs helped maintain lower ORPs, which were essential for the optimal activity of methanogenic enzymes such as hydrogenases and ferredoxin-linked oxidoreductases (Brabender et al., 2024). These enzymes facilitate electron flow during the conversion of acetate and hydrogen/carbon dioxide into methane. Furthermore, MNPs mitigated oxidative stress by transforming harmful ROS, such as hydroxyl radicals, into less reactive species (Kicheeva et al., 2023). This transformation thereby protected sensitive methanogens, including *Methanosarcina* and *Methanoculleus*, from oxidative stress. These combined effects enhanced both acetoclastic and hydrogenotrophic methanogenesis pathways. A schematic representation of these mechanistic roles is provided in **Figure 7** and **Figures S5–S6**.

Hydrolytic enzymatic activities increased by 16.2% and 7.0% in butyrate- and propionate-stressed systems, respectively, with the 50 nm MNP pretreatment groups exhibiting the greatest improvement. Pyruvate kinase, a key enzyme in converting monosaccharides to pyruvate, was more strongly inhibited in propionate-stressed systems (Sikora et al., 2019). MNP treatment mitigated this inhibition, which correlated with increased abundance of hydrolytic bacteria and improved degradation of particulate organic nitrogen.

Although enzymes involved in acetate and butyrate metabolic pathways did not increase significantly, MNPs regulated VFA levels and prevented their excessive accumulation. This suggested that MNPs enhanced DIET (**Fig. S9**), enabling faster electron flow between syntrophic partners (Zhang et al., 2019). DIET improved VFA consumption rates, maintained stable pH, and prevented acidification. It also mitigated ammonia inhibition by strengthening syntrophic interactions (Yan et al., 2020) and bypassing the use of hydrogen as an intermediate electron carrier, thus improving energy efficiency and microbial stability.

Moreover, MNPs stimulated the expression of functional genes and enzymes involved in nitrogen and sulphate reduction (**Figs. S5** and **S6**). The *acs* gene, linked to acetate metabolism, increased 1.4–3.9 times in treated groups of methanogens (Giangeri et al., 2023). Enhanced dissimilatory sulphate reduction, coupled with DIET, offered alternative electron sinks and alleviated typical bottlenecks under VFA stress. Enrichment of genes associated with dissimilatory sulphate reduction and the reverse Wood-Ljungdahl pathway enabled SRB to oxidise acetate into H_2 and CO_2, supporting syntrophic energy conservation and improving methanation efficiency (Giangeri et al., 2023).

The presence of Feammox (ammonium oxidation coupled to ferric iron reduction) in MNP-amended systems accelerated nitrogen removal, contributing to the stabilisation of the AD process and enhancing system resilience under VFA-induced stress (Tan et al., 2022). MNPs also influenced the ORP of the systems, creating a more reductive environment with values ranging from -316 to -309 mV. This shift contrasts with the higher ORP observed in untreated systems (-276 mV in butyrate-stressed and -268 mV in propionate-stressed reactors) and favoured methanogenic activity (Ao et al., 2021). By limiting the activity of propionate pathway enzymes under VFA stress, MNPs accelerated VFA methanation and mitigated metabolic bottlenecks. The reductive environment also regulated ROS generation (**Fig. S8**), thus enriching the activities of acetolactic methanogens (**Figs. S5** and **S6**) and helping the systems overcome oxidative stress induced by elevated VFAs. Moreover, MNP supplements upregulated genes involved in ROS response, particularly those linked to Fe-S cluster biosynthesis and repair. These Fe-S clusters are critical cofactors for key methanogenic enzymes, enabling enhanced methanogenesis efficiency, cell membrane integrity, and system resilience (Martins et al., 2019; Yang et al., 2019; Yan et al., 2023).

3.5. Implications

This study provides critical insights into the key factors affecting AD performance under VFA-induced stress and highlights the applications of MNPs as an effective mitigation strategy. The concentrations of butyric and

Please cite this article as: Zhu X., Blanco E., Bhatti M., Borrion A. Promoting methanogenesis and stability in anaerobic digestion with nano magnetite under VFA-induced stress. Biofuel Research Journal 46 (2025) 2432-2450. DOI: 10.18331/BRJ2025.12.2.5.

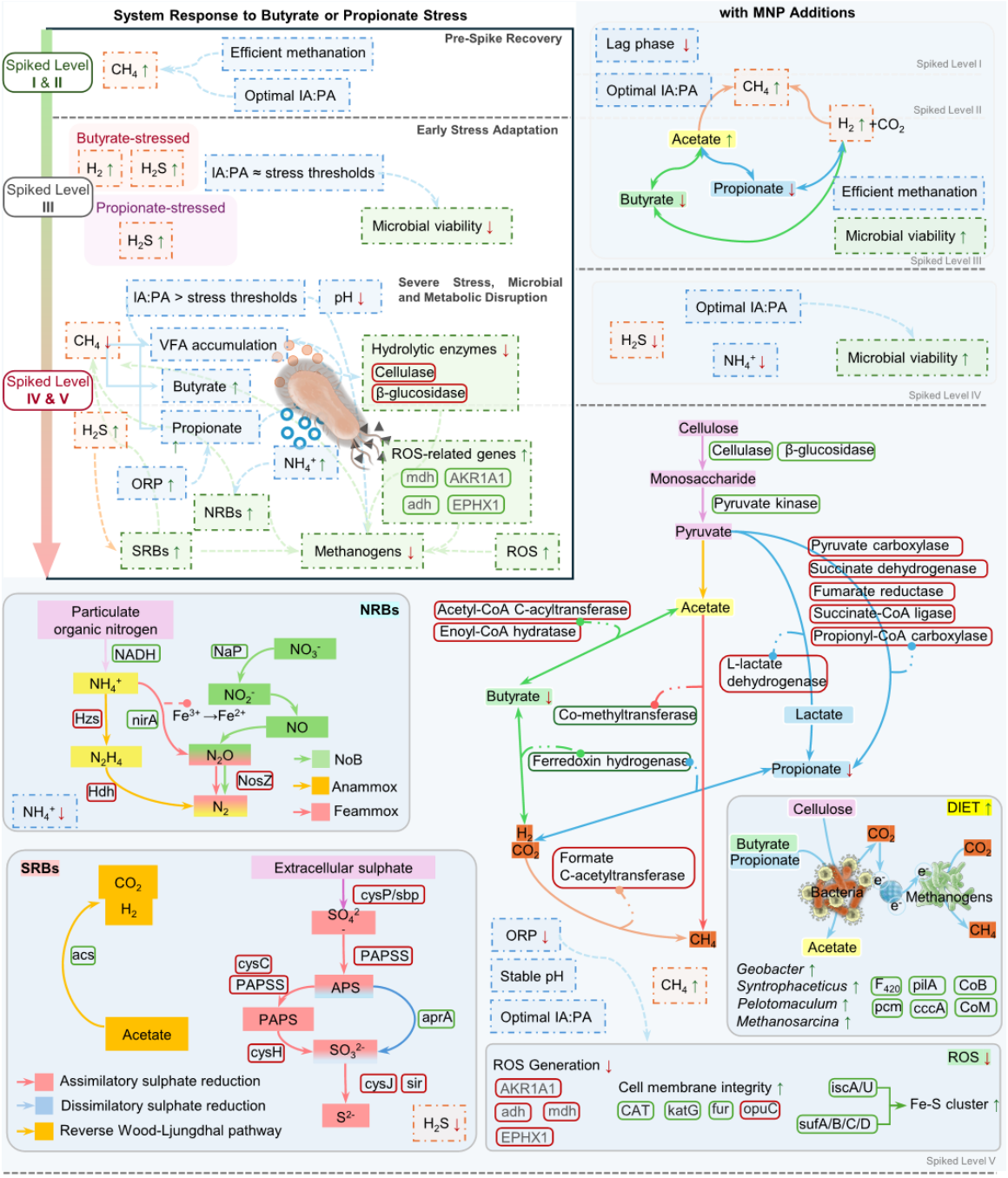

Fig. 7. Proposed mechanisms behind mitigation of butyrate and propionate stress by MNPs. The metabolic pathways are detailed in Figures S5 and S6, ROS-related enzyme activities in Figure S8, DIET-associated functional genes in Figure S9, and correlations between AD performance indicators and metabolic pathways via Mantel tests in Figure S7, the interplay between SRB, NRB, and methanogens under VFA-induced stress are presented in Figures S5 and S6.

Please cite this article as: Zhu X., Blanco E., Bhatti M., Borrion A. Promoting methanogenesis and stability in anaerobic digestion with nano magnetite under VFA-induced stress. Biofuel Research Journal 46 (2025) 2432-2450. DOI: 10.18331/BRJ2025.12.2.5.

propionic acids were shown to be reliable indicators of stress. Specifically, maintaining butyric acid below 900 mg/L and propionic acid below 300 mg/L (dosage level III) was essential to avoid metabolic bottlenecks in methanogenesis. These thresholds can serve as early warning indicators to ensure stable AD system operation and optimise methane recovery.

MNP treatments offer dual advantages depending on the application strategy. Post-treatment with MNPs enabled rapid recovery from VFA-induced stress by accelerating the methanation of accumulated VFAs, making it a promising option for addressing acute stress scenarios in AD systems. Meanwhile, pretreatment with MNPs provided a more stable microbial community structure, similar to that of the unstressed-control system. These strategies are particularly suitable for AD systems processing substrates that lead to rapid VFA accumulation, such as food waste and livestock manure (Khatami et al., 2021; Yin et al., 2022). In this study, methanation kinetics were initially assessed using batch assays; the same MNP and VFA concentrations were applied in semi-continuous experiments to simulate operational performance under sustained stress. This approach bridges controlled lab-scale testing with practical application in real-world AD systems.

The economic and environmental evaluations (**Table S7**) suggest that MNP use could significantly enhance the viability of industrial-scale AD plants treating cellulose-rich waste, such as municipal solid waste or agricultural residues (Van et al., 2020). Under stress conditions, MNP dosages improved methane production, increasing revenue from electricity generation by 8.8-12.8% while also reducing carbon dioxide emissions due to enhanced methane recovery. Moreover, smaller MNPs with 20 nm diameters presented better performance compared to 50 nm MNPs, achieving higher solid reduction rates, which further decreased slurry output and associated disposal costs. These findings indicate that MNP treatments not only enhance the economic viability of AD systems by increasing energy recovery but also contribute to environmental sustainability by minimising greenhouse gas emissions and waste outputs.

Although the MNP concentrations used in this study were far below the levels known to pose environmental risks (Thu et al., 2023), the long-term effects of low-concentration MNP exposure on ecosystems remain poorly understood. Owing to their high stability under environmental conditions, MNPs can persist and accumulate in ecosystems, potentially leading to adverse effects on soil microbial activity, plant growth, and aquatic life. For instance, studies have shown that MNPs can disrupt microbial enzymatic activities and hinder the synthesis of bioactive molecules, thereby affecting essential ecological processes (Klekotka et al., 2021; Yang et al., 2025). Moreover, the interaction of MNPs with beneficial microorganisms may lead to alterations in microbial community structures (Bondarenko et al., 2020), impacting nutrient cycling and soil fertility (Yamini et al., 2023). Given these potential risks, it is crucial to assess the fate and transport of MNPs in natural environments. Future research should also focus on developing strategies for the recovery and reuse of MNPs, such as magnetic separation techniques, to minimise their environmental footprint. Implementing closed-loop systems for MNP management aligns with circular economy principles and ensures the sustainable application of nanotechnology in waste treatment processes.

4. Conclusions

This study demonstrated the potential of MNPs as a mitigation strategy against VFA-induced stress in AD systems. MNPs facilitated a more balanced progression through hydrolysis, acetogenesis, and methanogenesis by enhancing enzymatic activity, regulating redox potential, and mitigating oxidative stress. These effects led to improved microbial viability and diversity, reduced VFA accumulation, and enhanced system stability. In both butyrate- and propionate-stressed systems, the addition of MNPs facilitated functional gene enrichment and metabolic adjustments, including enhanced sulphate and nitrogen reduction through dissimilatory sulphate reduction, the reverse Wood-Ljungdahl pathway, and Feammox processes.

Moreover, MNPs significantly enhanced DIET, promoting more efficient electron flow between syntrophic partners through improved microbial nanowire formation, upregulated multiheme cytochromes, and stable redox cycling. These changes mitigated microbial competition and supported efficient methanation of accumulated VFAs, indicating the ability of MNPs to resolve bottlenecks in methanogenesis. As a result, methane production improved by up to 8.7% in propionate-stressed systems and 7.9% in butyrate-stressed systems, highlighting the efficacy of MNP supplementation in reinforcing AD system resilience and energy recovery under adverse conditions.

Based on these findings, this study proposes practical recommendations for industrial-scale AD systems, particularly those treating cellulose-rich substrates such as municipal solid waste or agricultural residues. Maintaining butyric acid and propionic acid concentrations below 900 mg/L and 300 mg/L, respectively, is crucial to prevent metabolic inhibition. MNP post-treatment proved highly effective for rapid methanation of accumulated VFAs, making it suitable for acute stress scenarios. In contrast, pretreatment with MNPs enhanced long-term microbial stability and community resilience. Both strategies improved methane yields and solid degradation rates while reducing operational risks and costs. The scale-up assessment of this study indicated that MNP supplementation could increase electricity revenue by 8.8–12.8% and reduce carbon dioxide emissions through enhanced methane recovery. Smaller MNPs (20 nm) achieved better results, improving solid reduction and reducing disposal volumes and costs. These dual economic and environmental benefits suggest that MNPs hold promise for practical implementation in real-world AD operations. However, this study also faces several limitations. The use of a synthetic cellulose-rich feedstock, while simulating real-world waste, may not fully capture the complexities of heterogeneous organic waste streams. Additionally, while semi-continuous experiments better represent operational conditions than batch tests, full-scale continuous reactors would offer deeper insights into performance under dynamic loading and longer retention times.

The long-term environmental fate of MNPs also remains a concern. Although used concentrations (≤100 mg/L) were within safe limits, the potential accumulation and ecotoxicological effects of MNPs in natural systems warrant caution. As mentioned earlier, persistent MNPs could disrupt microbial ecology, affect nutrient cycles, or accumulate in aquatic and terrestrial environments. Future research should, therefore, explore advanced recovery methods, such as magnetic separation, to enable MNP reuse and reduce environmental impact. Comprehensive life cycle assessments and environmental risk evaluations are also essential to ensure the sustainable integration of MNPs into circular waste management systems.

In conclusion, this study lays a foundation for advancing AD process optimisation under stress conditions and sets the stage for future work focused on scaling, long-term monitoring, environmental safety, and recovery of nanomaterials in bioenergy systems.

References

[1] Ali, S., Hua, B., Huang, J.J., Droste, R.L., Zhou, Q., Zhao, W., Chen, L., 2019. Effect of different initial low pH conditions on biogas production, composition, and shift in the aceticlastic methanogenic population. Bioresour. Technol. 289, 121579.

[2] Andrade, M.F.C., Parussulo, A.L.A., Netto, C.G.C.M., Andrade, L.H., Toma, H.E., 2016. Lipase immobilized on polydopamine-coated magnetite nanoparticles for biodiesel production from soybean oil. Biofuel Res. J. 3(2), 403-409.

[3] Ao, T., Chen, L., Zhou, P., Liu, X., Li, D., 2021. The role of oxidation-reduction potential as an early warning indicator, and a microbial instability mechanism in a pilot-scale anaerobic mesophilic digestion of chicken manure. Renewable Energy 179, 223-232.

[4] APHA, 2012. Standard methods for the examination of water and wastewater. American Public Health Association, American Water Works Association, Water Pollution Control Federation, Washington DC.

[5] Augustine, R., Hasan, A., Primavera, R., Joyce, R., Thakor, A.S., Kevadiya, B.D., 2020. Cellular uptake and retention of nanoparticles: insights on particle properties and interaction with cellular components. Mater. Today Commun. 25, 101692.

[6] Bai, X., Rebosura, M.J., Jensen, P.D., 2025. Enhanced anaerobic digestion of lignocellulosic paunch waste using potassium hydroxide pre-treatment. Bioresour. Technol. 425, 132323.

[7] Bao, R., Wei, Y., Guan, R., Li, X., Lu, X., Rong, S., Zuo, X., Yuan, H., 2023. High-solids anaerobic co-digestion performances and microbial community dynamics in co-digestion of different mixing ratios with food waste and highland barley straw. Energy. 262(Part B),

Please cite this article as: Zhu X., Blanco E., Bhatti M., Borrion A. Promoting methanogenesis and stability in anaerobic digestion with nano magnetite under VFA-induced stress. Biofuel Research Journal 46 (2025) 2432-2450. DOI: 10.18331/BRJ2025.12.2.5.

125529.
[8] Barrena, R., Vargas-García, M. del C., Catacora-Padilla, P., Gea, T., Abo Markeb, A., Moral-Vico, J., Sánchez, A., Font, X., Aspray, T.J., 2023. Magnetite-based nanoparticles and nanocomposites for recovery of overloaded anaerobic digesters. Bioresour. Technol. 372, 128632.
[9] Bondarenko, L.S., Kovel, E.S., Kydralieva, K.A., Dzhardimalieva, G.I., Illés, E., Tombácz, E., Kicheeva, A.G., Kudryasheva, N.S., 2020. Effects of modified magnetite nanoparticles on bacterial cells and enzyme reactions. Nanomaterials. 10(8), 1499.
[10] Boyle, W.C., 1977. Energy recovery from sanitary landfills - a review. Microb. Energy Convers. 1977, 119-138.
[11] Brabender, M., Henriques, D.P., Mrnjavac, N., Laura, M., Kleinermanns, K., Tüysüz, H., Buckel, W., Martin, W.F., 2024. Ferredoxin reduction by hydrogen with iron functions as an evolutionary precursor of flavin- based electron bifurcation. Proc. Natl. Acad. Sci. 121(13), e2318969121.
[12] Campanaro, S., Treu, L., Kougias, P.G., Zhu, X., Angelidaki, I., 2018. Taxonomy of anaerobic digestion microbiome reveals biases associated with the applied high throughput sequencing strategies. Sci. Rep. 8(1), 1926.
[13] Chen, Q., Liu, C., Liu, X., Sun, D., Li, P., Qiu, B., Dang, Y., Karpinski, N.A., Smith, J.A., Holmes, D.E., 2020. Magnetite enhances anaerobic digestion of high salinity organic wastewater. Environ. Res. 189, 109884.
[14] Dogan, T., Ince, O., Oz, N.A., Ince, B.K., 2005. Inhibition of volatile fatty acid production in granular sludge from a UASB reactor. J. Environ. Sci. Health., Part A. 40(3), 633-644.
[15] Fan, Y.Y., Tang, Q., Li, Y., Sun, H., Xu, M., Yu, H.Q., 2024. Fabricating an advanced electrogenic chassis by activating microbial metabolism and fine-tuning extracellular electron transfer. Trends Biotechnol. 43(2), 383-407.
[16] Gahlot, P., Ahmed, B., Tiwari, S.B., Aryal, N., Khursheed, A., Kazmi, A.A., Tyagi, V.K., 2020. Conductive material engineered direct interspecies electron transfer (DIET) in anaerobic digestion: mechanism and application. Environ. Technol. Innovation. 20, 101056.
[17] Giangeri, G., Tsapekos, P., Gaspari, M., Ghofrani-Isfahani, P., Lin, M.K.T.H., Treu, L., Kougias, P., Campanaro, S., Angelidaki, I., 2023. Magnetite alters the metabolic interaction between methanogens and sulfate-reducing bacteria. Environ. Sci. Technol. 57(43), 16399-16413.
[18] Guan, Q., Qu, Y., Zhai, Y., Shi, W., Zhao, M., Huang, Z., Ruan, W., 2023. Enhancement of methane production in anaerobic digestion of high salinity organic wastewater: the synergistic effect of nano-magnetite and potassium ions. Chemosphere. 318, 137974.
[19] Guo, W.B., Wu, C., Yang, L., Pan, K., Miao, A.J., 2022. Nanoparticle pre- or co-exposure affects bacterial ingestion by the protozoan *Tetrahymena thermophila*. J. Hazard. Mater. 429, 128268.
[20] Hansen, J.C., Aanderud, Z.T., Reid, L.E., Bateman, C., Hansen, C.L., Rogers, L.S., Hansen, L.D., 2021. Enhancing waste degradation and biogas production by pre-digestion with a hyperthermophilic anaerobic bacterium. Biofuel Res. J. 8(3), 1433-1443.
[21] Holmes, D.E., Zhou, J., 2021. Mechanisms for Electron Uptake by *Methanosarcina acetivorans* during direct interspecies electron transfer. MBio 12(5).
[22] IEA, 2020. Outlook for biogas and biomethane. IEA, Paris.
[23] Isci, A., Demirer, G.N., 2007. Biogas production potential from cotton wastes. Renew. Energy. 32(5), 750-757.
[24] Jin, Y., Lu, Y., 2023. Syntrophic propionate oxidation: one of the rate-limiting steps of organic matter decomposition in anoxic environments. Appl. Environ. Microbiol. 89(5).
[25] Jung, H., Yu, H., Lee, C., 2023. Direct interspecies electron transfer enables anaerobic oxidation of sulfide to elemental sulfur coupled with CO2-reducing methanogenesis. iScience. 26(9), 107504.
[26] Khatami, K., Atasoy, M., Ludtke, M., Baresel, C., Eyice, Ö., Cetecioglu, Z., 2021. Bioconversion of food waste to volatile fatty acids: impact of microbial community, pH and retention time. Chemosphere. 275, 129981.
[27] Kicheeva, A.G., Sushko, E.S., Bondarenko, L.S., Kydralieva, K.A., Pankratov, D.A., Tropskaya, N.S., Dzeranov, A.A., Dzhardimalieva, G.I., Zarrelli, M., Kudryasheva, N.S., 2023. Functionalized magnetite nanoparticles: characterization, bioeffects, and role of reactive oxygen species in unicellular and enzymatic systems. Int. J. Mol. Sci. 24(2), 1133.
[28] Kim, M., Jung, S., Kang, S., Rhie, M.N., Song, M., Shin, J., Shin, S.G., Lee, J., 2024. Magnetite particles accelerate methanogenic degradation of highly concentrated acetic acid in anaerobic digestion process. Environ. Res. 255, 119132.
[29] Klekotka, U., Zambrzycka-Szelewa, E., Satuła, D., Kalska-Szostko, B., 2021. Stability studies of magnetite nanoparticles in environmental solutions. Materials. 14(17), 5069.
[30] Li, J., Chen, T., Yin, J., Shen, D., 2021. Effect of nano-magnetite on the propionic acid degradation in anaerobic digestion system with acclimated sludge. Bioresour. Technol. 334, 125143.
[31] Li, Q., Liu, Y., Yang, X., Zhang, J., Lu, B., Chen, R., 2020. Kinetic and thermodynamic effects of temperature on methanogenic degradation of acetate, propionate, butyrate and valerate. Chem. Eng. J. 396(13), 125366.
[32] Liu, P., Lu, Y., 2018. Concerted metabolic shifts give new insights into the syntrophic mechanism between propionate-fermenting *Pelotomaculum thermopropionicum* and hydrogenotrophic *Methanocella conradii*. Front. Energy Res. 9, 1–15.
[33] Lv, N., Zhao, L., Wang, R., Ning, J., Pan, X., Li, C., Cai, G., 2020. Novel strategy for relieving acid accumulation by enriching syntrophic associations of syntrophic fatty acid-oxidation bacteria and H_2/formate- scavenging methanogens in anaerobic digestion. Bioresour. Technol. 313, 123702.
[34] Martins, M.C., Romão, C. V., Folgosa, F., Borges, P.T., Frazão, C., Teixeira, M., 2019. How superoxide reductases and flavodiiron proteins combat oxidative stress in anaerobes. Free Radical Biol. Med. 140, 36-60.
[35] Mashkour, M., Rahimnejad, M., Raouf, F., Navidjouy, N., 2021. A review on the application of nanomaterials in improving microbial fuel cells. Biofuel Res. J. 8(2), 1400-1416.
[36] Morita, M., Malvankar, N.S., Franks, A.E., Summers, Z.M., Giloteaux, L., Rotaru, A.E., Rotaru, C., Lovleya, D.R., 2011. Potential for direct interspecies electron transfer in methanogenic wastewater digester aggregates. MBio. 2(4), 5-7.
[37] Peng, H., Zhang, Y., Tan, D., Zhao, Z., Zhao, H., Quan, X., 2018. Roles of magnetite and granular activated carbon in improvement of anaerobic sludge digestion. Bioresour. Technol. 249, 666-672.
[38] Rotaru, A., Paquete, C.M., Rosenbaum, M.A., Ba, L., 2022. Let's chat: communication between electroactive microorganisms. Bioresour. Technol. 347, 126705.
[39] Shu, W., Du, B., Wu, G., 2025. Strategies for enriching targeted sulfate-reducing bacteria and revealing their microbial interactions in anaerobic digestion ecosystems. Water Res. 270, 122842.
[40] Sihlangu, E., Luseba, D., Regnier, T., Magama, P., Chiyanzu, I., Nephawe, K.A., 2024. Investigating methane, carbon dioxide, ammonia, and hydrogen sulphide content in agricultural waste during biogas production. Sustainability. 16(12), 5145.
[41] Sikora, A., Detman, A., Mielecki, D., Chojnacka, A., Błaszczyk, M., 2019. Searching for metabolic pathways of anaerobic digestion: a useful list of the key enzymes. Anaerobic Digestion. pp. 1-19.
[42] Su, Y., Chen, Y., Wu, J., 2021. Methane production from propionate enhanced by Met@Fe_3O_4via increasing microbe-material attachment in a direct interspecies electron-transfer process. ACS Sustainable Chem. Eng. 9(1), 471-480.
[43] Subbarao, P.M.V., D' Silva, T.C., Adlak, K., Kumar, S., Chandra, R., Vijay, V.K., 2023. Anaerobic digestion as a sustainable technology for efficiently utilizing biomass in the context of carbon neutrality and circular economy. Environ. Res. 234, 116286.
[44] Tan, X., Xie, G., Nie, W., Xing, D., Liu, B., Ding, J., Ren, N., 2022. Fe(III)-mediated anaerobic ammonium oxidation: a novel microbial nitrogen cycle pathway and potential applications. Crit. Rev. Environ. Sci. Technol. 52(16), 2962-2994.
[45] Thu, H.E., Haider, M.A., Khan, S., Sohail, M., Hussain, Z., 2023. Nanotoxicity induced by nanomaterials: a review of factors affecting nanotoxicity and possible adaptations. OpenNano. 14, 100190.
[46] USEPA, 1983. Methods for chemical analysis of water and wastes, United States Environmental Protection Agency, Office of Research

Please cite this article as: Zhu X., Blanco E., Bhatti M., Borrion A. Promoting methanogenesis and stability in anaerobic digestion with nano magnetite under VFA-induced stress. Biofuel Research Journal 46 (2025) 2432-2450. DOI: 10.18331/BRJ2025.12.2.5.

and Development. Cincinnati, Ohio.
[47] Van, D.P., Fujiwara, T., Tho, B.L., Toan, P.P.S., Minh, G.H., 2020. A review of anaerobic digestion systems for biodegradable waste: Configurations, operating parameters, and current trends. Environ. Eng. Res. 25(1), 1-17.
[48] Wang, H., Byrne, J.M., Liu, P., Liu, J., Dong, X., Lu, Y., 2020. Brief report Redox cycling of Fe(II) and Fe(III) in magnetite accelerates aceticlastic methanogenesis by Methanosarcina mazei. Environ. Microbiol. Rep. 12(1), 97-109.
[49] Wang, Y., Zhang, Y., Wang, J., Meng, L., 2009. Effects of volatile fatty acid concentrations on methane yield and methanogenic bacteria. Biomass. Bioenergy. 33(5), 848-853.
[50] Westerholm, M., Calusinska, M., Dolfing, J., 2022. Syntrophic propionate-oxidizing bacteria in methanogenic systems. FEMS Microbiol. Rev. 46(2), fuab057.
[51] Wu, D., Li, L., Zhen, F., Liu, H., Xiao, F., Sun, Y., Peng, X., Li, Y., Wang, X., 2022. Thermodynamics of volatile fatty acid degradation during anaerobic digestion under organic overload stress: the potential to better identify process stability. Water Res. 214(2), 118187.
[52] Yamini, V., Shanmugam, V., Rameshpathy, M., Venkatraman, G., Ramanathan, G., AL Garalleh, H., Hashmi, A., Brindhadevi, K., Devi Rajeswari, V., 2023. Environmental effects and interaction of nanoparticles on beneficial soil and aquatic microorganisms. Environ. Res. 236(Part 1), 116776.
[53] Yan, M., Hu, Z., Duan, Z., Sun, Y., Dong, T., Sun, X., Zhen, F., Li, Y., 2023. Microbiome re-assembly boosts anaerobic digestion under volatile fatty acid inhibition: focusing on reactive oxygen species metabolism. Water Res. 246, 120711.
[54] Yan, W., Mukherjee, M., Zhou, Y., 2020. Direct interspecies electron transfer (DIET) can be suppressed under ammonia-stressed condition-reevaluate the role of conductive materials. Water Res. 183, 116094.
[55] Yang, H., Liu, L., Shu, Z., Zhang, W., Huang, C., Zhu, Y., Li, S., Wang, W., Li, G., Zhang, Q., Liu, Q., Jiang, G., 2025. Magnetic iron oxide nanoparticles: An emerging threat for the environment and human health. J. Environ. Sci. 152, 188-202.
[56] Yang, L., Mih, N., Anand, A., Park, J.H., Tan, J., Yurkovich, J.T., Monk, J.M., Lloyd, C.J., Sandberg, T.E., Seo, S.W., Kim, D., Sastry, A. V., Phaneuf, P., Gao, Y., Broddrick, J.T., Chen, K., Heckmann, D., Szubin, R., Hefner, Y., Feist, A.M., Palsson, B.O., 2019. Cellular responses to reactive oxygen species are predicted from molecular mechanisms. Proc. Natl. Acad. Sci. 116(28), 14368-14373.
[57] Yin, D.M., Uwineza, C., Sapmaz, T., Mahboubi, A., De Wever, H., Qiao, W., Taherzadeh, M.J., 2022. Volatile fatty acids (VFA) production and recovery from chicken manure using a high-solid anaerobic membrane bioreactor (AnMBR). Membranes. 12(11), 12111133.
[58] You, M., Zhao, Q., Liu, Y., Zhang, W., Shen, Z., Ren, Z., Xu, C., 2023. Insights into lignocellulose degradation: comparative genomics of anaerobic and cellulolytic *Ruminiclostridium*-type species. Front. Microbiol. 14, 1-12.
[59] Zhang, J., Lu, T., Wang, Z., Wang, Y., Zhong, H., Shen, P., Wei, Y., 2019. Effects of magnetite on anaerobic digestion of swine manure: attention to methane production and fate of antibiotic resistance genes. Bioresour. Technol. 291, 121847.
[60] Zhao, D., Zhang, P., Liu, Y., Li, Q., Wang, G., Chen, R., Li, Y.Y., 2024. Biochar-mediated synergistic promotion of DIET and IHT: kinetic and thermodynamic insights into propionate two-step syntrophic methanogenesis. Chem. Eng. J. 486(13), 150310.
[61] Zhu, X., Blanco, E., Bhatti, M., Borrion, A., 2021. Impact of metallic nanoparticles on anaerobic digestion: a systematic review. Sci. Total Environ. 757, 143747.
[62] Zhu, X., Blanco, E., Bhatti, M., Borrion, A., 2025. Improving anaerobic digestion process against acetate accumulation: insights into organic loading rates and nano magnetite additions. Chem. Eng. J. 512, 162641.
[63] Ziganshina, E.E., Belostotskiy, D.E., Bulynina, S.S., Ziganshin, A.M., 2021. Effect of magnetite on anaerobic digestion of distillers grains and beet pulp: Operation of reactors and microbial community dynamics. J. Biosci. Bioeng. 131(3), 290-298.
[64] Ziganshina, E.E., Ziganshin, A.M., 2023. Magnetite Nanoparticles and Carbon Nanotubes for Improving the Operation of Mesophilic Anaerobic Digesters. Microorganisms. 11(4), 938.

Xiaowen Zhu is a PhD candidate in the Department of Civil, Environmental, and Geomatic Engineering at University College London. Her research focuses on the application of metallic nanoparticles in anaerobic digestion to enhance performance and optimise processes. Her research profile is available at https://scholar.google.com/citations?hl=en&user=9vUh5NUAAAAJ.

Edgar Blanco is an accomplished research manager with over 26 years of experience in wastewater treatment and anaerobic digestion treatment, covering laboratory work, field monitoring, commercial operations, and project management. He holds an MSc in Environmental Technology and a Diploma in Water Management from Imperial College London, and a degree in Environmental Earth Science from the University of Greenwich. He has led research and innovation in senior roles at Anaero Technology and Andigestion Ltd, developing patented AD systems and transforming operations into profitable ventures. His ResearchGate profile can be found at: https://www.researchgate.net/profile/Edgar-Blanco-5.

Dr. Manni Bhatti is an Honorary Lecturer at UCL and graduated with a PhD in Medical Microbiology from the Eastman Dental Institute. Since moving to UCL from Imperial College London, she has been working on using various methods to eliminate plastics and other pollutants within the Environmental Engineering Research section. She has also worked on using plant extracts to eliminate pathogens in collaboration with Kew Gardens and Kingston University. She has worked on superhydrophobic materials and nanowires in collaboration with the Mechanical Engineering Department at UCL and has peer-reviewed a wide selection of papers on some leading journals. Her Research Gate profile can be found at https://www.researchgate.net/profile/Manni-Bhatti.

Professor Aiduan Borrion is a professor of environmental engineering who leads a research group on bioresource and sustainability. She is the Head of the Environmental Engineering Section at University College London (UCL) and Co-Director of the UCL Circular Economy Lab (CircEL). She was the European Editor of Environmental Engineering Science, the official journal of the Association of Environmental Engineering & Science Professors (AEESP), between 2017 and 2023, and the programme director of the MSc Environmental Systems Engineering, between 2019 and 2024. She holds a PhD in Environmental Engineering and Clean Energy Technology from UCL. Her research profile can be found at: https://scholar.google.co.uk/citations?user=mO5SErMAAAAJ&hl=en.

Please cite this article as: Zhu X., Blanco E., Bhatti M., Borrion A. Promoting methanogenesis and stability in anaerobic digestion with nano magnetite under VFA-induced stress. Biofuel Research Journal 46 (2025) 2432-2450. DOI: 10.18331/BRJ2025.12.2.5.

Supplementary Material

S1. Detailed analytical methods

The biogas production rate was continuously monitored using a Nautilus model datalogger. Gas composition, including methane (CH_4), carbon dioxide (CO_2), and hydrogen (H_2), was analysed using a GasData GFM436 gas analyser (UK). Liquid samples were collected via effluent tubes (**Fig. 1**) at the beginning and end of each spiked level. Ammonium (NH_4^+) levels were measured with a pH/ORP/ISE meter (HI-98191, UK) equipped with an ammonium ion-selective electrode (EDT directION, UK). Oxidation-reduction potential (ORP) and pH were determined using an ORP meter (Hanna, UK) and a pH meter (Mettler Toledo, UK), respectively. Partial and total alkalinity was assessed by titration to endpoints at pH 5.75 and 4.30, following established protocols (Jantsch and Mattiasson, 2003).

Volatile fatty acids (VFAs), including acetic, butyric, and propionic acids, were quantified using high-performance liquid chromatography (HPLC, PerkinElmer Series 200, USA) equipped with a UV/VIS detector and a Chrom-Clone 5 µm C18 100 Å LC Column (Phenomenex, UK). The mobile phase, a 10 mM potassium phosphate buffer, was delivered at 1.5 mL/min, with detection at 210 nm. The column temperature was maintained at 40ºC, and the injection volume was set to 20 µL. Dissolved iron concentrations at the conclusion of semi-continuous operations were determined using inductively coupled plasma mass spectrometry (ICP-MS, 7900, Agilent Technologies Inc., Santa Clara, CA, USA). Solid content analyses, including total solids (TS), volatile solids (VS), and volatile suspended solids (VSS), were performed on samples collected at the end of spike levels V and R, using standard analytical methods (USEPA, 1983; APHA, 2012).

S2. Detailed sequencing pipeline and metabolic analysis

Sludge samples were collected for microbial analysis by the end of spiked level V of semi-continuous operations. Genomic DNA was extracted using the DNeasy PowerSoil kit (QIAGEN, Germany) according to the manufacturer's instructions. The quality and quantity of extracted DNA were evaluated with a NanoDrop 2000 microvolume spectrophotometer (Thermo Fisher Scientific, USA). Absorbance readings at 260 nm and 280 nm were used to assess DNA purity, with 260/280 nm ratios ranging between 1.8 and 2.0, indicating high-purity DNA with minimal protein contamination. All DNA samples exceeded a concentration threshold of 10 ng/µL, ensuring sufficient yield for subsequent analyses.

To investigate microbial community diversity, the V4 hypervariable regions of 16S rRNA genes were amplified using the universal primer set 515F/806R (5'-GTGCCAGCMGCCGCGGTAA-3' and 5'-GGACTACHVGGGTWTCTAAT-3') (Campanaro et al., 2018). Amplicons were sequenced on the Illumina NovaSeq PE250 platform by Novogene Co. Ltd. (Cambridge, UK). Paired-end sequencing reads were merged using FLASH software (v1.2.7) to create contiguous sequences. Raw sequences underwent quality filtering with the Quantitative Insights Into Microbial Ecology (QIIME, v1.7.0) pipeline, producing high-quality clean tags. Chimera detection and removal were performed with the UCHIME algorithm by comparing sequences against the SILVA138 reference database.

Operational Taxonomic Units (OTUs) were clustered at 97% sequence similarity using Uparse software (v7.0.1090). Representative sequences from each OTU were phylogenetically classified, and taxonomic identities were assigned with the Ribosomal Database Project (RDP) classifier (v2.2). This comprehensive workflow provided insights into microbial diversity and composition, facilitating an in-depth understanding of microbial responses to VFA stress in the AD systems.

PICRUSt2 (Phylogenetic Investigation of Communities by Reconstruction of Unobserved States, version 2) was used to predict the functional potential of microbial communities using marker gene sequencing data (Douglas et al., 2020). The PICRUSt software package offers functional annotations by using the Kyoto Encyclopedia of Genes and Genomes (KEGG) pathway database to clarify variations in gene-encoding enzymes, including detailed reconstruction of microbial functions (Lv et al., 2020; You et al., 2023), nitrogen and sulphate cycling (Tan et al., 2022; Giangeri et al., 2023), direct interspecies electron transfer (DIET) (You et al., 2023), as well as reactive oxygen species (ROS) in AD process (Yan et al., 2023).

S3. Kinetic evaluation

S3.1 Methane Production

Data from the batch spike-to-recovery test were fitted with the modified Gompertz equation (**Eq. S1**) to access the kinetic parameters of butyrate and propionate methanation.

$$P_{(t)} = P_0 \cdot \exp\left\{-\exp\left[\frac{R_{max} \cdot e}{P_0}(\lambda - t) + 1\right]\right\} \quad \text{Eq. S1}$$

where $P_{(t)}$ stands for the cumulative methane production (mL) at time t of methanogenesis, P_0 represents the potential methane production (mL), R_{max} stands for the maximum methanation rate (mL/hour), e is the Euler's number (e=2.718), λ stands for the duration of lag phase (hour), and t donates the duration of each feeding cycle.

S3.2 Specific methanogenic activity and substrate utilisation efficiency

The link between methane production rate and biomass weight was investigated by the specific methanogenic activity (SMA, mL/g VSS/d). In this study, the results from batch experiments were used to calculate SMA and substrate utilisation efficiency (η) based on **Equations S2** and **S3** (Dogan et al., 2005).

$$SMA = \frac{r}{X} \quad \text{Eq. S2}$$

$$\eta = \frac{\sum_{i=1}^{3} r_i}{Y_{theoretical}} \quad \text{Eq. S3}$$

where r is the methane production rate (ml/L/d), X is the concentration of substrate (g VSS/L), $\sum_{i=1}^{3} r_i$ represents the total methane production over three days for one feeding cycle (mL/g·VS), and $Y_{theoretical}$ is the theoretical methane potential of the substrate VFA (mL/g·VS) derived from the modified Boyle equation (Boyle, 1977).

S3.3 Microbial growth

The growth of microbes inside the AD systems can be accessed by measured biomass concentrations (X, g/L) and then simulated as specific growth rate (µ, 1/d) with the Monod equation (**Eq. S4**).

$$\mu = \frac{\Delta X}{X \cdot \Delta t} = \mu_{max} \cdot \frac{S}{K_s + S} \quad \text{Eq. S4}$$

where ΔX represents the change in biomass concentration (g/L), Δt is the duration of each dosage level (d), S is the substrate concentration (g/L), whilst μ_{max} (1/d) and K_S (g/L) stands for two critical kinetic parameters, namely the maximum specific growth rate and substrate half-saturation constant, respectively.

S3.4 Microbial cell synthesis

The synthesis yield (Y, g cells/g consumed substrate) of substrate is calculated using **Equation S5**:

$$Y = -\frac{\Delta X}{\Delta t} \Big/ \frac{\Delta S}{\Delta t} \quad \text{Eq. S5}$$

where ΔS is the concentration of consumed substrate (g/L).

Please cite this article as: Zhu X., Blanco E., Bhatti M., Borrion A. Promoting methanogenesis and stability in anaerobic digestion with nano magnetite under VFA-induced stress. Biofuel Research Journal 46 (2025) 2432-2450. DOI: 10.18331/BRJ2025.12.2.5.

The overall stoichiometric oxidation-reduction reaction (R) of the substrate to methane could be described using **Equation S6** (Rittmann and McCarty., 2020).

$$R = f_e R_a + f_s R_c - R_d \quad \text{Eq. S6}$$

Assuming the reaction is a transformation of a single electron equivalent, when there is no electron donor other than the substrate, the total fractions of electrons used for methanation (f_e) and microbial cell synthesis (f_s) equals 1. R_d and R_a are the half-reactions for the electron donor and acceptor, respectively, and R_c is the cell biomass equation (with empirical cell formulation of $C_5H_7O_2N$), assuming ammonia as the nitrogen source for cell synthesis (Rittmann and McCarty., 2020).

S4. AD performances during semi-continuous operations to stepwise increased OLRs

The semi-continuous AD systems were initially incubated with OLRs and gradually increased from 2.0 to 4.0 gVS/L·d. During this phase, methane production (**Fig. S3a**) increased significantly to 471.0±89.3 mL/L·d, and the end-phase acetic acid concentrations (**Fig. S3f**) reached 489.8±211.8 mg/L.

At the start of the experiment (**Fig. S3**), the bacterial communities were predominantly composed of *Defluviitalea* (29.0%) and *HN-HF0106* (27.4%), both from the phylum *Firmicutes*. These genera are linked to the degradation of complex hydrocarbons, including cellulose, the main carbon source in this study (Rettenmaier et al., 2020; Rocamora et al., 2023). Methanogens made up 0.7% of the microbial population, dominated by *Methanosarcinaceae* (54.6%) and *Methanobacteriaceae* (30.5%).

When the OLR was increased to 5.0 gVS/L·d, reactor performance gradually declined. Average methane production decreased by 5.9% compared to the control group (**Fig. S3a**, $p<0.001$), while pH levels dropped to 7.0±0.3 (**Fig. S3d**). Acetic acid concentrations (**Fig. S3f**) neared the inhibition threshold of 1500 mg/L (Wang et al., 2023) in approximately 20% of measurements, averaging 1287.6±572.5 mg/L. Butyric and propionic acid levels (**Figs. S3g** and **S3h**) significantly increased to 96.6±117.4 mg/L ($p<0.001$) and 247.5±138.5 mg/L ($p<0.001$), respectively, accompanied by a rise in hydrogen content to 187.1±35.0 ppm ($p<0.001$). The IA:PA ratio (**Fig. S3c**) increased to 0.8±0.3 ($p<0.001$), exceeding the optimal range for AD (Bai et al., 2025; Zhang et al., 2019), which was mirrored by a reduction in microbial viability to 85.8±9.9% (Fig. S3E, $p<0.001$).

Compared to the phase operated at 4.0 gVS/L·d, the OLR increase to 5.0 gVS/L·d resulted in a doubling of the average concentrations of individual VFAs (**Figs. S3f-h**). Ammonium and free ammonia nitrogen (FAN) levels also surged, increasing by 93.6% ($p<0.001$) and 28.8% ($p<0.05$), respectively. Despite these changes, none of the inhibitory compounds reached their reported threshold concentrations for inhibition (Zhang et al., 2019; Bai et al., 2025).

At the end of the semi-continuous operations ("Control" in **Fig. 5**), the bacterial communities were enriched with *Defluviitalea* (21.2%), *Fastidiosipila* (18.6%), and *Ruminiclostridium* (10.5%), all within the phylum *Firmicutes*, and known for their roles in hydrolysis and VFA production (Rettenmaier et al., 2020; You et al., 2023). Notably, bacteria involved in butyrate and propionate degradation were more abundant compared with the initial sample, with *Syntrophomonadaceae* increasing from 3.4% to 6.1% and *Pelotomaculum* slightly rising from 0.3% to 0.4% (Zheng et al., 2019; Ziels et al., 2019). Methanogen abundance rose to 5.2%, with a community shift dominated by *Methanomicrobiaceae* (85.1%) and *Methanosarcinaceae* (11.8%). This shift correlated with increased hydrogen levels (124.6±23.8 ppm) and enhanced activity of hydrogen-producing acetogens (Yan et al., 2023).

Under feedstock overload, hydrolytic activity significantly increased (**Fig. S4**), while the bacterial community structure remained largely consistent with the control (**Fig. 5a**). The elevated organic loading rate (OLR) introduced more complex substrates, requiring enhanced breakdown by hydrolytic and acidogenic bacteria, resulting in increased relative abundances of these groups (**Fig. 5a**). This reflects the rising demand for substrate degradation to manage the increased organic load. Although microbial diversity and richness improved (**Fig. 5b**), the system shifted toward the less energy-efficient "propionate metabolic pathway" (**Fig. 5d**), leading to greater propionate production instead of acetate (Sikora et al., 2019).

The relative abundance of *Pelotomaculum*, a key propionate-degrading bacterium, rose from 0.3% to 3.1%, indicating an enhanced microbial capacity for propionate metabolism (Zheng et al., 2019). However, the reliance on this pathway slowed the AD process due to the more energy-intensive nature of propionate conversion (Sikora et al., 2019). To adapt, the methanogenic community shifted toward dominance by H_2-dependent methanogens, such as *Methanomicrobiaceae*, which accounted for 86.9% of the methanogenic population (**Fig. 5a**), enhancing their ability to consume with elevated hydrogen levels.

Additionally, *Nitrososphaeraceae*, crucial for ammonia oxidation, increased in relative abundance from 0.2% to 1.4% in response to elevated ammonium concentrations. The rise in ammonium levels correlated with increased activity of ammonium-forming enzymes, including NirBD, NrfAH, and urease (**Fig. S4e**). Although enzymes linked to denitrification (NoB) and anaerobic ammonium oxidation (Anammox) also showed enhanced activity (**Fig. S4e**), these responses were insufficient to prevent ammonium accumulation within the system. This imbalance highlights the challenges of managing elevated OLRs in AD processes.

Table S1.
Detailed characteristics of inoculum.

Parameter	Units	Inoculum
Total solids, TS	g/L	42.1
Volatile solids, VS	g/L	27.1
Volatile suspended solids, VSS	g/L	21.5
pH	-	7.53
Alkalinity	g $CaCO_3$/L	5906
Ammonium	mg NH_4^+/L	4966
Phosphorus, P	mg/L	783
Sodium, Na	mg/L	2366
Calcium, Ca	mg/L	1793
Magnesium, Mg	mg/L	79.7
Sulphur, S	mg/L	386
Potassium, K	mg/L	1188
Selenium, Se	mg/L	0.07
Cobalt, Co	mg/L	0.78
Iron, Fe	mg/L	418
Copper, Cu	mg/L	1.85
Nickel, Ni	mg/L	1.09
Zinc, Zn	mg/L	10.8
Molybdenum, Mo	mg/L	0.19
Manganese, Mg	mg/L	6.36

Table S2.
Composition of the basal medium (Isci and Demirer, 2007; Morita et al., 2011).

Component	Amount (mg/L)
$NaHCO_3$	9000
$Na_2S·9H_2O$	300
NH_4Cl	1200
$MgSO_4·7H_2O$	400
$KH_2PO_4·3H_2O$	300
K_2HPO_4	1500
$CaCl_2$	3000
$FeCl_2·4H_2O$	1500
H_3BO_3	5
$ZnCl_2$	15
$CuCl_2·2H_2O$	5
$MnCl_2·4H_2O$	5
$(NH_4)_6Mo_7O_{24}·4H_2O$	0.5
$AlCl_3·6H_2O$	45
$CoCl_2·6H_2O$	2.5
$NiCl_2·6H_2O$	7.5
$Na_2SeO·5H_2O$	0.25
NaCl	5.2
Urea	8000
H_2SO_4	3

Please cite this article as: Zhu X., Blanco E., Bhatti M., Borrion A. Promoting methanogenesis and stability in anaerobic digestion with nano magnetite under VFA-induced stress. Biofuel Research Journal 46 (2025) 2432-2450. DOI: 10.18331/BRJ2025.12.2.5.

Table S3.
Gene expressions and relative KEGG description involved in this study, including detailed reconstruction of microbial functions (Lv et al., 2020; You et al., 2023), nitrogen and sulphate cycling (Tan et al., 2022; Giangeri et al., 2023), direct interspecies electron transfer (DIET) (You et al., 2023), as well as reactive oxygen species in AD process (Yan et al., 2023).

KO	Role	KEGG Description
K00691		mapA; maltose phosphorylase [EC:2.4.1.8]
K01176		AMY, amyA, malS; alpha-amylase [EC:3.2.1.1]
K01178		SGA1; glucoamylase [EC:3.2.1.3]
K01179		E3.2.1.4; endoglucanase [EC:3.2.1.4]
K01180		E3.2.1.6; endo-1,3(4)-beta-glucanase [EC:3.2.1.6]
K01181		E3.2.1.8, xynA; endo-1,4-beta-xylanase [EC:3.2.1.8]
K01182		IMA, malL; oligo-1,6-glucosidase [EC:3.2.1.10]
K01183		E3.2.1.14; chitinase [EC:3.2.1.14]
K01184		E3.2.1.15; polygalacturonase [EC:3.2.1.15]
K01185		E3.2.1.17; lysozyme [EC:3.2.1.17]
K01186		NEU1; sialidase-1 [EC:3.2.1.18]
K01187		malZ; alpha-glucosidase [EC:3.2.1.20]
K01188		E3.2.1.21; beta-glucosidase [EC:3.2.1.21]
K01190		lacZ; beta-galactosidase [EC:3.2.1.23]
K01191		MAN2C1; alpha-mannosidase [EC:3.2.1.24]
K01192		E3.2.1.25, MANBA, manB; beta-mannosidase [EC:3.2.1.25]
K01193		INV, sacA; beta-fructofuranosidase [EC:3.2.1.26]
K01194		TREH, treA, treF; alpha,alpha-trehalase [EC:3.2.1.28]
K01195		uidA, GUSB; beta-glucuronidase [EC:3.2.1.31]
K01197		hya; hyaluronoglucosaminidase [EC:3.2.1.35]
K01198		xynB; xylan 1,4-beta-xylosidase [EC:3.2.1.37]
K01200		pulA; pullulanase [EC:3.2.1.41]
K01201		GBA, srfJ; glucosylceramidase [EC:3.2.1.45]
K01205		NAGLU; alpha-N-acetylglucosaminidase [EC:3.2.1.50]
K01206		FUCA; alpha-L-fucosidase [EC:3.2.1.51]
K01207		nagZ; beta-N-acetylhexosaminidase [EC:3.2.1.52]
K01208	Hydrolysis	cd, ma, nplT; cyclomaltodextrinase / maltogenic alpha-amylase / neopullulanase [EC:3.2.1.54 3.2.1.133 3.2.1.135]
K01209		abfA; alpha-N-arabinofuranosidase [EC:3.2.1.55]
K01210		E3.2.1.58; glucan 1,3-beta-glucosidase [EC:3.2.1.58]
K01212		sacC, levB; levanase [EC:3.2.1.65]
K01214		ISA, treX; isoamylase [EC:3.2.1.68]
K01215		dexB; glucan 1,6-alpha-glucosidase [EC:3.2.1.70]
K01216		E3.2.1.73; licheninase [EC:3.2.1.73]
K01218		gmuG; mannan endo-1,4-beta-mannosidase [EC:3.2.1.78]
K01219		E3.2.1.81; beta-agarase [EC:3.2.1.81]
K01220		E3.2.1.85, lacG; 6-phospho-beta-galactosidase [EC:3.2.1.85]
K01222		E3.2.1.86A, celF; 6-phospho-beta-glucosidase [EC:3.2.1.86]
K01223		E3.2.1.86B, bglA; 6-phospho-beta-glucosidase [EC:3.2.1.86]
K01224		E3.2.1.89; arabinogalactan endo-1,4-beta-galactosidase [EC:3.2.1.89]
K01226		treC; trehalose-6-phosphate hydrolase [EC:3.2.1.93]
K01227		E3.2.1.96; mannosyl-glycoprotein endo-beta-N-acetylglucosaminidase [EC:3.2.1.96]
K01230		MAN1; mannosyl-oligosaccharide alpha-1,2-mannosidase [EC:3.2.1.113]
K01232		glvA; maltose-6'-phosphate glucosidase [EC:3.2.1.122]
K01233		csn; chitosanase [EC:3.2.1.132]
K01235		aguA; alpha-glucuronidase [EC:3.2.1.139]
K01236		treZ, glgZ; maltooligosyltrehalose trehalohydrolase [EC:3.2.1.141]
K01811		xylS, yicI; alpha-D-xyloside xylohydrolase [EC:3.2.1.177]
K02438		glgX; glycogen debranching enzyme [EC:3.2.1.196]
K03332		fruA; fructan beta-fructosidase [EC:3.2.1.80]
K04844		ycjT; hypothetical glycosyl hydrolase [EC:3.2.1.-]
K05349		bglX; beta-glucosidase [EC:3.2.1.21]

Please cite this article as: Zhu X., Blanco E., Bhatti M., Borrion A. Promoting methanogenesis and stability in anaerobic digestion with nano magnetite under VFA-induced stress. Biofuel Research Journal 46 (2025) 2432-2450. DOI: 10.18331/BRJ2025.12.2.5.

Table S3.
continued.

KO	Role	KEGG Description
K05350		bglB; beta-glucosidase [EC:3.2.1.21]
K05988		dexA; dextranase [EC:3.2.1.11]
K05989		ramA; alpha-L-rhamnosidase [EC:3.2.1.40]
K05991		E3.2.1.123; endoglycosylceramidase [EC:3.2.1.123]
K05992		amyM; maltogenic alpha-amylase [EC:3.2.1.133]
K06113		abnA; arabinan endo-1,5-alpha-L-arabinosidase [EC:3.2.1.99]
K07405		E3.2.1.1A; alpha-amylase [EC:3.2.1.1]
K07406		melA; alpha-galactosidase [EC:3.2.1.22]
K07407		E3.2.1.22B, galA, rafA; alpha-galactosidase [EC:3.2.1.22]
K07964		HPSE; heparanase [EC:3.2.1.166]
K08068		siaA, neuC1; UDP-N-acetylglucosamine 2-epimerase (hydrolysing) [EC:3.2.1.183]
K08254		E3.2.1.59; glucan endo-1,3-alpha-glucosidase [EC:3.2.1.59]
K12111		ebgA; evolved beta-galactosidase subunit alpha [EC:3.2.1.23]
K12308		bgaB, lacA; beta-galactosidase [EC:3.2.1.23]
K12373		HEXA_B; hexosaminidase [EC:3.2.1.52]
K13381		chiA; bifunctional chitinase/lysozyme [EC:3.2.1.14 3.2.1.17]
K15524		mngB; mannosylglycerate hydrolase [EC:3.2.1.170]
K15531		rexA; oligosaccharide reducing-end xylanase [EC:3.2.1.156]
K15532		yteR, yesR; unsaturated rhamnogalacturonyl hydrolase [EC:3.2.1.172]
K15538		MANEA; glycoprotein endo-alpha-1,2-mannosidase [EC:3.2.1.130]
K15719		NCOAT, MGEA5; protein O-GlcNAcase / histone acetyltransferase [EC:3.2.1.169 2.3.1.48]
K15855		csxA; exo-1,4-beta-D-glucosaminidase [EC:3.2.1.165]
K15921		xynD; arabinoxylan arabinofuranohydrolase [EC:3.2.1.55]
K15922		yihQ; sulfoquinovosidase [EC:3.2.1.199]
K15923		AXY8, FUC95A, afcA; alpha-L-fucosidase 2 [EC:3.2.1.51]
K15924		xynC; glucuronoarabinoxylan endo-1,4-beta-xylanase [EC:3.2.1.136]
K16559		exoK; endo-1,3-1,4-beta-glycanase ExoK [EC:3.2.1.-]
K17108		GBA2; non-lysosomal glucosylceramidase [EC:3.2.1.45]
K17624		engCP, engBF, endoEF; endo-alpha-N-acetylgalactosaminidase [EC:3.2.1.97]
K18429		legG, neuC2; GDP/UDP-N,N'-diacetylbacillosamine 2-epimerase (hydrolysing) [EC:3.2.1.184]
K18579		6GAL; galactan endo-1,6-beta-galactosidase [EC:3.2.1.164]
K18581		ugl; unsaturated chondroitin disaccharide hydrolase [EC:3.2.1.180]
K18650		pehX; exo-poly-alpha-galacturonosidase [EC:3.2.1.82]
K18775		lf2; levanbiose-producing levanase [EC:3.2.1.64]
K19355		MAN; mannan endo-1,4-beta-mannosidase [EC:3.2.1.78]
K19668		CBH2, cbhA; cellulose 1,4-beta-cellobiosidase [EC:3.2.1.91]
K00024	VFA metabolism	mdh; malate dehydrogenase
K05606		MCEE, epi; methylmalonyl-CoA/ethylmalonyl-CoA epimerase
K01966		PCCB, pccB; propionyl-CoA carboxylase beta chain
K01913		acetate/butyrate---CoA ligase [EC:6.2.1.1 6.2.1.2]
K01903		sucC; succinyl-CoA synthetase beta subunit [EC:6.2.1.5]
K01902		sucD; succinyl-CoA synthetase alpha subunit
K01847		MUT; methylmalonyl-CoA mutase
K01715		crt; enoyl-CoA hydratase
K01692		paaF, echA; enoyl-CoA hydratase
K01573		oadG; oxaloacetate decarboxylase, gamma subunit [EC:4.1.1.3]
K01572		oadB; oxaloacetate decarboxylase, beta subunit [EC:4.1.1.3]
K01571		oadB; oxaloacetate decarboxylase, beta subunit [EC:4.1.1.3]
K01026		pct; propionate CoA-transferase
K00925		ackA; acetate kinase
K00656		pflD; formate C-acetyltransferase
K00626		atoB; acetyl-CoA C-acetyltransferase

Please cite this article as: Zhu X., Blanco E., Bhatti M., Borrion A. Promoting methanogenesis and stability in anaerobic digestion with nano magnetite under VFA-induced stress. Biofuel Research Journal 46 (2025) 2432-2450. DOI: 10.18331/BRJ2025.12.2.5.

Table S3.
continued.

KO	Role	KEGG Description
K00625		pta; phosphate acetyltransferase
K00248		ACADS, bcd; butyryl-CoA dehydrogenase
K00244		frdA; fumarate reductase flavoprotein subunit
K00240		sdhB, frdB; succinate dehydrogenase / fumarate reductase, iron-sulfur subunit
K00239		sdhA, frdA; succinate dehydrogenase / fumarate reductase, flavoprotein subunit
K00074		paaH, hbd, fadB, mmgB; 3-hydroxybutyryl-CoA dehydrogenase
K03422		mcrD; methyl-coenzyme M reductase subunit C
K03421		mcrD; methyl-coenzyme M reductase subunit D
K01895		ACSS, acs; acetyl-CoA synthetase
K01499		mch; methenyltetrahydromethanopterin cyclohydrolase []
K00672		DLAT, aceF, pdhC; pyruvate dehydrogenase E2 component (dihydrolipoamide acetyltransferase) [EC:2.3.1.12]
K00584		mtrH; tetrahydromethanopterin S-methyltransferase subunit H [EC:2.1.1.86]
K00583		mtrG; tetrahydromethanopterin S-methyltransferase subunit G [EC:2.1.1.86]
K00582		mtrF; tetrahydromethanopterin S-methyltransferase subunit F [EC:2.1.1.86]
K00581		mtrE; tetrahydromethanopterin S-methyltransferase subunit E [EC:2.1.1.86]
K00580		mtrD; tetrahydromethanopterin S-methyltransferase subunit D [EC:2.1.1.86]
K00579		mtrC; tetrahydromethanopterin S-methyltransferase subunit C [EC:2.1.1.86]
K00578		mtrB; tetrahydromethanopterin S-methyltransferase subunit B [EC:2.1.1.86]
K00577		mtrA; tetrahydromethanopterin S-methyltransferase subunit A
K00534		E1.12.7.2S; ferredoxin hydrogenase small subunit [EC:1.12.7.2]
K00533		E1.12.7.2L; ferredoxin hydrogenase large subunit [EC:1.12.7.2]
K00532	Methanogenesis	E1.12.7.2; ferredoxin hydrogenase [EC:1.12.7.2]
K00436		hoxH; NAD-reducing hydrogenase large subunit [EC:1.12.1.2]
K00400		methyl coenzyme M reductase system, component A2
K00320		mer; 5,10-methylenetetrahydromethanopterin reductase [EC:1.5.98.2]
K00319		mtd; methylenetetrahydromethanopterin dehydrogenase [EC:1.5.98.1]
K00203		fwdD, fmdD; formylmethanofuran dehydrogenase subunit D [EC:1.2.7.12]
K00202		fwdC, fmdC; formylmethanofuran dehydrogenase subunit C [EC:1.2.7.12]
K00201		fwdB, fmdB; formylmethanofuran dehydrogenase subunit B [EC:1.2.7.12]
K00200		fwdA, fmdA; formylmethanofuran dehydrogenase subunit A [EC:1.2.7.12]
K00197		cdhE, acsC; acetyl-CoA decarbonylase/synthase complex subunit gamma [EC:2.1.1.245]
K00194		cdhD, acsD; acetyl-CoA decarbonylase/synthase complex subunit delta [EC:2.1.1.245]
K00193		cdhC; acetyl-CoA decarbonylase/synthase complex subunit beta [EC:2.3.1.-]
K00192		cdhA; acetyl-CoA decarbonylase/synthase complex subunit alpha
K00125		fdhB; formate dehydrogenase (coenzyme F420) beta subunit [EC:1.17.98.3 1.8.98.6]
K00124		fdoH, fdsB; formate dehydrogenase iron-sulfur subunit
K00123		fdoG, fdhF, fdwA; formate dehydrogenase major subunit [EC:1.17.1.9]
K12234		cofE, fbiB; coenzyme F420-0:L-glutamate ligase / coenzyme F420-1:gamma-L-glutamate ligase [EC:6.3.2.31 6.3.2.34]
K06937		K06937; 7,8-dihydro-6-hydroxymethylpterin dimethyltransferase [EC:1.21.98.5]
K05847		opuA; osmoprotectant transport system ATP-binding protein
K05846		opuBD; osmoprotectant transport system permease protein
K05845		opuC; osmoprotectant transport system substrate-binding protein
K05020	Membrane permeability/osmoprotectant	opuD, betL; glycine betaine transporter
K03549		kup; KUP system potassium uptake protein
K02002		proX; glycine betaine/proline transport system substrate-binding protein
K02001		proW; glycine betaine/proline transport system permease protein
K02000		proV; glycine betaine/proline transport system ATP-binding protein [EC:3.6.3.32]
K01950		NADSYN1, QNS1, nadE; NAD+ synthase (glutamine-hydrolysing) [EC:6.3.5.1]
K01919		gshA; glutamate--cysteine ligase [EC:6.3.2.2]
K00266		gltD; glutamate synthase (NADPH/NADH) small chain [EC:1.4.1.13 1.4.1.14]

Please cite this article as: Zhu X., Blanco E., Bhatti M., Borrion A. Promoting methanogenesis and stability in anaerobic digestion with nano magnetite under VFA-induced stress. Biofuel Research Journal 46 (2025) 2432-2450. DOI: 10.18331/BRJ2025.12.2.5.

Table S3.
continued.

KO	Role	KEGG Description
K00262		E1.4.1.4, gdhA; glutamate dehydrogenase (NADP+) [EC:1.4.1.4]
K00261		GLUD1_2, gdhA; glutamate dehydrogenase (NAD(P)+) [EC:1.4.1.3]
K00260		gudB, rocG; glutamate dehydrogenase [EC:1.4.1.2]
K09825	ROS defense system	perR; Fur family transcriptional regulator, peroxide stress response regulator
K04565		SOD1; superoxide dismutase, Cu-Zn family [EC:1.15.1.1]
K04564		SOD2; superoxide dismutase, Fe-Mn family [EC:1.15.1.1]
K03782		katG; catalase-peroxidase [EC:1.11.1.21]
K03781		katE, CAT, catB, srpA; catalase [EC:1.11.1.6]
K03711		fur, zur, furB; Fur family transcriptional regulator, ferric uptake regulator
K02588		nifH; nitrogenase iron protein NifH
K01915		glnA, GLUL; glutamine synthetase [EC:6.3.1.2]
K00432		gpx; glutathione peroxidase [EC:1.11.1.9]
K01253	ROS generation system	EPHX1; microsomal epoxide hydrolase [EC:3.3.2.9]
K00002		AKR1A1, adh; alcohol dehydrogenase (NADP+)
K13628	ROS response	iscA; iron-sulfur cluster assembly protein
K11717		sufS; cysteine desulfurase / selenocysteine lyase [EC:2.8.1.7 4.4.1.16]
K09015		sufD; Fe-S cluster assembly protein SufD
K09014		sufB; Fe-S cluster assembly protein SufB
K09013		sufC; Fe-S cluster assembly ATP-binding protein
K05997		sufA; Fe-S cluster assembly protein SufA
K04759		feoB; ferrous iron transport protein B
K04758		feoA; ferrous iron transport protein A
K04488		iscU, nifU; nitrogen fixation protein NifU and related proteins
K03284		corA; magnesium transporter
K02016		ABC.FEV.S; iron complex transport system substrate-binding protein
K02013		ABC.FEV.A; iron complex transport system ATP-binding protein []
K00245		frdB; fumarate reductase iron-sulfur subunit [EC:1.3.5.4]
K00188		vorD; 2-oxoisovalerate ferredoxin oxidoreductase, delta subunit [EC:1.2.7.7]
K00187		vorB; 2-oxoisovalerate ferredoxin oxidoreductase, beta subunit [EC:1.2.7.7]
K00186		vorA; 2-oxoisovalerate ferredoxin oxidoreductase, alpha subunit [EC:1.2.7.7]
K00573	DIET	E2.1.1.77, pcm; protein-L-isoaspartate(D-aspartate) O-methyltransferase [EC:2.1.1.77]
K02650		pilA; type IV pilus assembly protein PilA
K13300		cccA; cytochrome c550
K02048	Sulphate cycle	cysP, sbp; sulphate transport system substrate-binding protein
K00394		aprA; adenylylsulphate reductase, subunit A [EC:1.8.99.2]
K13811		PAPSS; 3'-phosphoadenosine 5'-phosphosulfate synthase [EC:2.7.7.4 2.7.1.25]
K00860		cysC; adenylylsulphate kinase [EC:2.7.1.25]
K00390		cysH; phosphoadenosine phosphosulphate reductase [EC:1.8.4.8 1.8.4.10]
K00392		sir; sulphite reductase (ferredoxin) [EC:1.8.7.1]
K00380		cysJ; sulphite reductase (NADPH) flavoprotein alpha-component [EC:1.8.1.2]

Please cite this article as: Zhu X., Blanco E., Bhatti M., Borrion A. Promoting methanogenesis and stability in anaerobic digestion with nano magnetite under VFA-induced stress. Biofuel Research Journal 46 (2025) 2432-2450. DOI: 10.18331/BRJ2025.12.2.5.

Table S4.
Enzyme activities and relative KEGG description involved in this study, including detailed reconstruction of microbial functions (Lv et al., 2020; You et al., 2023), nitrogen and sulphate cycling (Tan et al., 2022; Giangeri et al., 2023), direct interspecies electron transfer (DIET) (You et al., 2023), as well as reactive oxygen species in AD process (Yan et al., 2023).

EC	Role	Description
EC:3.2.1.1	Hydrolysis	Alpha-amylase
EC:3.2.1.10		Oligo-1,6-glucosidase
EC:3.2.1.11		Dextranase
EC:3.2.1.113		Mannosyl-oligosaccharide 1,2-alpha-mannosidase
EC:3.2.1.122		Maltose-6'-phosphate glucosidase
EC:3.2.1.123		Endoglycosylceramidase
EC:3.2.1.130		Glycoprotein endo-alpha-1,2-mannosidase
EC:3.2.1.132		Chitosanase
EC:3.2.1.135		Neopullulanase
EC:3.2.1.136		Glucuronoarabinoxylan endo-1,4-beta-xylanase
EC:3.2.1.139		Alpha-glucuronidase
EC:3.2.1.14		Chitinase
EC:3.2.1.141		4-alpha-D-((1->4)-alpha-D-glucano)trehalose trehalohydrolase
EC:3.2.1.15		Polygalacturonase
EC:3.2.1.156		Oligosaccharide reducing-end xylanase
EC:3.2.1.164		Galactan endo-1,6-beta-galactosidase
EC:3.2.1.165		Exo-1,4-beta-D-glucosaminidase
EC:3.2.1.166		Heparanase
EC:3.2.1.169		Protein O-GlcNAcase
EC:3.2.1.17		Lysozyme
EC:3.2.1.170		Mannosylglycerate hydrolase
EC:3.2.1.172		Unsaturated rhamnogalacturonyl hydrolase
EC:3.2.1.177		Alpha-D-xyloside xylohydrolase
EC:3.2.1.18		Exo-alpha-sialidase
EC:3.2.1.180		Unsaturated chondroitin disaccharide hydrolase
EC:3.2.1.183		UDP-N-acetylglucosamine 2-epimerase (hydrolyzing)
EC:3.2.1.184		UDP-N,N'-diacetylbacillosamine 2-epimerase (hydrolyzing)
EC:3.2.1.20		Alpha-glucosidase
EC:3.2.1.21		Beta-glucosidase
EC:3.2.1.22		Alpha-galactosidase
EC:3.2.1.23		Beta-galactosidase
EC:3.2.1.24		Alpha-mannosidase
EC:3.2.1.25		Beta-mannosidase
EC:3.2.1.26		Beta-fructofuranosidase
EC:3.2.1.28		Alpha,alpha-trehalase
EC:3.2.1.3		Glucan 1,4-alpha-glucosidase
EC:3.2.1.31		Beta-glucuronidase
EC:3.2.1.35		Hyaluronoglucosaminidase
EC:3.2.1.37		Xylan 1,4-beta-xylosidase
EC:3.2.1.4		Cellulase
EC:3.2.1.40		Alpha-L-rhamnosidase
EC:3.2.1.41		Pullulanase
EC:3.2.1.45		Glucosylceramidase
EC:3.2.1.50		Alpha-N-acetylglucosaminidase
EC:3.2.1.51		Alpha-L-fucosidase
EC:3.2.1.52		Beta-N-acetylhexosaminidase
EC:3.2.1.54		Cyclomaltodextrinase
EC:3.2.1.55		Non-reducing end alpha-L-arabinofuranosidase
EC:3.2.1.58		Glucan 1,3-beta-glucosidase
EC:3.2.1.59		Glucan endo-1,3-alpha-glucosidase

Please cite this article as: Zhu X., Blanco E., Bhatti M., Borrion A. Promoting methanogenesis and stability in anaerobic digestion with nano magnetite under VFA-induced stress. Biofuel Research Journal 46 (2025) 2432-2450. DOI: 10.18331/BRJ2025.12.2.5.

Table S4.
continued.

EC	Role	Description
EC:3.2.1.6		Endo-1,3(4)-beta-glucanase
EC:3.2.1.64		2,6-beta-fructan 6-levanbiohydrolase
EC:3.2.1.65		Levanase
EC:3.2.1.68		Isoamylase
EC:3.2.1.70		Glucan 1,6-alpha-glucosidase
EC:3.2.1.73		Licheninase
EC:3.2.1.78		Mannan endo-1,4-beta-mannosidase
EC:3.2.1.8		Endo-1,4-beta-xylanase
EC:3.2.1.80		Fructan beta-fructosidase
EC:3.2.1.81		Beta-agarase
EC:3.2.1.82		Exo-poly-alpha-galacturonosidase
EC:3.2.1.85		6-phospho-beta-galactosidase
EC:3.2.1.86		6-phospho-beta-glucosidase
EC:3.2.1.89		Arabinogalactan endo-beta-1,4-galactanase
EC:3.2.1.91		Cellulose 1,4-beta-cellobiosidase (non-reducing end)
EC:3.2.1.93		Alpha,alpha-phosphotrehalase
EC:3.2.1.96		Mannosyl-glycoprotein endo-beta-N-acetylglucosaminidase
EC:3.2.1.97		Endo-alpha-N-acetylgalactosaminidase
EC:3.2.1.99		Arabinan endo-1,5-alpha-L-arabinosidase
EC:2.4.1.8		Maltose phosphorylase
EC: 1.2.7.1	VFA metabolism	Pyruvate synthase
EC: 6.2.1.1		Acetate--CoA ligase
EC:2.7.2.1		Acetate kinase
EC: 2.3.1.8		Phosphate acetyltransferase
EC:2.3.1.16		Acetyl-CoA C-acyltransferase
EC:4.2.1.17		Enoyl-CoA hydratase
EC: 6.2.1.2		Butyrate--CoA ligase
EC: 1.3.8.1		Short-chain acyl-CoA dehydrogenase
EC: 4.2.1.17		Enoyl-CoA hydratase
EC: 1.1.1.157		3-hydroxybutyryl-CoA dehydrogenase
EC: 2.3.1.9		Acetyl-CoA C-acetyltransferase
EC: 4.2.1.54		lactoyl-CoA dehydratase
EC: 1.3.1.84		Acrylyl-CoA reductase (NADPH)
EC: 6.4.1.1		Pyruvate carboxylase
EC: 1.1.1.27		L-lactate dehydrogenase
EC: 2.8.3.1		Propionate CoA-transferase
EC: 6.4.1.3		Propionyl-CoA carboxylase
EC: 5.1.99.1		Methylmalonyl-CoA epimerase
EC: 5.4.99.2		methylmalonyl-CoA mutase
EC: 6.2.1.5		Succinate--CoA ligase (ADP-forming)
EC: 1.3.5.1		Succinate dehydrogenase (quinone)
EC: 1.3.5.4		Fumarate reductase (quinol)
EC: 1.1.1.37		Malate dehydrogenase
EC: 4.1.1.3		Oxaloacetate decarboxylase
EC:2.1.1.245	Methanogenesis	Co-methyltransferase
EC: 2.1.1.86		Tetrahydromethanopterin S-methyltransferase
EC: 1.8.98.1		CoB--CoM heterodisulfide reductase
EC: 2.3.1.54		Formate C-acetyltransferase
EC: 1.12.7.2		Ferredoxin hydrogenase
EC: 1.2.7.12		formylmethanofuran dehydrogenase
EC: 2.3.1.101		formyltransferase
EC: 3.5.4.27		Methenyltetrahydromethanopterin cyclohydrolase

Please cite this article as: Zhu X., Blanco E., Bhatti M., Borrion A. Promoting methanogenesis and stability in anaerobic digestion with nano magnetite under VFA-induced stress. Biofuel Research Journal 46 (2025) 2432-2450. DOI: 10.18331/BRJ2025.12.2.5.

Table S4.
continued.

EC	Role	Description
EC: 1.5.98.2		5,10-methylenetetrahydromethanopterin reductase
EC: 1.5.98.1		Methylenetetrahydromethanopterin dehydrogenase
EC:2.7.2.1	DIET	Acetate kinase
EC:2.3.1.8		Acetyl_CoA, phosphate acetyltransferase
EC:6.2.1.1		Acetyl_CoA syntheyases
EC:3.5.4.27		Methenylterhydromethanopterin cyclohydrolase
EC:1.5.98.1		Methanylenetetrahydromethanopterin dehydrogenase
EC:1.5.98.2		5,10-methanlenetetrahydromethanopterin reductase
EC:1.12.98.1		Coenzyme F420 hydrogenase
EC:2.3.1.101		Formylmethanofuran---tetrahydromethanopterin N-formyltransferase
EC:1.2.7.12		Formylmethanofuran dehydrogenase
EC:1.8.98.1		CoB--CoM heterodisulfide reductase
EC:2.1.1.86		Tetrahydromethanopterin S-methyltransferase
EC:1.3.5.4		Fumarate reductase (quinol)
EC:1.3.5.1		Succinate dehydrogenase (quinol)
EC:1.7.1.15	Ammonium metabolism	Nitrite reductase (NADH)
EC:1.7.7.1		Ferredoxin--nitrite reductase
EC:1.7.2.1		Nitrite reductase (NO-forming)
EC:1.7.2.5		Nitric-oxide reductase (cytochrome c)
EC:1.7.99.4		Nitrate reductase
EC:1.7.1.8		Hydrazine synthase (HZS)
EC:1.7.2.7		Hydrazine dehydrogenase (HDH)
EC:1.7.2.4		Nitrous-oxide reductase
EC:1.7.2.2		Nitrite reductase (cytochrome; ammonia-forming)
EC:3.5.1.5		Urease

Please cite this article as: Zhu X., Blanco E., Bhatti M., Borrion A. Promoting methanogenesis and stability in anaerobic digestion with nano magnetite under VFA-induced stress. Biofuel Research Journal 46 (2025) 2432-2450. DOI: 10.18331/BRJ2025.12.2.5.

Table S5.
Metabolic response of reactors with evaluated butyrate and propionate dosage.

	Feeding Cycle	Butyrate			Propionate		
		Control	20 nm MNP	50 nm MNP	Control	20 nm MNP	50 nm MNP
fe	I	0.928	0.956	0.957	0.938	0.979	0.977
	II	0.934	0.961	0.964	0.935	0.982	0.979
	III	0.928	0.968	0.959	0.936	0.982	0.976
	IV	0.922	0.967	0.964	0.930	0.983	0.978
	V	0.889	0.950	0.944	0.928	0.985	0.979
fs	I	0.067	0.088	0.084	0.032	0.038	0.037
	II	0.066	0.092	0.085	0.034	0.037	0.037
	III	0.066	0.094	0.086	0.033	0.039	0.038
	IV	0.065	0.091	0.086	0.030	0.038	0.037
	V	0.060	0.089	0.083	0.028	0.036	0.036
fe+fs	I	0.995	1.044	1.040	0.971	1.018	1.014
	II	1.000	1.052	1.049	0.969	1.020	1.016
	III	0.994	1.061	1.045	0.969	1.021	1.015
	IV	0.987	1.058	1.050	0.961	1.020	1.015
	V	0.950	1.040	1.027	0.956	1.021	1.015
Y	I	0.101	0.132	0.126	0.058	0.069	0.067
	II	0.099	0.138	0.128	0.061	0.067	0.068
	III	0.100	0.141	0.130	0.060	0.070	0.069
	IV	0.097	0.137	0.130	0.055	0.068	0.066
	V	0.091	0.131	0.125	0.050	0.065	0.065
λ	I	3.506	2.881	3.031	5.376	5.085	5.036
	II	5.029	3.925	3.829	4.032	3.278	3.206
	III	7.009	5.166	5.324	15.718	7.097	7.057
	IV	12.203	9.666	10.180	14.106	11.854	12.368
	V	20.817	12.518	12.651	16.054	12.637	12.842
R_{max}	I	5.382	6.353	6.339	1.598	2.438	2.378
	II	10.482	12.482	12.090	1.989	2.969	2.647
	III	12.132	16.218	15.703	3.157	3.353	3.167
	IV	13.813	15.626	15.718	2.591	3.127	3.007
	V	12.721	12.137	11.574	2.608	2.867	2.787
η	I	95.061	97.890	97.963	94.341	98.465	97.784
	II	94.375	98.403	98.677	94.039	98.767	98.578
	III	94.886	99.101	98.168	94.077	97.368	98.124
	IV	93.045	98.066	97.830	93.774	97.453	97.566
	V	90.127	96.640	96.057	92.117	96.868	97.163

f_e: Fraction of electrons for methanation from donor;
f_s: Fraction of electrons for cell synthesis from donor;
$f_e + f_s$: Total fraction of electrons from the donor;
Y: Overall synthesis yield from the substrate, g cells/g substrate consumed;
λ: Duration of lag phase, hour;
R_{max}: Maximum methanation rate, ml/hour;
η: Substrate utilisation efficiency, %.

Please cite this article as: Zhu X., Blanco E., Bhatti M., Borrion A. Promoting methanogenesis and stability in anaerobic digestion with nano magnetite under VFA-induced stress. Biofuel Research Journal 46 (2025) 2432-2450. DOI: 10.18331/BRJ2025.12.2.5.

Table S6.
ANOVA results for the control group during the semi-continuous VFA spike-to-recovery test.

Treatment		Methane		Hydrogen		H_2S		pH		Live microorganism %		IA:PA		Acetic acid concentration		Butyric acid concentration		Propionic acid concentration		Total VFA concentration		Ammonium concentration	
		p-value	Sig.[1]	p-value	Sig.	p-value	Sig.	p-value	Sig.	p-value	Sig.	p-value	Sig.	p-value	Sig.	p-value	Sig.	p-value	Sig.	p-value	Sig.	p-value	Sig.
Control		0.85	ns	0.35	ns	0.63	ns	0.23	ns	0.80	ns	0.523	ns	0.15	ns	0.06	ns	0.66	ns	0.08	.	0.33	ns
Butyrate-spiking	Acid-spiking	<2e-16	***	0.000	***	<2e-16	***	0.00	***	0.00	***	<2e-16	***	0.02	*	<2e-16	***	0.00	**	0.00	***	0.00	***
	with 20 nm MNP pretreatment	0.00	***	0.05	*	0.55	ns	0.00	***	0.00	***	0.00	***	0.20	ns	0.08	.	0.00	**	0.13	ns	0.01	**
	with 50 nm MNP pretreatment	0.00	***	0.6	ns	0.84	ns	0.00	**	0.00	***	0.00	***	0.25	ns	0.34	ns	0.02	*	0.27	ns	0.01	**
	with 20 nm MNP post-treatment	0.01	*	0.94	ns	0.00	***	0.86	ns	0.06	.	0.11	Ns	0.60	ns	0.84	ns	0.66	ns	0.59	ns	0.94	ns
	with 50 nm MNP post-treatment	0.02	*	0.40	ns	0.00	***	0.30	ns	0.01	*	0.27	Ns	0.94	ns	0.12	ns	0.26	ns	0.69	ns	0.53	ns
Propionate-spiking	Acid-spiking	<2e-16	***	0.07	.	0.00	***	0.00	***	0.00	***	<2e-16	***	0.00	***	0.01	*	<2e-16	***	0.00	***	<2e-16	***
	with 20 nm MNP pretreatment	0.00	***	0.09	.	0.10	ns	0.12	ns	0.00	***	0.00	***	0.02	*	0.02	*	0.11	ns	0.01	*	0.00	**
	with 50 nm MNP pretreatment	0.00	***	0.06	.	0.66	ns	0.26	ns	0.00	**	0.00	***	0.43	ns	0.01	**	0.23	ns	0.34	ns	0.00	***
	with 20 nm MNP post-treatment	0.01	**	0.39	ns	0.84	ns	0.39	ns	0.18	ns	0.28	Ns	0.64	ns	0.13	ns	0.76	ns	0.75	ns	0.06	.
	with 50 nm MNP post-treatment	0.05	.	0.07	.	0.89	ns	0.19	ns	0.16	ns	0.23	Ns	0.95	ns	0.08	.	0.32	ns	0.90	ns	0.03	*

[1] The significance codes in the "Sig." columns indicate the statistical relevance of the corresponding p-values: "***" $p < 0.001$ (highly significant), "**" $p < 0.01$ (very significant), "*" $p < 0.05$ (significant), "." $p < 0.1$ (marginally significant; considered a trend), and "ns" denotes $p \geq 0.1$ (not significant).

Please cite this article as: Zhu X., Blanco E., Bhatti M., Borrion A. Promoting methanogenesis and stability in anaerobic digestion with nano magnetite under VFA-induced stress. Biofuel Research Journal 46 (2025) 2432-2450. DOI: 10.18331/BRJ2025.12.2.5.

Table S7.
Economic and environmental analyses of AD systems under feedstock overload and VFA stress.

	Parameter	Value
General parameter	Weight of the feedstock, ton waste/d	7 [a]
	Hydraulic retention time (HRT), d	30
	Operation temperature, ºC	35
	Refuse generation, %	1.93 [a]
	Conversion efficiency of methane to power energy, %	40 [b,c]
	Energy generation associated CO_2 emission, kg CO_2/kWh	1.05 [b]
	Energy from methane, kWh/kg CH_4	16.00 [d]
	Operation energy, kWh/ton waste	3.82 [a]
	Cost of slurry transportation and disposal. USD/ton	55 [a]
	Power price, USD/kWh	0.15 [a]
Control system	TS reduction, %	98.10 [e]
	VS reduction, %	83.50 [e]
	Slurry output, ton/day	4.13 [a]
	Methane production, kg/CH_4·d	215.43 [f]
	Energy produced from methane, kWh/d	5246.51
	Electricity generated, kWh/d	2098.60
	Net energy generated, kWh/d	2071.83
	Avoided CO_2 emission due to methane production, kg CO_2/d	2203.53
	Slurry disposal cost, USD/yr	82925.21
	Revenue from electricity production, USD/yr	113432.72
Overfed system	TS reduction, %	97.72 [a,f]
	VS reduction, %	77.84 [a,f]
	Slurry output, ton/d	4.39 [a,f]
	Methane production, kg/CH_4·d	172.75[f]
	Energy produced from methane, kWh/d	4207.04
	Electricity generated, kWh/d	1682.82
	Net energy generated, kWh/d	1656.04
	Avoided CO_2 emission due to methane production, kg CO_2/d	1766.96
	Slurry disposal cost, USD/yr	88118.52
	Revenue from electricity production, USD/yr	90668.28
Butyrate-stressed system	TS reduction, %	97.00 [a,f]
	VS reduction, %	67.00 [a,f]
	Slurry output, ton/day	4.89 [a,f]
	Methane production, kg/CH_4·d	172.35[f]
	Energy produced from methane, kWh/d	4197.21
	Electricity generated, kWh/d	1678.88
	Net energy generated, kWh/d	1652.11
	Avoided CO_2 emission due to methane production, kg CO_2/d	1762.83
	Slurry disposal cost, USD/yr	98075.99
	Revenue from electricity production, USD/yr	90453.00
Butyrate-stressed system with 50 nm MNP pretreatment	TS reduction, %	97.34 [a,f]
	VS reduction, %	71.64 [a,f]
	Slurry output, ton/day	4.67 [a,f]
	Methane production, kg/CH_4·d	188.97 [f]
	Energy produced from methane, kWh/d	4602.03
	Electricity generated, kWh/d	1840.81
	Net energy generated, kWh/d	1814.04
	Avoided CO_2 emission due to methane production, kg CO_2/d	1932.85
	Slurry disposal cost, USD/yr	93843..9
	Revenue from electricity production, USD/yr	99318.56
Butyrate-stressed system with 20 nm MNP pretreatment	TS reduction, %	97.42 [a,f]
	VS reduction, %	74.22 [a,f]
	Slurry output, ton/d	4.55 [a,f]

Please cite this article as: Zhu X., Blanco E., Bhatti M., Borrion A. Promoting methanogenesis and stability in anaerobic digestion with nano magnetite under VFA-induced stress. Biofuel Research Journal 46 (2025) 2432-2450. DOI: 10.18331/BRJ2025.12.2.5.

Table S7.
continued.

	Parameter	Value
	Methane production, kg/CH_4·d	189.64 [f]
	Energy produced from methane, kWh/d	4618.34
	Electricity generated, kWh/d	1847.34
	Net energy generated, kWh/d	1820.56
	Avoided CO_2 emission due to methane production, kg CO_2/d	1939.70
	Slurry disposal cost, USD/yr	91390.41
	Revenue from electricity production, USD/yr	99675.82
	TS reduction, %	97.13 [a,f]
	VS reduction, %	71.13 [a,f]
	Slurry output, ton/day	4.69 [a,f]
Butyrate-stressed system with 50 nm MNP post-treatment	Methane production, kg/CH_4·d	187.24 [f]
	Energy produced from methane, kWh/d	4559.98
	Electricity generated, kWh/d	1823.99
	Net energy generated, kWh/d	1797.22
	Avoided CO_2 emission due to methane production, kg CO_2/d	1915.19
	Slurry disposal cost, USD/yr	94142.93
	Revenue from electricity production, USD/yr	98397.78
	TS reduction, %	97.34 [a,f]
	VS reduction, %	72.16 [a,f]
	Slurry output, ton/d	4.65 [a,f]
	Methane production, kg/CH_4·d	188.22 [f]
Butyrate-stressed system with 20 nm MNP post-treatment	Energy produced from methane, kWh/d	4583.70
	Electricity generated, kWh/d	1833.48
	Net energy generated, kWh/d	1806.71
	Avoided CO_2 emission due to methane production, kg CO_2/d	1925.15
	Slurry disposal cost, USD/yr	93336.180
	Revenue from electricity production, USD/yr	5581.01
	TS reduction, %	97.04 [a,f]
	VS reduction, %	67.00 [a,f]
	Slurry output, ton/d	4.89 [a,f]
	Methane production, kg/CH_4·d	169.92 [f]
Propionate-stressed system	Energy produced from methane, kWh/d	4137.96
	Electricity generated, kWh/d	1655.18
	Net energy generated, kWh/d	1628.41
	Avoided CO_2 emission due to methane production, kg CO_2/d	1737.94
	Slurry disposal cost, USD/yr	98117.52
	Revenue from electricity production, USD/yr	89155.52
	TS reduction, %	97.30 [a,f]
	VS reduction, %	72.67 [a,f]
	Slurry output, ton/d	4.62 [a,f]
	Methane production, kg/CH_4·d	189.00 [f]
Propionate-stressed system with 50 nm MNP pretreatment	Energy produced from methane, kWh/d	4602.69
	Electricity generated, kWh/d	1841.08
	Net energy generated, kWh/d	1814.30
	Avoided CO_2 emission due to methane production, kg CO_2/d	1933.13
	Slurry disposal cost, USD/yr	92787.44
	Revenue from electricity production, USD/yr	99333.02
	TS reduction, %	97.64 [a,f]
	VS reduction, %	73.70 [a,f]
	Slurry output, ton/d	4.59 [a,f]
Propionate-stressed system with 20 nm MNP pretreatment	Methane production, kg/CH_4·d	191.30 [f]
	Energy produced from methane, kWh/d	4658.73
	Electricity generated, kWh/d	1863.49
	Net energy generated, kWh/d	1836.72

Please cite this article as: Zhu X., Blanco E., Bhatti M., Borrion A. Promoting methanogenesis and stability in anaerobic digestion with nano magnetite under VFA-induced stress. Biofuel Research Journal 46 (2025) 2432-2450. DOI: 10.18331/BRJ2025.12.2.5.

Table S7.
continued.

	Parameter	Value
	Avoided CO_2 emission due to methane production, kg CO_2/d	1956.66
	Slurry disposal cost, USD/yr	92105.29
	Revenue from electricity production, USD/yr	100560.25
Propionate-stressed system with 50 nm MNP post-treatment	TS reduction, %	97.34 [a,f]
	VS reduction, %	73.19 [a,f]
	Slurry output, ton/day	4.60 [a,f]
	Methane production, kg/CH_4d	186.61 [f]
	Energy produced from methane, kWh/d	4544.45
	Electricity generated, kWh/d	1817.78
	Net energy generated, kWh/d	1791.01
	Avoided CO_2 emission due to methane production, kg CO_2/d	1908.67
	Slurry disposal cost, USD/yr	92321.76
	Revenue from electricity production, USD/yr	98057.68
Propionate-stressed system with 20 nm MNP post-treatment	TS reduction, %	97.68 [a,f]
	VS reduction, %	75.25 [a,f]
	Slurry output, ton/d	4.51 [a,f]
	Methane production, kg/CH_4d	185.66 [f]
	Energy produced from methane, kWh/d	4521.44
	Electricity generated, kWh/d	1808.58
	Net energy generated, kWh/d	1781.80
	Avoided CO_2 emission due to methane production, kg CO_2/d	1899.01
	Slurry disposal cost, USD/yr	90625.20
	Revenue from electricity production, USD/yr	97553.70

[a]: Refer to Weligama Thuppahige and Babel (2022).
[b]: Refer to Wei et al. (2017).
[c]: Refer to Carballa et al. (2011).
[d]: Refer to Tchobanoglous et al. (2003).
[e]: Refer to Van et al. (2020) and Zhang et al. (2017) for similar operation conditions.
[f]: Calculated based on the results from this study. For VFA-stressed systems, the results from last dosage level were used.

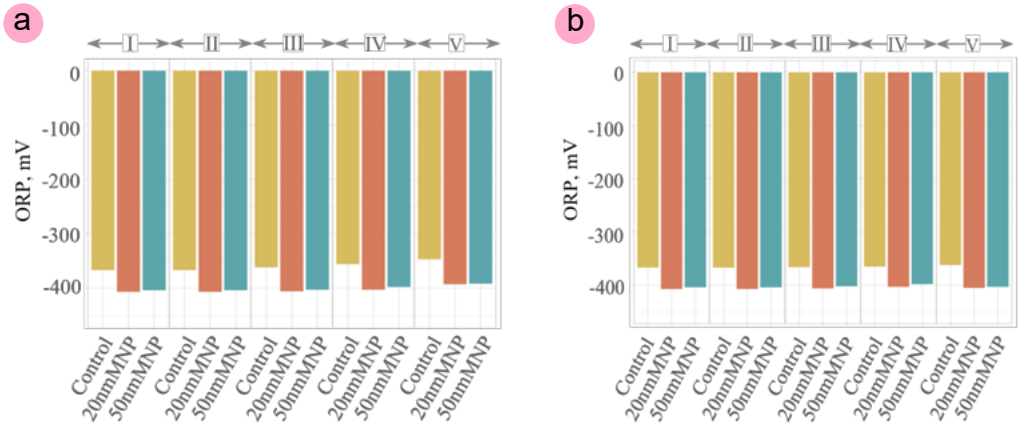

Fig. S1. Changes of ORP levels with evaluated VFA dosage: **(a)** substrate as butyric acid; and **(b)** substrate as propionic acid.

Please cite this article as: Zhu X., Blanco E., Bhatti M., Borrion A. Promoting methanogenesis and stability in anaerobic digestion with nano magnetite under VFA-induced stress. Biofuel Research Journal 46 (2025) 2432-2450. DOI: 10.18331/BRJ2025.12.2.5.

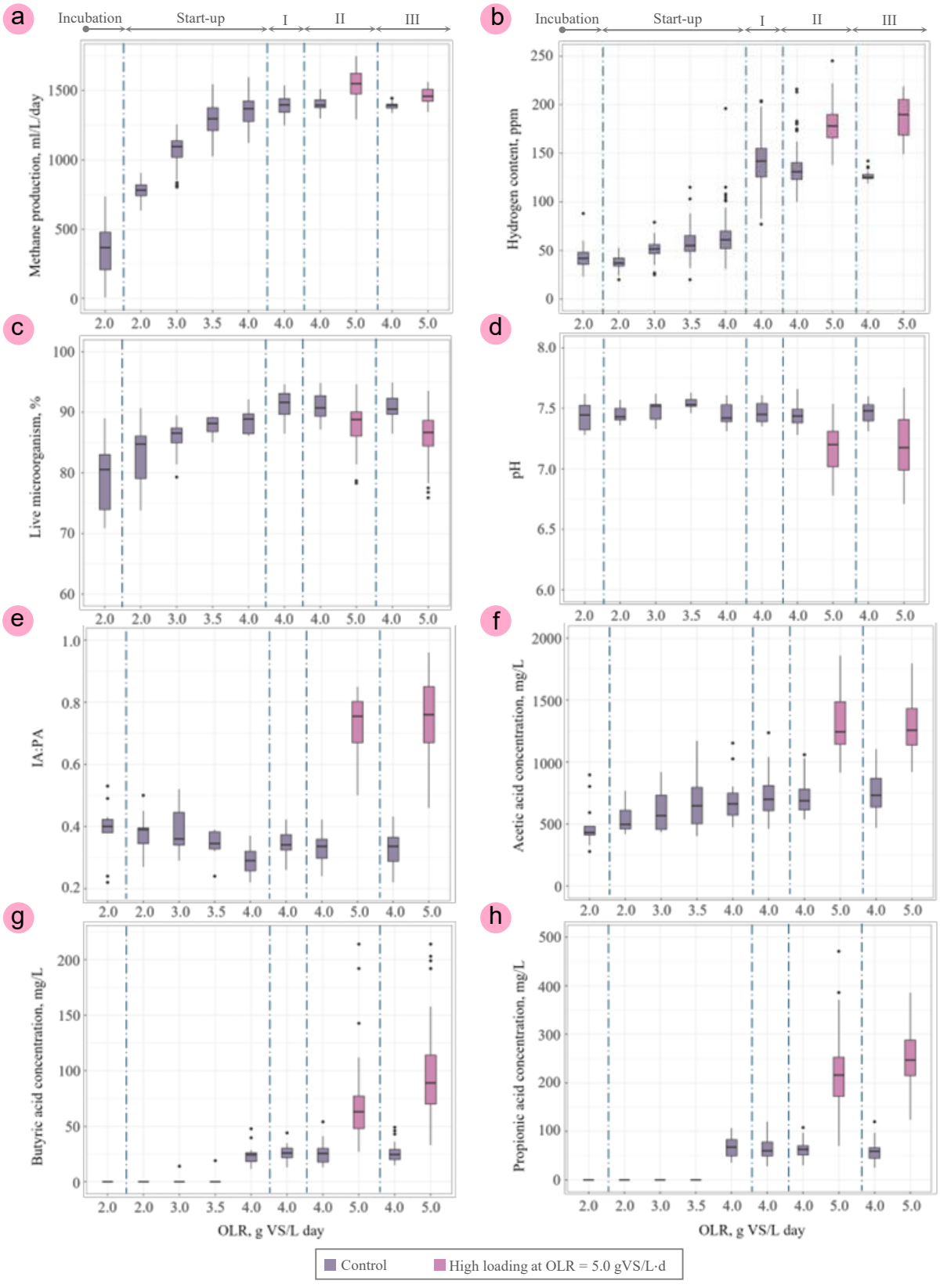

Fig. S2. Reactor performance at stepwise increased OLRs. **(a)** methane production; **(b)** hydrogen content; **(c)** microbial viability; **(d)** pH; **(E)** IA:PA; **(f)** acetic acid concentration; **(g)** butyric acid concentration; and **(h)** propionic acid concentration.

Please cite this article as: Zhu X., Blanco E., Bhatti M., Borrion A. Promoting methanogenesis and stability in anaerobic digestion with nano magnetite under VFA-induced stress. Biofuel Research Journal 46 (2025) 2432-2450. DOI: 10.18331/BRJ2025.12.2.5.

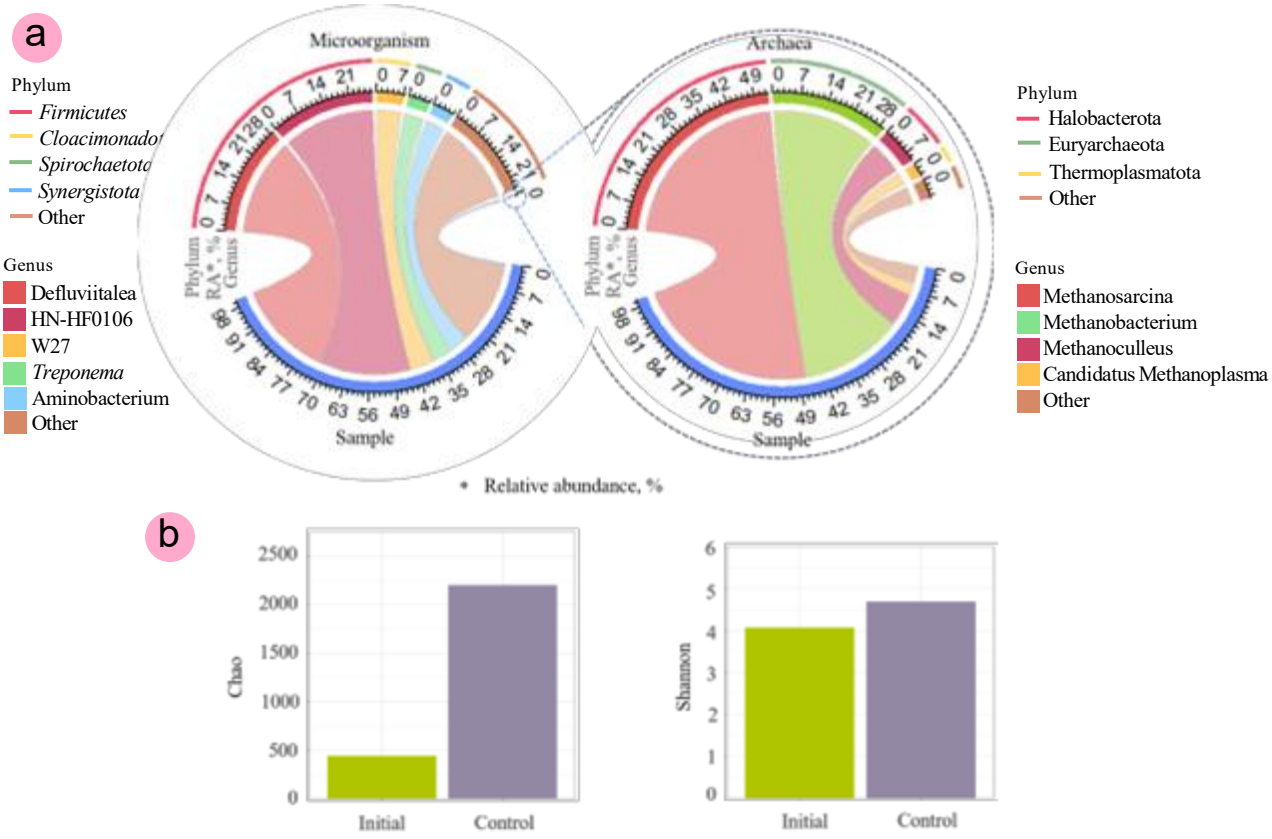

Fig. S3. **(a)** Circos plot of initial microorganism community at genus level, and **(b)** Alpha diversity comparing initial inoculum and control system after long-term operation.

Please cite this article as: Zhu X., Blanco E., Bhatti M., Borrion A. Promoting methanogenesis and stability in anaerobic digestion with nano magnetite under VFA-induced stress. Biofuel Research Journal 46 (2025) 2432-2450. DOI: 10.18331/BRJ2025.12.2.5.

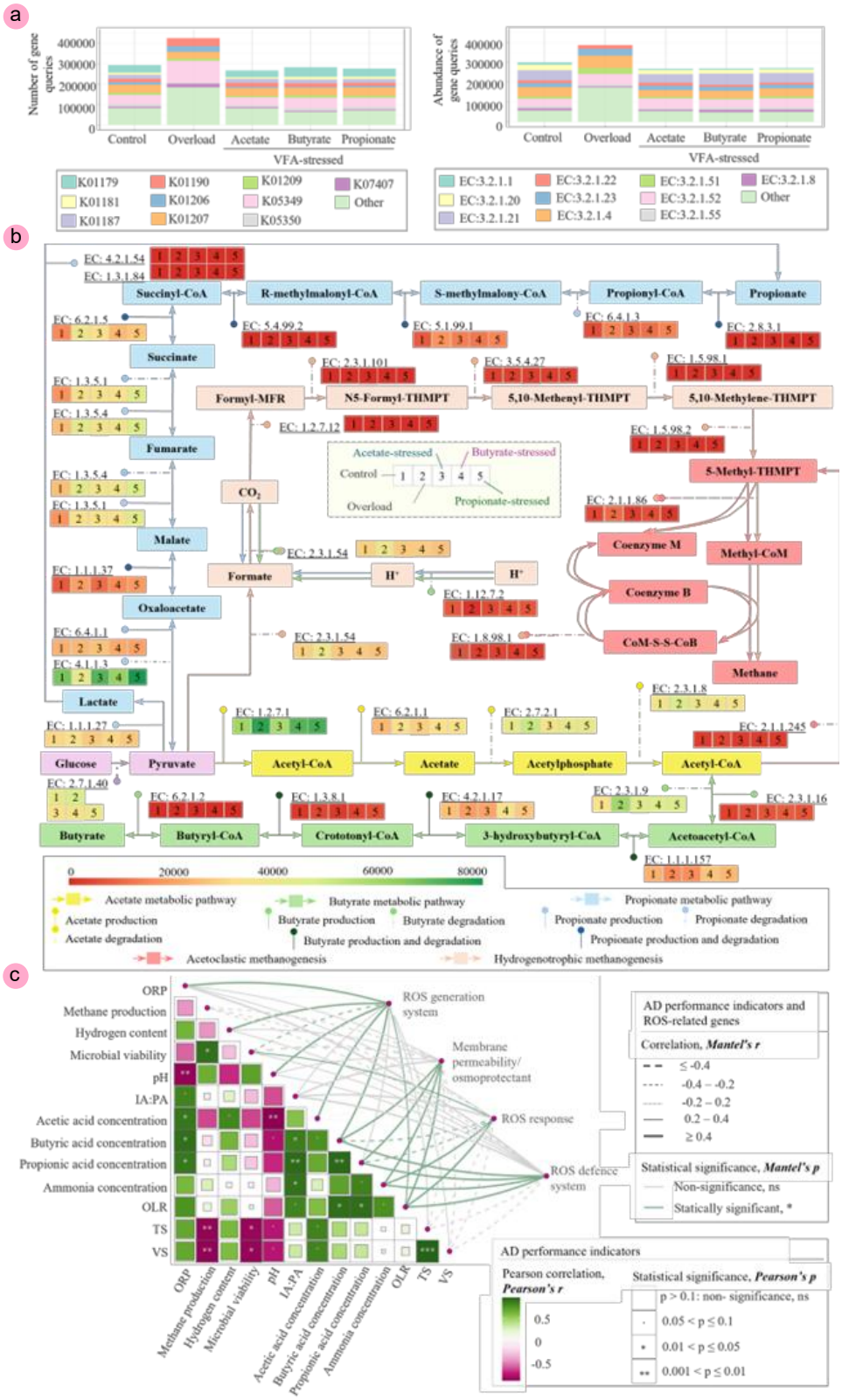

Fig. S4. Microbial and metabolic response to feedstock overload and VFA-induced stress. **(a)** Number and abundance of the top 10 gene queries encoding enzymes involved in the hydrolysis process; **(b)** The abundance variations of relevant enzymes involved in acetate, butyrate, and propionate metabolic pathways and methanogenesis in control, feedstock overload and VFA-stressed systems. Information on the corresponding enzymes within control, feedstock overload, and manually induced acetate stress was derived from (Lv et al., 2020; Wang et al., 2023); and **(c)** Correlations between ROS-related genes and AD performance indicators throughout control, feedstock overload and VFA-stressed systems.

Please cite this article as: Zhu X., Blanco E., Bhatti M., Borrion A. Promoting methanogenesis and stability in anaerobic digestion with nano magnetite under VFA-induced stress. Biofuel Research Journal 46 (2025) 2432-2450. DOI: 10.18331/BRJ2025.12.2.5.

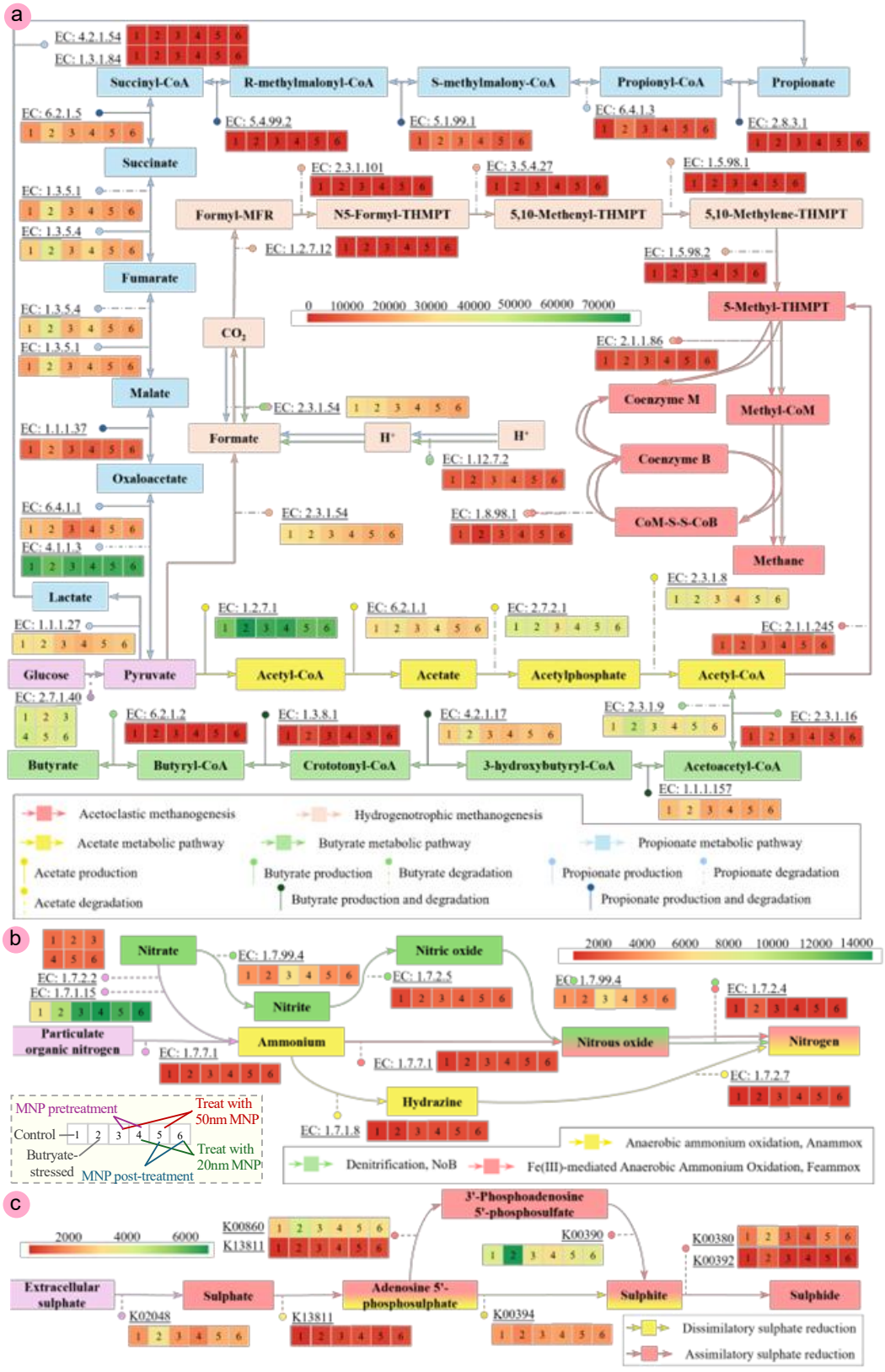

Fig. S5. Metabolic response to butyrate-induced stress and MNP additions. **(a)** The abundance variations of relevant enzymes involved in acetate, butyrate, and propionate metabolic pathways and methanogenesis. Information on the corresponding enzymes was derived from (Lv et al., 2020; Wang et al., 2023); **(b)** The abundance variations of relevant enzymes involved in nitrogen cycle (Tan et al., 2022); and **(C)** The abundance variations of relevant enzymes involved in sulphate cycle (Giangeri et al., 2023).

Please cite this article as: Zhu X., Blanco E., Bhatti M., Borrion A. Promoting methanogenesis and stability in anaerobic digestion with nano magnetite under VFA-induced stress. Biofuel Research Journal 46 (2025) 2432-2450. DOI: 10.18331/BRJ2025.12.2.5.

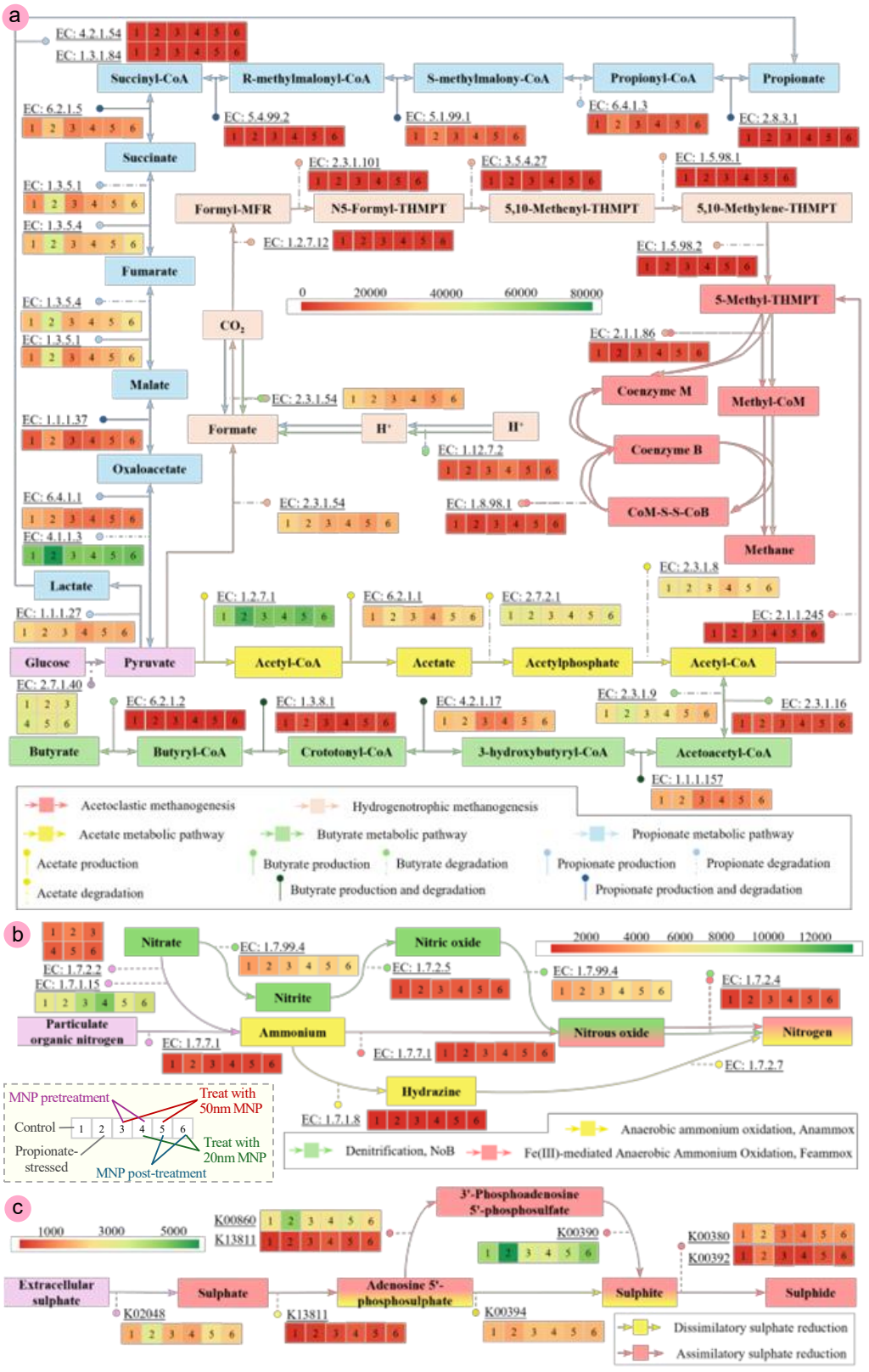

Fig. S6. Metabolic response to propionate-induced stress and MNP additions. **(a)** The abundance variations of relevant enzymes involved in acetate, butyrate, and propionate metabolic pathways and methanogenesis. Information on the corresponding enzymes was derived from (Lv et al., 2020; Wang et al., 2023); **(b)** The abundance variations of relevant enzymes involved in nitrogen cycle (Tan et al., 2022); and **(c)** The abundance variations of relevant enzymes involved in sulphate cycle (Giangeri et al., 2023).

Please cite this article as: Zhu X., Blanco E., Bhatti M., Borrion A. Promoting methanogenesis and stability in anaerobic digestion with nano magnetite under VFA-induced stress. Biofuel Research Journal 46 (2025) 2432-2450. DOI: 10.18331/BRJ2025.12.2.5.

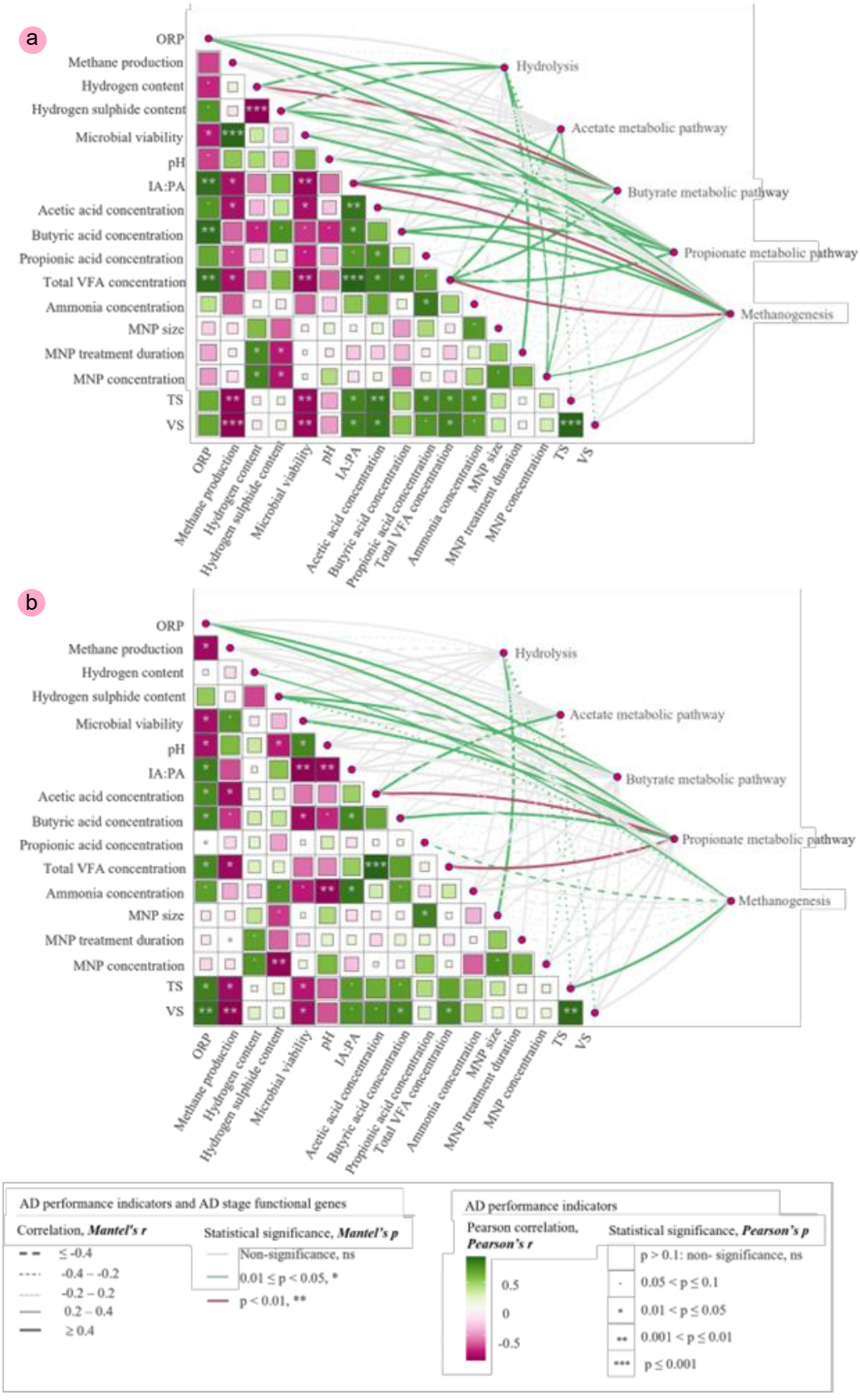

Fig. S7. Correlations between genes of AD process and performance indicators. **(a)** In butyrate-stressed systems with MNP additions; and **(b)** In propionate-stressed systems with MNP additions.

Please cite this article as: Zhu X., Blanco E., Bhatti M., Borrion A. Promoting methanogenesis and stability in anaerobic digestion with nano magnetite under VFA-induced stress. Biofuel Research Journal 46 (2025) 2432-2450. DOI: 10.18331/BRJ2025.12.2.5.

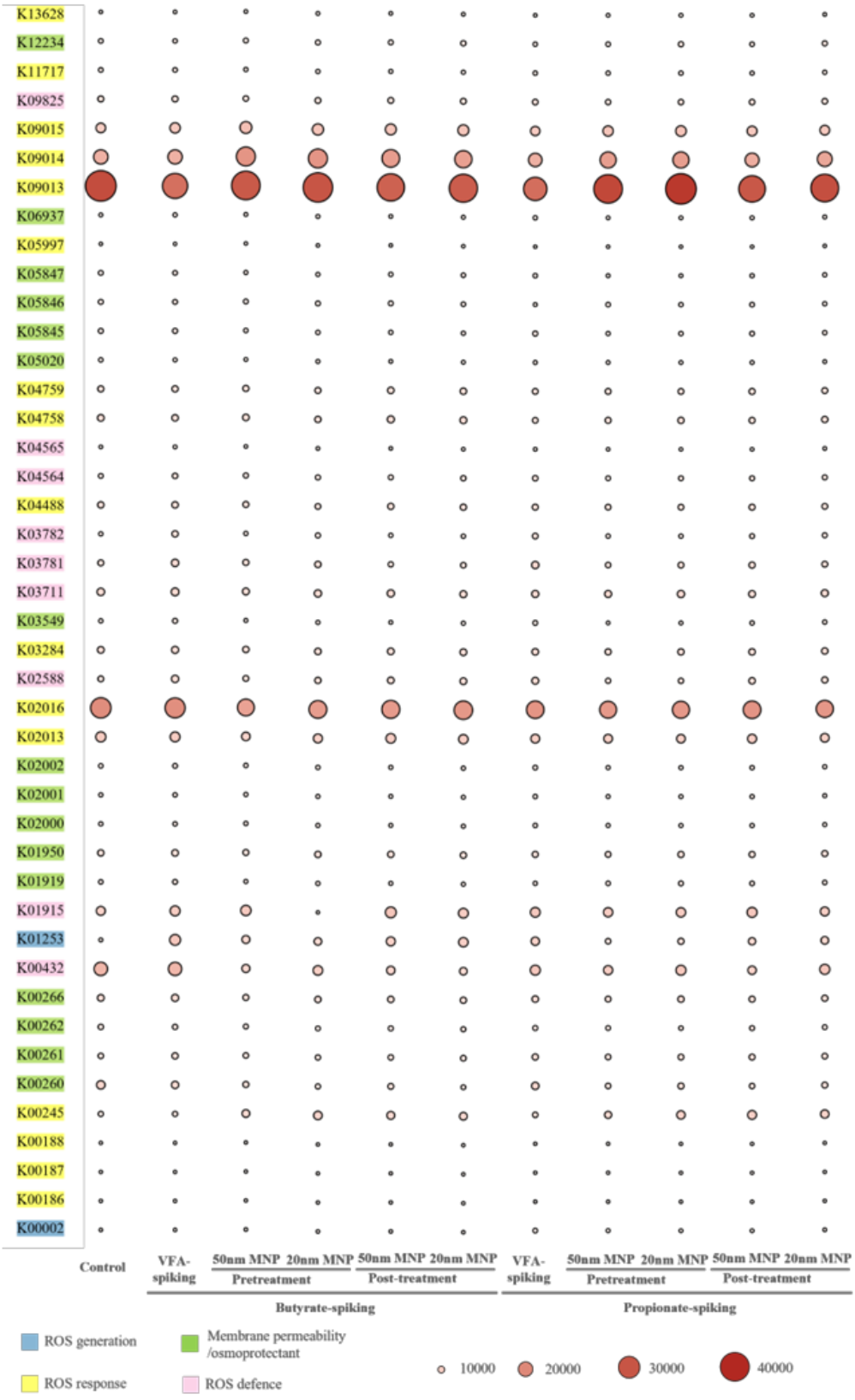

Fig. S8. The abundance variations of ROS-related genes. Information on the corresponding functional genes was derived from a previous study (Yan et al., 2023).

Please cite this article as: Zhu X., Blanco E., Bhatti M., Borrion A. Promoting methanogenesis and stability in anaerobic digestion with nano magnetite under VFA-induced stress. Biofuel Research Journal 46 (2025) 2432-2450. DOI: 10.18331/BRJ2025.12.2.5.

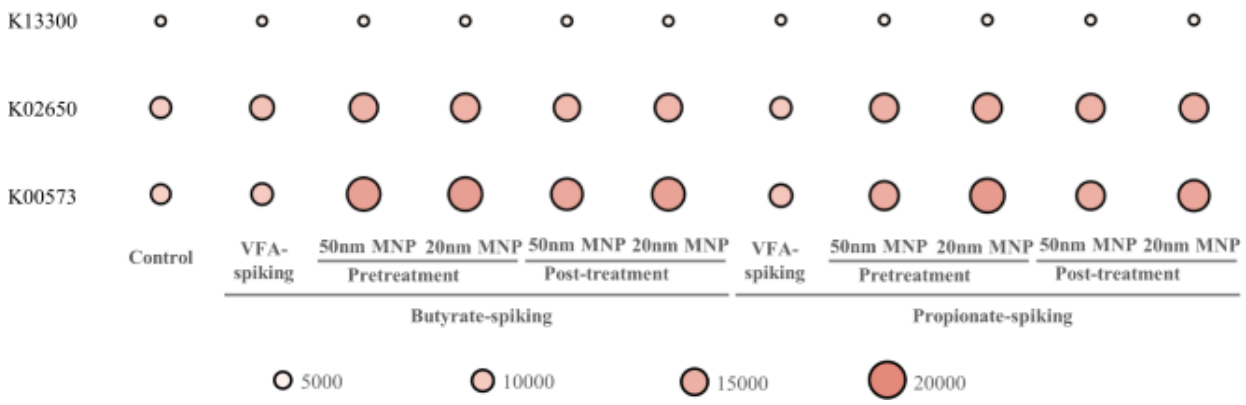

Fig. S9. The abundance variations of DIET-related enzymes (Xu et al., 2019; Holmes and Zhou, 2021).

References

[1] APHA, 2012. Standard methods for the examination of water and wastewater. American Public Health Association, American Water Works Association, Water Pollution Control Federation. Washington DC. 56(3), 387-388.
[2] Bai, X., Rebosura, M.J., Jensen, P.D., 2025. Enhanced anaerobic digestion of lignocellulosic paunch waste using potassium hydroxide pre-treatment. Bioresour. Technol. 425, 132323.
[3] Boyle, W.C., 1977. Energy recovery from sanitary landfills-a Review. Microb. Energy Convers. 119-138.
[4] Campanaro, S., Treu, L., Kougias, P.G., Zhu, X., Angelidaki, I., 2018. Taxonomy of anaerobic digestion microbiome reveals biases associated with the applied high throughput sequencing strategies. Sci. Rep. 8(1), 1926.
[5] Carballa, M., Duran, C., Hospido, A., 2011. Should we pretreat solid waste prior to anaerobic digestion? an assessment of its environmental cost. Environ. Sci. Technol. 45(24), 10306-10314.
[6] Dogan, T., Ince, O., Oz, N.A., Ince, B.K., 2005. Inhibition of volatile fatty acid production in granular sludge from a UASB reactor. J. Environ. Sci. Health., Part A. 40(3), 633-644.
[7] Douglas, G.M., Maffei, V.J., Zaneveld, J.R., Yurgel, S.N., Brown, J.R., Taylor, C.M., Huttenhower, C., Langille, M.G.I., 2020. PICRUSt2 for prediction of metagenome functions. Nat. Biotechnol. 38(6), 669-673.
[8] Giangeri, G., Tsapekos, P., Gaspari, M., Ghofrani-Isfahani, P., Lin, M.K.T.H., Treu, L., Kougias, P., Campanaro, S., Angelidaki, I., 2023. Magnetite alters the metabolic interaction between methanogens and sulfate-reducing bacteria. Environ. Sci. Technol. 57(43), 16399-16413.
[9] Holmes, D.E., Zhou, J., 2021. Mechanisms for Electron Uptake by *Methanosarcina acetivorans* during Direct Interspecies Electron Transfer. MBio. 12(5).
[10] Isci, A., Demirer, G.N., 2007. Biogas production potential from cotton wastes. Renewable Energy. 32(5), 750-757.
[11] Jantsch, T.G., Mattiasson, B., 2003. A simple spectrophotometric method based on ph-indicators for monitoring partial and total alkalinity in anaerobic processes. Environ. Technol. 24(9), 1061-1067.
[12] Lv, N., Zhao, L., Wang, R., Ning, J., Pan, X., Li, C., Cai, G., 2020. Novel strategy for relieving acid accumulation by enriching syntrophic associations of syntrophic fatty acid-oxidation bacteria and H_2/formate- scavenging methanogens in anaerobic digestion. Bioresour. Technol. 313, 123702.
[13] Morita, M., Malvankar, N.S., Franks, A.E., Summers, Z.M., Giloteaux, L., Rotaru, A.E., Rotaru, C., Lovleya, D.R., 2011. Potential for direct interspecies electron transfer in methanogenic wastewater digester aggregates. MBio. 2(4), 5-7.
[14] Rettenmaier, R., Schneider, M., Munk, B., Lebuhn, M., Jünemann, S., Sczyrba, A., Maus, I., Zverlov, V., Liebl, W., 2020. Importance of defluviitalea raffinosedens for hydrolytic biomass degradation in co-culture with hungateiclostridium thermocellum. Microorganisms. 8(6), 1-18.
[15] Rittmann, B., McCarty., P.L., 2020. Environmental biotechnology: principles and applications.
[16] Rocamora, I., Wagland, S.T., Hassard, F., Villa, R., Peces, M., Simpson, E.W., Fernández, O., Bajón-Fernández, Y., 2023. Inhibitory mechanisms on dry anaerobic digestion: Ammonia, hydrogen and propionic acid relationship. Waste Manage. 161, 29-42.
[17] Sikora, A., Detman, A., Mielecki, D., Chojnacka, A., Błaszczyk, M., 2019. Searching for Metabolic Pathways of Anaerobic Digestion: A Useful List of the Key Enzymes, in: Anaerobic Digestion. pp. 1-19.
[18] Tan, X., Xie, G., Nie, W., Xing, D., Liu, B., Ding, J., Ren, N., 2022. Fe(III)-mediated anaerobic ammonium oxidation: a novel microbial nitrogen cycle pathway and potential applications. Crit. Rev. Environ. Sci. Technol. 52(16), 2962-2994.
[19] Tchobanoglous, G., Burton, F.L., Stensel, H.D., 2003. Wastewater engineering: treatment and reuse, 4th ed. McGraw-Hill, New York.
[20] USEPA, 1983. Methods for chemical analysis of water and wastes. United States Environmental Protection Agency, Office of Research and Development. Cincinnati, Ohio.
[21] Van, D.P., Fujiwara, T., Tho, B.L., Toan, P.P.S., Minh, G.H., 2020. A review of anaerobic digestion systems for biodegradable waste: Configurations, operating parameters, and current trends. Environ. Eng. Res. 25(1), 1-17.
[22] Wang, S., Li, D., Zhang, K., Ma, Y., Liu, F., Li, Z., Gao, X., Gao, W., Du, L., 2023. Effects of initial volatile fatty acid concentrations on process characteristics , microbial communities , and metabolic pathways on solid-state anaerobic digestion. Bioresour. Technol. 369, 128461.
[23] Wei, W., Zhou, X., Wang, D., Sun, J., Wang, Q., 2017. Free ammonia pre-treatment of secondary sludge significantly increases anaerobic methane production. Water Res. 118, 12-19.
[24] Weligama Thuppahige, R.T., Babel, S., 2022. Environmental impact assessment of organic fraction of municipal solid waste treatment by anaerobic digestion in Sri Lanka. Waste Manage. Res. 40(2), 236-243.
[25] Xu, H., Chang, J., Wang, H., Liu, Y., Zhang, X., Liang, P., Huang, X., 2019. Enhancing direct interspecies electron transfer in syntrophic-methanogenic associations with (semi) conductive iron oxides: effects and mechanisms. Sci. Total Environ. 695, 133876.
[26] Yan, M., Hu, Z., Duan, Z., Sun, Y., Dong, T., Sun, X., Zhen, F., Li, Y., 2023. Microbiome re-assembly boosts anaerobic digestion under volatile fatty acid

Please cite this article as: Zhu X., Blanco E., Bhatti M., Borrion A. Promoting methanogenesis and stability in anaerobic digestion with nano magnetite under VFA-induced stress. Biofuel Research Journal 46 (2025) 2432-2450. DOI: 10.18331/BRJ2025.12.2.5.

inhibition: focusing on reactive oxygen species metabolism. Water Res. 246, 120711.
[27] You, M., Zhao, Q., Liu, Y., Zhang, W., Shen, Z., Ren, Z., Xu, C., 2023. Insights into lignocellulose degradation: comparative genomics of anaerobic and cellulolytic Ruminiclostridium-type species. Front. Microbiol. 14, 1-12.
[28] Zhang, J., Loh, K.C., Li, W., Lim, J.W., Dai, Y., Tong, Y.W., 2017. Three-stage anaerobic digester for food waste. Appl. Energy 194, 287-295.
[29] Zhang, W., Zhang, F., Li, Y.X., Jianxiong Zeng, R., 2019. Inhibitory effects of free propionic and butyric acids on the activities of hydrogenotrophic methanogens in mesophilic mixed culture fermentation. Bioresour. Technol. 272(September 2018), 458-464.
[30] Zheng, D., Wang, H.Z., Gou, M., Nobu, M.K., Narihiro, T., Hu, B., Nie, Y., Tang, Y.Q., 2019. Identification of novel potential acetate-oxidizing bacteria in thermophilic methanogenic chemostats by DNA stable isotope probing. Appl. Microbiol. Biotechnol. 103(20), 8631-8645.
[31] Ziels, R.M., Nobu, M.K., Sousa, D.Z., 2019. Elucidating Syntrophic Butyrate-Degrading Populations in Anaerobic Digesters Using Stable-Isotope-Informed Genome-Resolved Metagenomics. mSystems. 4(4), 1-16.

Please cite this article as: Zhu X., Blanco E., Bhatti M., Borrion A. Promoting methanogenesis and stability in anaerobic digestion with nano magnetite under VFA-induced stress. Biofuel Research Journal 46 (2025) 2432-2450. DOI: 10.18331/BRJ2025.12.2.5.